

# **University of Alberta**

Paleomagnetic studies of volcanic rocks in Siberia and sedimentary rocks  
in Southern Alberta: From long-term geomagnetic field variations to age  
determinations.

by

Dunia Blanco Acuña

A thesis submitted to the Faculty of Graduate Studies and Research  
in partial fulfillment of the requirements for the degree of

Doctor of Philosophy  
in  
Geophysics

Department of Physics

©Dunia Blanco Acuña  
Fall 2013  
Edmonton, Alberta

Permission is hereby granted to the University of Alberta Libraries to reproduce single copies of this thesis and to lend or sell such copies for private, scholarly or scientific research purposes only. Where the thesis is converted to, or otherwise made available in digital form, the University of Alberta will advise potential users of the thesis of these terms.

The author reserves all other publication and other rights in association with the copyright in the thesis and, except as herein before provided, neither the thesis nor any substantial portion thereof may be printed or otherwise reproduced in any material form whatsoever without the author's prior written permission.

## **Abstract**

Paleomagnetism is a fundamental tool to understand the ancient variations of Earth's magnetic field through time. Important applications to geochronology and paleography come from interpreting the variations of the planetary magnetic vector. This dissertation explores the different applications of paleomagnetism to uncover important characteristics of the paleointensity magnetic field during the Permo-Triassic boundary and the nature of the apparent polar wander path (APWP) of Siberia, and to create geochronological frameworks for kimberlites in the Siberian platform and for sediments at the Western Canada Sedimentary Basin.

Detailed absolute paleointensity measurements from Permo-Triassic sills at the Siberian platform are studied to determine the existence of a low dipole field, which has been previously reported in the area. We found a mean virtual dipolar moment value of  $6.01 \pm 1.45 \times 10^{22}$  Am<sup>2</sup> which is over 50% higher than the results previously obtained by other authors.

Diamondiferous kimberlite pipes are exposed across the north-central part of the Siberian platform. The age of the magmatic activity cannot be clearly determined from isotopic age data – this is the reason why new paleomagnetic poles from four kimberlite pipes are obtained to study their paleomagnetic age. On the basis of a comparison with the Siberian APWP, we estimate the age of the kimberlite

magmatism. The acquired paleomagnetic ages span from the Early Silurian to the Middle Late Jurassic.

Magnetostratigraphic analysis is used as a dating tool on three deep drilling cores that penetrate Santonian-Campanian strata in southern Alberta, Canada. Chrons 34n and 33r are clearly identified from the studied sections - providing a high-resolution age boundary that creates new age boundaries between adjacent stratigraphic units. In addition, normal polarity zones are observed within C33r, previously described as reverse polarity over its entire length.

Siberian APWP contains long unresolved segments; therefore, the nature of the path depends largely on the curve fitting method used. A least square fitting method computed through singular value decomposition is applied to create the path. The method is compared to a smoothing cubic spline fitting and to the most recent version of the Siberian APWP from the literature. For the Mesozoic Era two possible scenarios are explored.

## Acknowledgments

I would like to offer my special thanks to my supervisor Dr. Vadim A. Kravchisnky. His constant support, constructive suggestions and patient guidance were fundamental for the development of my Ph.D. I would also like to extend my thanks to my supervisory committees Dr. Thomas Stachel, Dr. Frank Hegmann, Dr. Mathieu Dumberry, Dr. Moritz Heimpel and Dr. William Harbert for their careful and constructive review of my thesis.

Special thanks should be given to the Paleomagnetic group at the University of Alberta: Ted Evans, Lei Wu and Taslima Anwar, as well to the laboratory technicians: Luda P. Kuokhar, Len Tober and Lucas Duerkensen, for their support during my studies. I would also like to thank Dr. Rui Zhang and Prof. Yue Leping for allowing me to contribute to their research and for giving me the opportunity to visit their laboratories at the Northwestern University in Xi'an, China. In addition, I would like to extend my gratitude to Andrew J. Mumpy for giving the opportunity to participate in his research project, which resulted in the magnetostratigraphy study presented in Chapter 4 of this contribution.

Thanks to the University of Alberta, Department of Physics for opening me spaces to grow as a scientist and as professional. I would like to give special thanks to Sarah Derr and Dr. Sharon Morsink for their continuous help and support to graduate students.

This thesis as well as the completion of my studies would not have been possible without the support of my family and friends. I wish to thank my parents for their continuous support in this path I have chosen to take. Without them I would not be who I am.

# Table of Contents

## Chapter 1

### Introduction

<b>1.1 Geomagnetic Principles .....</b>	<b>1</b>
1.1.1 Magnetic Properties of Solids .....	2
1.1.2 Rock Magnetism .....	5
<b>1.2 Earth's Ancient Magnetic Field .....</b>	<b>8</b>
1.2.1 Paleomagnetic Principles .....	8
1.2.2 Paleomagnetic Methods .....	9
1.2.3 Paleointensity and Virtual Dipolar Moment .....	13
<b>1.3 Geochronological Applications .....</b>	<b>18</b>
1.3.1 Geomagnetic Polarity Time Scale .....	19
1.3.2 Magnetostratigraphy .....	20
1.3.3 Dating Using Apparent Polar Wander Paths .....	21
<b>1.4 Construction of Apparent Polar Wander Paths.....</b>	<b>22</b>
<b>1.5 Major Goals of the Thesis .....</b>	<b>25</b>

## Chapter 2

### Does the Permo-Triassic geomagnetic dipole low exist?

<b>2.1 Introduction .....</b>	<b>34</b>
<b>2.2 Geological Settings .....</b>	<b>36</b>
<b>2.3 Methodology .....</b>	<b>38</b>
2.3.1 Magnetic Mineralogy .....	38
2.3.2 Directions .....	39
2.3.3 Absolute Paleointensity .....	39
<b>2.4 Results .....</b>	<b>43</b>
2.4.1 Thermomagnetic and Hysteresis Measurements .....	43
2.4.2 Directions .....	45
2.4.3 Absolute Paleointensity .....	50
<b>2.5 Discussion .....</b>	<b>52</b>
<b>2.6 Conclusions .....</b>	<b>55</b>

## **Chapter 3**

### **Paleomagnetic dating of Phanerozoic kimberlites in Siberia**

<b>3.1 Introduction .....</b>	<b>65</b>
<b>3.2 Geological Settings .....</b>	<b>65</b>
<b>3.3 Methods .....</b>	<b>70</b>
3.3.1 Laboratory Techniques .....	70
3.3.2 Paleomagnetic Dating Techniques .....	71
<b>3.4 Paleomagnetic Results .....</b>	<b>72</b>
3.4.1 Rock-Magnetic Properties of the Studied Kimberlites .....	71
3.4.2 Kimberlite from the Eastern Udachnaya Pipe .....	75
3.4.3 Sediments Near the Eastern Udachnaya Kimberlite Pipe .....	78
3.4.4 Kimberlites from the Western Udachnaya Pipe .....	80
3.4.5 Sedimentary Rocks from the Baked Contact of the Western Udachnaya Kimberlite Pipe .....	82
3.4.6 International Kimberlite Pipe .....	84
3.4.7 Obnazhennaya Kimberlite Pipe .....	86
<b>3.5 Discussion .....</b>	<b>88</b>
<b>3.6 Conclusions .....</b>	<b>94</b>

## **Chapter 4**

### **Upper Cretaceous magnetostratigraphy in Western Canada: Evidence for normal polarity zones in chron 33r and high resolution age correlation between stratigraphic units**

<b>4.1 Introduction .....</b>	<b>102</b>
<b>4.2 Geological Background .....</b>	<b>103</b>
4.2.1 Regional Setting and Stratigraphic Units .....	103
4.2.2 Studied Cores .....	107
4.2.3 Age Control .....	108
<b>4.3 Methodology .....</b>	<b>110</b>
<b>4.4 Results .....</b>	<b>112</b>
4.4.1 Rock Magnetism Results .....	112
4.4.2 Paleomagnetic Results .....	113
4.4.3 Magnetostratigraphy .....	117
<b>4.5 Discussion .....</b>	<b>122</b>
<b>4.6 Conclusions .....</b>	<b>126</b>

## **Chapter 5**

### **Revised apparent polar wander path for Siberia during the Phanerozoic: Application of a new fitting technique**

<b>5.1 Introduction .....</b>	<b>136</b>
<b>5.2 Methodology .....</b>	<b>137</b>
5.2.1 Paleomagnetic Data Selection .....	137
5.2.2 Mathematical Approach .....	144
<b>5.3 Results .....</b>	<b>149</b>
5.3.1 European APWP .....	149
5.3.2 APWP for the Siberia Platform .....	153
<b>5.4 Conclusions and Future Work .....</b>	<b>158</b>

## **Chapter 6**

<b>Conclusions .....</b>	<b>165</b>
--------------------------	------------

## List of Tables

<b>Table 1.1.</b>	Summary of the remanent magnetizations observed in nature .....	7
<b>Table 1.2.</b>	Summary of the different check applied in thermal paleointensity measurements .....	16
<b>Table 1.3.</b>	Statistical parameters to determine the goodness of the paleointensity determination .....	17
<b>Table 1.4.</b>	Summary of the different methods used in the calculation of APW paths .....	24
<b>Table 2.1.</b>	Late Permian – Early Triassic basalt mean directions of the high temperature primary stable component of NRM for the Eastern Siberian traps (Aikhal (66.17°N, 111.33° E), Sytikanskaya (66.11°N, 111.80°E), Yubileinaya (66.0°N,111.7°E) kimberlite mine pit areas) and northwestern Noril'sk sill intrusion (69.21°N, 88.03°E). N is the number of directions for specimens or sites accepted for calculation; D (I) is the declination (inclination) of the NRM in geographic (g) or stratigraphic (s) system of coordinates; k, $\alpha_{95}$ - precision parameter and half angle radius of the 95% probability confidence cone .....	49
<b>Table 2.2.</b>	Statistical parameters of the paleointensity results. Site: Nomenclature for each of the studied sites. Class: Category for each of the samples as defined in the text. $\Delta T$ : Temperature range of the linear segment. Prot: paleointensity protocol applied: ZI, Coe protocol; IZ, Atkin protocol. $B_{lab}$ : Applied laboratory magnetic field. N: Number of successive data points used for paleointensity calculations. $\beta$ : measure of linearity (Selkin and Tauxe, 2000). f, is the fraction of the NRM, as defined by Coe et al. (1978) and Prévot et al. (1985). MAD: maximum angular deviation .....	53

<b>Table 2.3.</b>	Paleointensity results. Site: Nomenclature for each of the studied sites. $B \pm \sigma_b$ : paleointensity result with its associated standard deviation. $VDM \pm \sigma_{VDM}$ : Virtual dipolar moment and its associated standard deviation .....	54
<b>Table 3.1.</b>	Site mean paleomagnetic directions for the high temperature components for the Eastern Udachnaya pipe ( $66.9^{\circ}\text{N}$ , $112.5^{\circ}\text{E}$ ); the Western Udachnaya pipe ( $66.9^{\circ}\text{N}$ , $112.5^{\circ}\text{E}$ ); and the host sediments and sediments from the baked contact zone .....	77
<b>Table 3.2.</b>	Paleomagnetic high temperature components mean directions for the International Pipe ( $62.4^{\circ}\text{N}$ , $113.7^{\circ}\text{E}$ ) and the Obnazhennaya Pipe ( $70.5^{\circ}\text{N}$ , $120.5^{\circ}\text{E}$ ) .....	86
<b>Table 3.3.</b>	Paleomagnetic poles and estimated ages for the studied pipes. Lat (Long): Latitude (Longitude) of the sampling sites of paleomagnetic pole. $dp/dm$ : semi-axes of the oval of 95% confidence of the paleomagnetic pole; $A_{95}$ : radius of the 95% confidence circle .....	91
<b>Table 5.1.</b>	Selected paleomagnetic poles for Siberian platform and their reliability. Selected paleomagnetic poles for Siberian platform. Formation – Geological formation name were sample was acquired, B(N) – number of sites (poles) included in the statistics, Mean Age – age in Ma. Q – classification factor due to Van der Voo (1993) (7 is the best score) Pole Lat (Long) – Paleomagnetic pole latitude (longitude), $dp/dm$ – semi-axes of the confidence cone of the paleomagnetic pole, Site Lat (Long) – sampling site coordinates. Ref – Reference.....	141

# List of Figures

<b>Figure 1.1.</b> The geomagnetic field can be described by total magnitude ( <b>H</b> ), declination (D) and inclination (I) .....	1
<b>Figure 1.2.</b> Present magnetic field of the Earth .....	2
<b>Figure 1.3.</b> Magnetization ( <b>M</b> ) versus applied field ( <b>H</b> ) for a diamagnetic material.....	3
<b>Figure 1.4.</b> Magnetization ( <b>M</b> ) versus applied field ( <b>H</b> ) for a paramagnetic material .....	4
<b>Figure 1.5.</b> a) M versus H plot for a ferromagnetic material. $M_s$ represents the magnetization of saturation. b) Categories for spin alignment. AFM: antiferromagnetism. Modified from Dunlop and Özdemir (2007) .....	5
<b>Figure 1.6.</b> a. Single domain spherical particle. Surface charges are shown by the plus and minus signs. b. Multidomain spherical particle. Region separating the domains are known as domain walls. Modified from Butler (1992).....	6
<b>Figure 1.7.</b> Magnetic flux lines produced by a geomagnetic axial dipole .....	8
<b>Figure 1.8.</b> Principles of spherical geometry are applied to determine the geomagnetic pole position P from magnetic field directions measured at S. S is the site location and has latitude $\lambda_s$ and a longitude $\phi_s$ and D and I as magnetic field mean directions.; <b>M</b> is the geomagnetic dipole that creates the observed magnetic field directions; P is the magnetic pole position at $\lambda_p$ and $\phi_p$ ; p is the magnetic colatitude; N is the geographic north pole; $\beta$ is the difference in longitude between the P and S. Modified from Tauxe (2002).....	11

**Figure 1.9.** Typical representation of a demagnetized sample. a) Orthogonal projection obtained after stepwise thermal demagnetization process. Open and solid circles represent vector endpoints projected onto the vertical and horizontal planes, respectively. In this case, the secondary component of magnetization is clearly removed after 300°C. b) Equal area projection of the same sample. Closed (open) dots represent projection onto the lower (upper) hemisphere. NRM: natural remanent magnetization ..... 12

**Figure 1.10.** Typical Arai diagram ..... 15

**Figure 1.11.** Variations of the VDM/VADM for the past a) 5 Ma, b) 300 Ma and c) 3500 Ma. Red dashed line represents the present value for Earth's dipolar moment ( $7.8 \times 10^{22} \text{ Am}^2$ ) ..... 18

**Figure 1.12.** Geomagnetic polarity time scale and Chronostratigraphy scale for the Cenozoic Era. Time scale created TimeScale Creator online by Ogg et al. (<http://www.tscreator.com/>) ..... 20

**Figure 1.13.** Apparent polar wander path for North America between 40Ma and 300Ma (Torsvik et al. 2001) ..... 22

**Figure 1.14.** a) Moving continents with a fixed pole. The resulting path of pole position is the apparent polar wander path. b) Wandering pole with respect to a fixed continent ..... 23

**Figure 2.1.** Occurrences of the Late Permian – Early Triassic magmatism in the structures of the Siberian platform and West Siberian plain (modified from Kuzmin et al., 2010). Our study areas are shown as red stars (1 – East Siberian intrusives, 2 – Noril'sk intrusion). 1 – extrusive volcanic rock exposure; 2 – intrusive volcanic rock exposure; 3 – West Siberian Rift basalts, tuffs, and tuffites; 4 – Taimyr Early Triassic traps; 5 – folded surrounding; 6 – major tectonic dislocations ..... 37

**Figure 2.2.** Results of the rock magnetic experiments for specimens from Sytikanskaya, Aikhal and Yubileinaya, respectively. Top row: thermomagnetic curves (using the VFTB) and thermal dependent magnetic susceptibility (using the Bartington susceptibility meter). The red (blue)

curves represent the heating (cooling) curves. Bottom row: magnetic hysteresis loops (using the VFTB) ..... 44

**Figure 2.3.** Modified day diagram (based on Dunlop, 2002) of the hysteresis parameters at room temperature for Sytikanskaya (triangles), Aikhal (diamonds) and Yubileinaya (circles) localities. Magnetite SD + SP and SD + MD theoretical mixing lines of Dunlop (2002) are also shown (the fainter lines) ..... 45

**Figure 2.4.** Representative vector end-point diagrams of stepwise thermal demagnetization of natural remanent magnetization for the studied localities. Demagnetization steps are in \_C, open and solid circles represent vector endpoints projected onto the vertical and horizontal planes, respectively. (a) Aikhal, (b) Sytikanskaya, (c, d) Yubileinaya, and (e) Noril'sk ..... 46

**Figure 2.5** Equal area projections of primary stable paleomagnetic directions for the eastern and northwestern specimens of the Siberian trap basalts. Closed (open) dots represent positive (negative) inclinations. The red star represents the mean direction for the studied localities. The green star corresponds to the expected mean direction calculated from the Permo-Triassic trap reference paleomagnetic poles from Pavlov et al. (2007). Circles around the directions represent the alpha 95 parameter for each sill/outcrop ..... 48

**Figure 2.6.** Typical examples of the paleointensity results for some specimens that met the three criteria listed in the methodology section. NRM vs. pTRM (left hand figures) and NRM as a function of temperature (right hand figures) are shown. Triangles on the NRM vs pTRM plots represent pTRM checks and the faint straight lines represent the temperature interval used for estimating the intensity. Squares on the NRM as a function of temperature plots represent the tail check measurements. (a) Aikhal specimen. (b) Sytikanskaya specimen. (c, d) Yubileinaya specimens. Noril'sk specimens are not presented because they did not fulfill the paleointensity selection criteria ..... 51

**Figure 3.1.** Simplified equal are projection geological map of the northeastern part of the Siberian platform (Kravchinsky et al., 2002). Sampling localities are as follows: 1 — Daldyn kimberlite pipe field (Eastern and Western

Udachnaya pipes); 2 — Malo-Botuoba kimberlite pipe field (International pipe); 3 — Kuoika kimberlite pipe field (Obnazhennaya pipe) ..... 68

**Figure 3.2.** Procedure used to determine the error in the paleomagnetic age determination. The pole and the circle of confidence are projected over the minimum distance point on the APWP. The intersection points will constrain the error in age. The final uncertainty is given by an average of the two intersection points ..... 72

**Figure 3.3.** Typical results of rock magnetic experiments for kimberlite samples from the Eastern Vostochnaya, Western Udachnaya, International, and Obnazhennaya pipes. Isothermal remanent magnetization (IRM) acquisition curves (left), Curie point thermomagnetic curves  $J_s$  (T) (center), and hysteresis loop (right).  $J$  is the isothermal remanence intensity ( $10^{-4} \text{ Am}^2 \times \text{m}^3/\text{kg}$ ),  $H$  is the magnetizing field intensity in millitesla and  $T$  is the temperature in Celsius degrees, respectively ..... 74

**Figure 3.4.** (A) Typical equal-area projections illustrating demagnetization paths during experiments, and thermal demagnetization orthogonal vector plots in-situ coordinates (Zijderveld, 1967) for samples from the Eastern Udachnaya pipe. Closed (open) symbols in orthogonal plots represent projections onto the horizontal (vertical) plane; temperature steps are indicated in Celsius degrees ( $^{\circ}\text{C}$ ). NRM: natural remanent magnetization. M/Max: ratio of the measured magnetization respect to the maximum magnetization value (in amperes per meter). (B) Equal-area projections of site-mean directions of high temperature (HTC) component, with circles of 95% confidence. Open symbols: upward inclinations. Star: mean formation direction D: declination, I: inclination, k: precision parameter,  $\alpha_{95}$ : radius of the 95% probability confidence circle, N: number of specimens at site level..... 76

**Figure 3.5.** (A) Typical equal-area projections, orthogonal vector plots and remanence intensity decay plots for the host sediments near the kimberlite pipe Udachnaya. Plotting conventions as in Figure 3.4A. (B) Equal-area projections of the low temperature component (LTC) and high temperature component (HTC) for the host sediments. Plotting conventions as in Figure 3.4B, except n: number of specimens at sample level ..... 79

**Figure 3.6.** (A) Typical equal-area projections, orthogonal vector plots and remanence intensity decay plots for the Western Udachnaya pipe. Plotting

conventions as in Figure 3.4A. (B) Equal-area projections of the high temperature component (HTC) for the pipe. Plotting conventions as in Figure 3.4B..... 81

**Figure 3.7.** (A) Typical equal-area projections, orthogonal vector plots and remanence intensity decay plots for the remagnetized sediments from the baked contact zone. Plotting conventions as in Figure 3.4A. (B) Equal-area projections of high temperature component (HTC) for the remagnetized sediments. Plotting conventions as in Figure 3.4B. ..... 83

**Figure 3.8.** (A) Typical equal-area projections, orthogonal vector plots and remanence intensity decay plots for the International pipe. Plotting conventions as in Figure 3.4A. (B) Equal-area projections of the low temperature component (LTC) and high temperature component (HTC) for the pipe. Plotting conventions as in Figure 3.4B, except n: number of specimens at sample level ..... 85

**Figure 3.9.** (A) Typical equal-area projections, orthogonal vector plots and remanence intensity decay plots for the Obnazhennaya kimberlite pipe. Plotting conventions as in Figure 3.4A. (B) Equal-area projections of the high temperature component (HTC) for the pipe. Plotting conventions as in Figure 3.4B..... 87

**Figure 3.10.** Equal-area projections of site-mean directions of high temperature (HTC) components for each studied pipe, with circles of 95% confidence. Open (close) symbols: upward (downward) inclinations. Star: mean formation direction. D: declination, I: inclination, k: precision parameter,  $\alpha_{95}$ : radius of the 95% probability confidence circle, N: number of specimens at site level ..... 89

**Figure 3.11.** Equal area projection of paleomagnetic poles from kimberlites pipes and sediments (diamonds) with ellipses of 95% confidence (shadow areas). Triangles represent the Siberian platform poles between 430 and 470 Myr with their corresponding 95% confidence ellipses (dashed ellipses). Circles represent the Siberian APWP of Cocks and Torsvik (2007) interpolated to 2 Myr intervals and the European APWP of Besse and Courtillot (2002) between 130 and 200 Ma interpolated to 2 Myr intervals. Obn: Obnazhennay pipe paleomagnetic pole; Int: International pipe paleomagnetic poles; EU: Eastern Udachnnaya pipe paleomagnetic pole; BCT: baked contact test paleomagnetic pole; Sed: sediments near the

Eastern Udachnya kimberlite pipe paleomagnetic pole. The Western Udachnaya paleomagnetic pole is not included in this figure ..... 92

**Figure 4.1.** Study area. Left: approximate distribution of Campanian marine deposits of the Western Interior Seaway (after Kauffman (1984) and Couillard and Irving (1975)). Right: locations of studied cores and localities referenced in the text. 1. Amoco B-1 Youngstown (ABY) well (51.61N, 111.05W). 2. ARC Brooks/Princess (ABP) well (50.66N, 111.55W). 3. Nexen Medhat (NM) well (50.21N, 110.13W). Star marks location of Writing-On-Stone Provincial Park ..... 104

**Figure 4.2.** Results from thermal-dependent magnetic susceptibility (MS, left hand side) and isothermal remnant magnetization (IRM, right hand side) experiments for Amoco B-1 Youngstown and Nexen Medhat cores ..... 112

**Figure 4.3.** Equal-area projections, demagnetization orthogonal diagrams (Zijderveld, 1967) and intensity decay plots for the studied cores. Open (close) symbols in orthogonal plots represent projections onto the vertical (horizontal) plane. NRM: natural remanent magnetization ..... 115

**Figure 4.4.** Inclination histograms for ABY, ABP and NM cores. The expected inclinations for each site are marked by the black straight lines ( $\pm 65.4^\circ$ ,  $\pm 64.8^\circ$ ,  $\pm 64.3^\circ$ , respectively) ..... 116

**Figure 4.5.** Inclination profiles and polarization zonations numbered from the top of each core. Close (open) diamonds represent core sections with inclination higher (lower) than  $\pm 30^\circ$ . Open circles represent low quality core sections. Dashed sections of the inclination profile represent core segments that were not considered as polarization zones. Subsea depth (m) with respect to ground elevation at well is shown. Error bars represent the standard deviation of the average inclination per core segment ..... 118

**Figure 4.6.** Time correlation between the studied magnetostratigraphic sections. Lithostratigraphic units are also illustrated for each location. Green lines represent the C33n-C33r and C33r-C34 boundaries in each of the studied cores as well as those established by Leahy and Lerbekmo (1995) in the Milk River Valley. Chron boundaries are correlated to the Geomagnetic Polarity Timescale (GPTS) (Ogg and Smith, 2004). Black lines present our correlation of microchrons. T1-T5 denote established timelines referenced

in the text. Red short-dashed line represent the base of the Pakowki Formation, M1. Small question marks represent the Pakowki transgression (refer to manuscript for discussion). Large question mark represents the ambiguity to determine the C33n-C33r. Inclination profile plotting convention as in Figure 4.5, error bars are not illustrated..... 121

**Figure 4.7.** Correlation between composed magnetostratigraphic profile of the studied cores and Upper Cretaceous cores. Shade area represents our interpretation. Black arrows represent tiny wiggles *a* and *b* of Boulingand et al. (2006). 1. This study. 2. Leahy and Lerbeckmo (1995). 3. Montgomery et al. (1998). 4. He et al. (2012), second interpretation of their core. 5. Boulingand et al. (2006) ..... 123

**Figure 5.1.** Simplified geological structure of Siberia and surrounding regions modified from Kravchinsky et al. (2002). 1: Precambrian shields; 2: Riphean and Palaeozoic sediment cover; 3: Permo-Triassic traps; 4: Viluy palaeorift; 5: edge of Precambrian platform; 6: Middle–Late Palaeozoic border of Siberian block. Names of blocks: TMn: Tuva-Mongolian, Jun: Jungar ; 7: paleomagnetic study sampling localities ..... 140

**Figure 5.2.** Selected paleomagnetic poles with 95% confidence ovals for the Siberian APWP construction. Left hand side plot represents the selected poles without rotation for Wenlock to Emsian times. Right hand side corrected poles respect an Euler pole of latitude 60°N, longitude 120°E and angle of 13°. Poles from 75 Ma to 200 Ma are not presented ..... 141

**Figure 5.3.** Comparison between European APWPs constrained with SVD least squares method using different set of polynomials. Circles: polynomial function with  $t^k$  set of polynomials. Crosses: rational functions as a set of polynomials. The 95% confidence circles are not shown for clarity. Number of polynomials is the same ( $m=10$ ) for both curves. The individual poles are taken from the Table 1b of Torsvik et al. (2001). Ages are in Ma..... 150

**Figure 5.4.** Comparison between European APWPs constructed with the SVD least squares method using different number of polynomials. The 95% confidence circles are not shown for clarity. Number of polynomials is 6 for the blue curve (squares), and 10 for the purple path (triangles). Red crosses and path is the APWP of Europe from Torsvik et al. (2001) (their Table 2). Individual paleomagnetic poles from Table 1b of Torsvik et al.

(2001) are shown as green circles, nearby numbers indicate the ages (in Ma) of the individual poles. Black arrow marks the European APWP Mesozoic cusp reported by Torsvik et al. (2001)..... 151

**Figure 5.5.** Comparison between European APWPs constructed with the smoothing spline method using different smoothing parameter  $S$  (squares  $S=15$  and triangles  $S=30$ ). The 95% confidence circles are not shown for clarity. The APW paths are plotted in 10 Myr step poles. Red crosses and path is the APWP of Europe from Torsvik et al. (2001) (their Table 2). Individual paleomagnetic poles from Table 1b of Torsvik et al. (2001) are shown as green circles, nearby numbers indicate the ages (in Ma) of the individual poles. Black arrow marks the European APWP Mesozoic cusp reported by Torsvik et al. (2001)..... 152

**Figure 5.6.** Comparison between Siberian APWP's for 200 Ma to 538.5Ma (Table 5.1). Left hand side: APWP's created using least square method solve through SVD. Squares:  $m=5$ . Triangles:  $m=6$ . Downward triangles:  $m=7$ . Diamonds:  $m=10$ . Right hand side: APWPs constructed with cubic smoothing method. Squares:  $S=10$ . Crosses:  $S=20$ . Triangles:  $S=30$ . Diamonds:  $S=40$ . Right hand side: APWP's created using cubic smoothing. Squares:  $S=10$ . Crosses:  $S=20$ . Triangles:  $S=30$ . Diamonds:  $S=40$ . Siberian poles are shown as black circles and their corresponding A95 circle of confidence is shown as a grey shaded area. The 95% confidence circles for the APWP's are not shown for clarity. A 10 Ma windows was used for the APWP's construction ..... 154

**Figure 5.7.** a) Best fitting lines obtained using LSM using SVD ( $m=6$ ) and cubic smoothing ( $S= 30$ ) techniques and Cocks and Torsvik (2007) Siberian APWP's. b) Latitudinal drift for the three paths presented in a) ..... 155

**Figure 5.8.** Left hand side: APWP constructed with SVD least squares method. Right hand side, APWP constructed with smoothing method. Comparison paths including Metelkin et al. (2010) Siberian poles vs. European poles from Torsvik et al. (2001) during the Mesozoic are shown. Individual paleomagnetic poles for this interval are not shown. Green squares/diamonds: Metelkin's poles and Siberian poles; purple triangles (up/down): European and Siberian poles ..... 156

**Figure 5.9.** A: Latitudinal drift for a reference point at 65 N and 105 E. B: APWP migration velocity. Both plots where based on SVD least squares APWP path from Figure 5.8 ..... 158

# Chapter 1

## Introduction

### 1.1 Geomagnetic Principles

Electric currents in the liquid outer core of the Earth generate the vast majority of its magnetic field, which can be described by a magnitude  $H$  and a direction, defined by two angles: declination and inclination. The declination  $D$  is the angle between the geographic north and the horizontal component, ranging from  $0^\circ$  to  $360^\circ$ , positive clockwise. The inclination  $I$  is the angle at which the magnetic vector dips below the horizontal, ranging from  $-90^\circ$  to  $+90^\circ$ , defined as positive downward (Figure 1.1). The relation between the Cartesian ( $x$ ,  $y$  and  $z$ ) and spherical polar coordinates ( $H$ ,  $D$  and  $I$ ) of the field is given by:

$$x = H \cos I \cos D; y = H \cos I \sin D; z = H \sin I; \quad (1.1)$$

and

$$H^2 = x^2 + y^2 + z^2; \quad D = \tan^{-1} \left( \frac{x}{y} \right); \quad I = \tan^{-1} \left( \frac{z}{\sqrt{x^2+y^2}} \right). \quad (1.2)$$

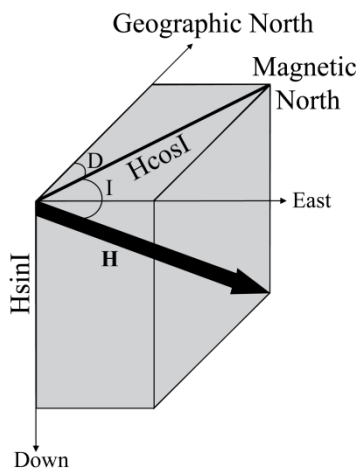


**Figure 1.1** The geomagnetic field can be described by total magnitude ( $H$ ), declination ( $D$ ) and inclination ( $I$ ).

The Earth's present magnetic field is mainly internal in origin, and at the surface, it can be well approximated by a dipole, which is  $11.5^\circ$  inclined from the rotation axis (Figure 1.2). The magnitude of the dipolar moment is  $7.8 \times 10^{22} \text{ Am}^2$  (Finlay et al. 2010).

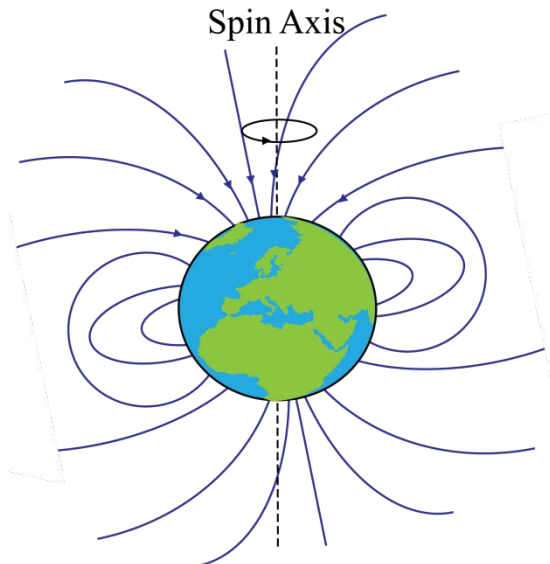


**Figure 1.2.** Present magnetic field of the Earth.

### 1.1.1 Magnetic Properties of Solids

Moving electric charges create magnetic fields. In solids, magnetism is produced by the magnetic moment of the atoms, which is related to the orbital movements and spin of the electrons. Some materials are able to carry magnetization only in the presence of an external magnetic field. This phenomenon is known as induced magnetization. Others stay magnetized in the absence of external magnetic fields, thereby maintaining a remanent magnetization.

Whether a material exhibits induced or remanent magnetization depends on the nature of its response to an externally applied magnetic field. The relationship between the induced magnetization and the applied magnetic field is given by:

$$\mathbf{M} = \chi \mathbf{H}, \quad (1.3)$$

where  $\mathbf{M}$  is the magnetization,  $\mathbf{H}$  is the applied magnetic field and  $\chi$  is a proportionality factor, called the magnetic susceptibility. This relationship can be complex (it depends on crystal shape, lattice structure, state of stress, amongst others) and in general  $\chi$  can be anisotropic and nonlinear (Butler, 1992; Tauxe, 2002). There are three different magnetic properties observed in materials: diamagnetism, paramagnetism and ferromagnetism.

### Diamagnetism

Diamagnetism is created as a result of the changes on the orbital motions of the electrons when a magnetic Lorentz force is added to the electrostatic Coulomb force (Dunlop and Özdemir, 2007). The magnetic susceptibility is negative, linearly dependent on the applied field and temperature independent (Figure 1.3). Although this effect is observed in all types of materials, it is relatively weak compared to the other types of magnetism.

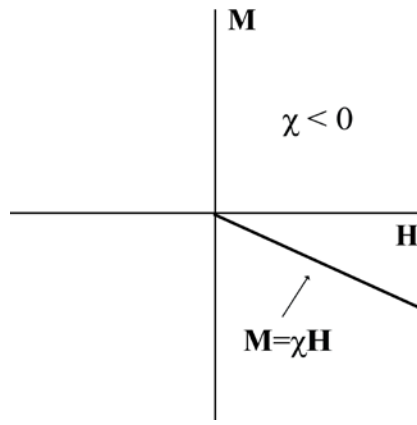


**Figure 1.3.** Magnetization ( $\mathbf{M}$ ) versus applied field ( $\mathbf{H}$ ) for a diamagnetic material.

### Paramagnetism

This is a property created by the permanent dipolar moments of atoms; formed when the presence of unpaired electrons are aligned with the applied field,  $\mathbf{H}$ . In this case the magnetic moments do not interact.  $\mathbf{M}$  is linearly proportional to  $\mathbf{H}$  and tends to zero when the magnetization field is removed, similar to diamagnetic materials (Figure 1.4). Paramagnetic susceptibility is positive, larger than

diamagnetism, and inversely proportional to temperature (a feature known as Curie's law of paramagnetism). Paramagnetism becomes of great importance at very low temperatures and in studies of anisotropy of magnetic susceptibility (Tauxe, 2002; Dunlop and Özdemir, 2007).

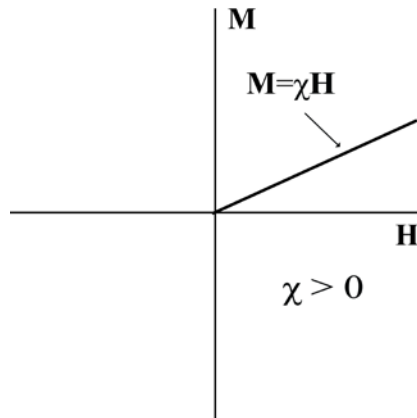


**Figure 1.4.** Magnetization ( $\mathbf{M}$ ) versus applied field ( $\mathbf{H}$ ) for a paramagnetic material.

## Ferromagnetism

This property is produced by the strong interaction of the atomic magnetic moments of the electrons in the material. It is characterized by a large magnetic susceptibility and by the ability to maintain magnetization in zero applied magnetic fields (a magnetic field referred to as a remanent magnetization). During the demagnetization process, the magnetization does not return to zero but retains information of the applied field. This phenomenon is demonstrated by hysteresis loops in plots of  $M$  versus  $H$  (see Figure 1.5a for example). This characteristic of ferromagnetic material implies that the relation between the induced magnetization and the applied magnetic field is no longer linear and the magnetic susceptibility presents complicated characteristic. Hysteresis is created due to the presence of magnetic domains formed by groups of paired spins.

The interaction of the electronic spins is determined by the exchange energy (related to the quantum mechanical characteristics of the atoms); spins can be parallel or anti-parallel, depending on the crystal structure of the material. In fact,

there are three categories of spin alignment: ferromagnetism, antiferromagnetism and ferrimagnetism (Figure 1.5b).

In ferromagnetism, the exchange energy is minimized when the spins are parallel to each other. When the spins are completely antiparallel so that no net magnetization is observed, the material exhibits antiferromagnetism. If the spins are antiparallel, but the magnitude of the moments in each direction are not equal, a resulting net moment is observed and the magnetization of the material is characterized by ferrimagnetism. The spin ordering is temperature dependent in ferromagnetic and ferrimagnetic materials, as the temperature increases, the scatter in the spin directions also increases. Above a certain temperature, known as the Curie temperature, the material will become paramagnetic. In some cases (e.g. hematite), the spin of antiferromagnetic materials are not perfectly antiparallel to each other ( i.e are canted by a few degrees). This feature creates a weak net magnetic moment that varies weakly with temperature (Tauxe, 2002).

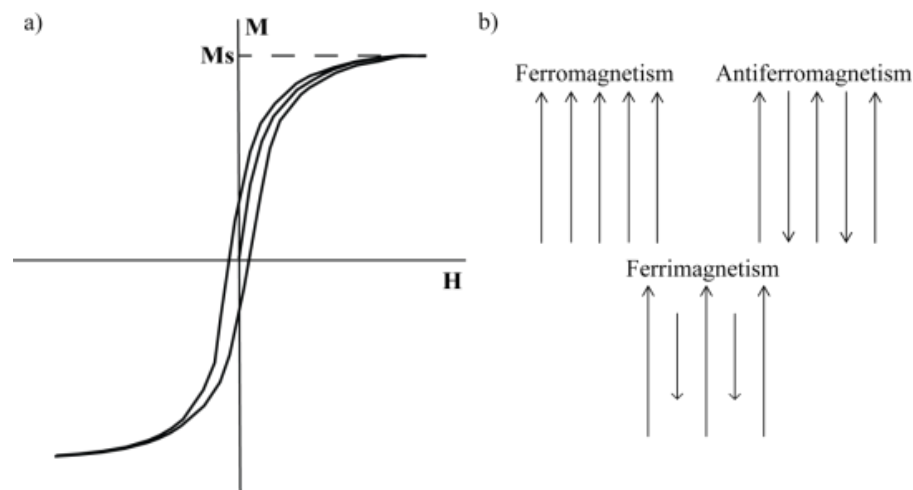


**Figure 1.5.** a)  $M$  versus  $H$  plot for a ferromagnetic material.  $M_s$  represents the magnetization of saturation. b) Categories for spin alignment. AFM: antiferromagnetism. Modified from Dunlop and Özdemir (2007).

### 1.1.2 Rock Magnetism

Rocks are heterogeneous materials, and therefore exhibit complex magnetization properties. Their magnetization results from a mixture of ferromagnetic,

paramagnetic and diamagnetic particles. A magnetic grain can be composed of one or more magnetic domains (Figure 1.6). Magnetic domains are formed as a result of the magnetic energy created by the charge distribution at the surface of the particle. The magnetic energy increases with grain volume. Formation of magnetic domain decreases the magnetic energy as this reduces the associated magnetic field (Figure 1.6b). If the grain is sufficiently small, it will consist of a single domain (Figure 1.6a). In zero magnetic field, the domain will be aligned with respect to a preferred axis that will depend on the shape or the crystalline anisotropy of the grain (Cox and Doell, 1960; Buttler, 1992). If a magnetic field is applied, the grain will align with it, but if the field is not strong enough to counteract the magnetic energy barriers, the grain will return to its original position after the field is removed, i.e., the acquired field is reversible. This is typical of induced magnetization.

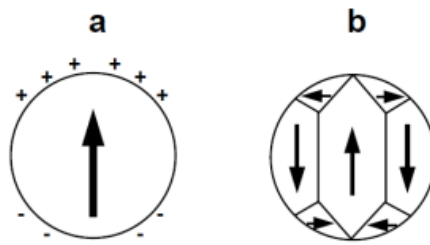


**Figure 1.6.** a. Single domain spherical particle. Surface charges are shown by the plus and minus signs. b. Multidomain spherical particle. Region separating the domains are known as domain walls. Modified from Butler (1992).

If the applied magnetic field is higher than a critical value (known as the coercive force), the magnetic particle will cross the magnetic energy barrier and after the applied magnetic field is removed, the magnetic vector remain in the new direction, acquiring a remanent magnetization (Tauxe, 2002). In 1955, Louis Néel developed the theory that explains the acquisition of remanent magnetization by single domain particles. Pseudo-single and multidomain grains follow similar principles.

There are a number of different natural processes that permit different rock types to acquire remanent magnetization. In general, rocks collected from geological

formations carry a natural remanent magnetization (NRM), which is usually composed of several components denoted as either primary or secondary, depending on whether the remanence was acquired during or after the rock formation, respectively. Table 1.1 summarizes the principal characteristics of primary and secondary magnetizations found in nature.

**Table 1.1.** Summary of the remanent magnetizations observed in nature.

Component	Remanent Magnetization	Characteristics
<i>Primary</i>	Thermal (TRM)	Remanent magnetization acquired during cooling from temperatures above the Curie temperature. Type of remanent magnetization acquired by igneous rocks. Is stable over geological times. Orientation of the particles tends to be parallel to the direction of the applied field. Intensity of thermal remanence is linearly related with the intensity of the applied field.
	Detrital (DRM)	Also known as depositional remanent magnetization. Is typical of sedimentary rocks and is usually acquired when magnetic grains settle in water reservoirs. The grain will align with the magnetic field, a feature that is maintained during consolidation imparting a remanent magnetization to the sediment.
	Chemical (CRM)	Usually observed in sedimentary rocks. Created as a result of chemical changes to ferromagnetic grains by changes in the preexisting minerals or precipitation on ferromagnetic minerals. Can be considered as a secondary component of the NRM if it is acquired long after deposition.
<i>Secondary</i>	Viscous (VRM)	Gradually acquired during long exposures of weak magnetic fields. Remanent magnetization acquired long after the formation of the rock.
	Isothermal (IRM)	Acquired by ferromagnetic particles with coercive force less than the applied field at constant temperature. Natural samples obtain IRM as a result of short term exposure to strong magnetic fields, such as ones created by ground strikes of lightning.

## 1.2 Earth's Ancient Magnetic Field

Understanding the Earth's ancient geomagnetic field is fundamental to comprehending how it will behave in the future, and so Earth's evolution through time. Paleomagnetism provides the tools to study the magnetic properties of rocks, and therefore has broad application to the study of the characteristics of the ancient magnetic field, geochronology, sedimentology and tectonics.

### 1.2.1 Paleomagnetic Principles

The geocentric axial dipole (GAD) model, assumes that Earth's time-averaged magnetic field is produced by a single magnetic dipole that is aligned with the rotation axis at the center of the planet (Butler 1992). It is fundamental for the paleomagnetic applications. In addition, it is also essential to have a clear understanding of how material acquires and conserves information of the ancient magnetic field.

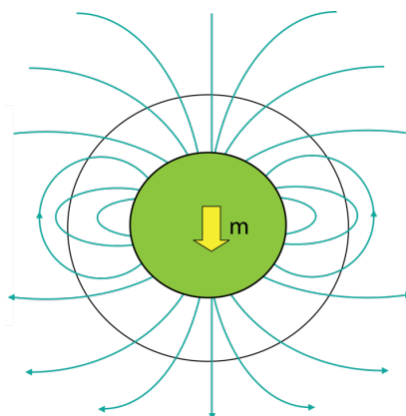


**Figure 1.7.** Magnetic flux lines produced by a geocentric axial dipole.

The best dipole fit to the present magnetic field is inclined  $11.5^\circ$  with respect to the rotation axis of the Earth. The points where the magnetic field of the best fit dipole intersects the surface of the planet are known as geomagnetic poles. Moreover, points where the magnetic field is vertical ( $I=\pm 90^\circ$ ) are called magnetic poles.

In the GAD model the inclination of the magnetic field can be related to the latitude ( $\lambda$ ) by the *dipole equation*:

$$2 \tan \lambda = \tan I, \quad (1.4)$$

which is one of the most important relations in paleomagnetism. The dipole equation implies that if the GAD model is assumed for different geological times, the paleomagnetic latitude can be derived from the mean magnetic inclination.

Furthermore, the magnitude of the field will also depend on the paleolatitude

$$H = \frac{M}{r^3} (1 + 3\sin^2 \lambda)^{1/2}, \quad (1.5)$$

where M is the dipole moment of the GAD and r is the radius of the Earth (McElhinny, 1973; Tauxe, 2002).

Although a dipolar model represents a convenient way to describe the magnetic field, it is important to notice that non-dipolar elements of the field also exist and can affect the paleomagnetic data. For example, magnetic field variations with periods between 1yr to  $10^5$  yr, known as *geomagnetic secular variations*, are considered to be due to variations in strength and direction of the non-dipolar and dipolar elements of the magnetic field (McElhinny, 1973).

### 1.2.2. Paleomagnetic Methods

The objective of paleomagnetic measurements is to isolate the different components of the magnetization, identify their origin and relate the measured magnetic inclination and declination with the position of the ancient geomagnetic pole. The pole position is defined as the geographic location where the projection of the magnetic dipole axis intersects the Earth's surface (Figure 1.8; McElhinny, 1973; Butler, 1992). If the position between the ancient and the present magnetic pole differ, this implied that either the magnetic pole has moved through

geological time, or the poles have remained stationary (aligned with Earth rotation axis) and the samples location has moved. It is widely accepted now that the wandering of the magnetic poles with respect to the geographic poles is unlikely, as all theoretical models predict a dominant dipole parallel to the Earth's rotation axis average over time; therefore, paleomagnetic measurements are a useful tool to describe continental motion (Kearey et al. 2009), as well as polar motion (i.e. changes in the direction of axis of Earth's rotation).

Spherical geometry can be used to determine a pole position (see Figure 1.8). The first step in the calculation is to determine the magnetic colatitude,  $p$ , which is the angular distance from the site (S) to the pole (P), and can be determined from equation 1.4:

$$p = \tan^{-1} \left( \frac{2}{\tan I} \right). \quad (1.6)$$

The paleolatitude can be determined using the law of cosines and is given by:

$$\lambda_p = \sin^{-1} (\sin \lambda_s \cos p + \cos \lambda_s \sin p \cos D), \quad (1.7)$$

where  $\lambda_p$  is the latitude of the pole,  $\lambda_s$  is the latitude of the site,  $p$  is the colatitudes and  $D$  is the declination.  $\beta$ , the longitudinal difference between pole and the site longitudes is defined positive toward the East and can be determined using the Law of Sines:

$$\beta = \sin^{-1} \left( \frac{\sin p \sin D}{\cos \lambda_p} \right). \quad (1.8)$$

If  $\cos p \geq \sin \lambda_s \sin \lambda_p$  the pole longitude will be  $\varphi_p = \varphi_s + \beta$ . If  $\cos p < \sin \lambda_s \sin \lambda_p$  the pole longitude will be given by  $\varphi_p = \varphi_s + 180 - \beta$ .

Sign conventions define positive latitude in the northern hemisphere and negative latitude in the southern hemisphere, whilst longitudes east of the Greenwich Meridian are positive and west of the meridian are negative (Butler, 1992).

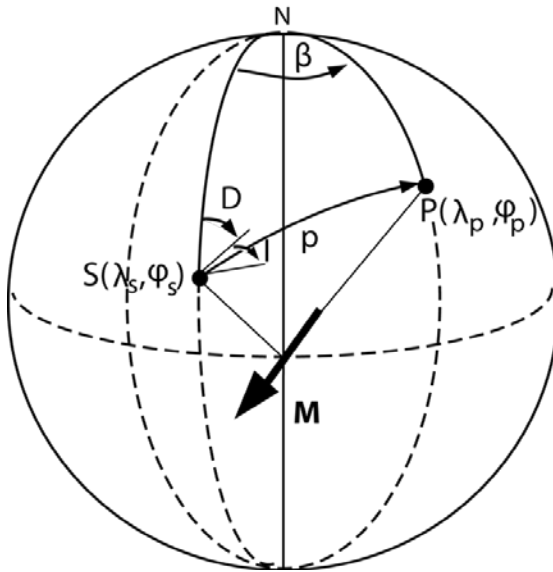


**Figure 1.8.** Principles of spherical geometry are applied to determine the geomagnetic pole position  $P$  from magnetic field directions measured at  $S$ .  $S$  is the site location and has latitude  $\lambda_s$  and a longitude  $\varphi_s$  and  $D$  and  $I$  are the magnetic field mean directions.;  $M$  is the geomagnetic dipole that creates the observed magnetic field directions;  $P$  is the magnetic pole position at  $\lambda_p$  and  $\varphi_p$ ;  $p$  is the magnetic colatitude;  $N$  is the geographic north pole;  $\beta$  is the angular difference in longitude between the  $P$  and  $S$ . Modified from Tauxe (2002).

If the pole calculation is done only for one observation of the direction of the geomagnetic field, the determined pole is called a *virtual geomagnetic pole* (VGP). VGP's can only provide information of the ancient magnetic field at a single location and point in time. This type of pole is strongly influenced by secular variations. If the pole calculation is done with a data set that averages the secular variation, the pole is called a *paleomagnetic pole*. It can be calculated from the average of the paleomagnetic field directions or by the average of the VGP's (McElhinny, 1973; Butler, 1992).

To determine the directions of the magnetic components acquired by the rocks, different laboratory demagnetization processes are applied. Alternating field (AF) is based on the assumption that the secondary magnetization will have low coercivity and uses increasing magnetic field steps. Thermal demagnetization uses progressive heating steps that randomize the magnetic components with low coercive force. After each heating or AF step, the magnetization of the samples is measured in a magnetometer. During the demagnetization, the remanent

magnetization will change until the most stable component is isolated and the vector will tend to zero in an orthogonal projection representation (Zijderveld diagrams, Zijderveld, 1967; Figure 1.9). From the orthogonal projection, a principal component analysis (PCA, Kirschvink, 1980) is done, and the mean direction of the magnetic vector for each sample is determined.

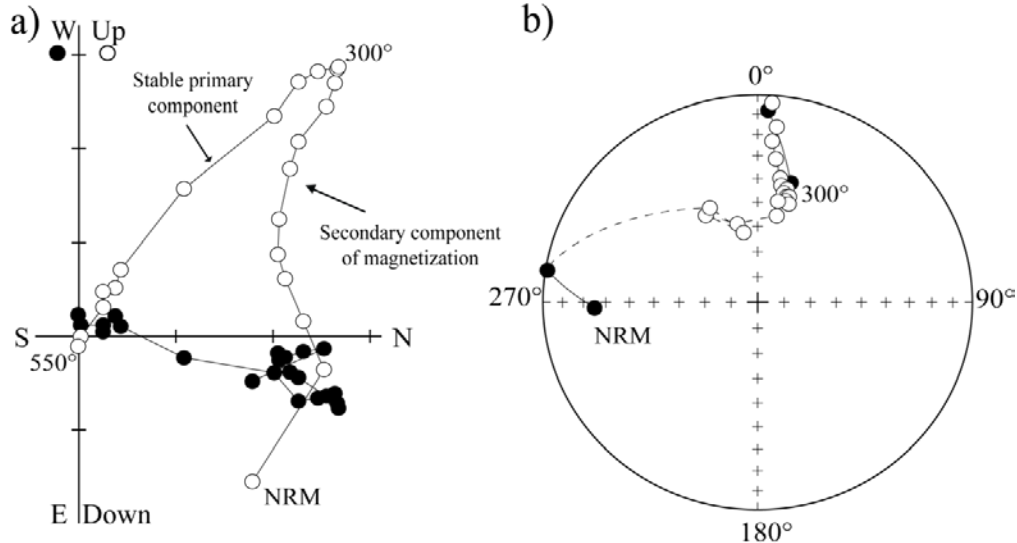


**Figure 1.9.** Typical representations of a demagnetized sample (Blanco et al. 2013). a) Orthogonal projection obtained after stepwise thermal demagnetization process. Open and solid circles represent vector endpoints projected onto the vertical and horizontal planes, respectively. In this case, the secondary component of magnetization is clearly removed after 300°C. b) Equal area projection of the same sample. Closed (open) dots represent projection onto the lower (upper) hemisphere. NRM: natural remanent magnetization.

There are several methods to guarantee the quality of the acquired paleomagnetic field. On the one hand, field-acquiring techniques are fundamental to determining the moment of acquisition of the primary paleomagnetic field (fold test) or the possible secondary paleomagnetic field overprints (conglomerate test, baked contact test). Furthermore, to average the secular variation and noise, several samples from different sites are required. On the other hand, Fisher's statistical test (Fisher, 1953) is used to quantify the confidence intervals with respect to the mean direction calculation. This test allows one to estimate the dispersion of the points ( $k$ , known as the precision parameter) and the semi-angle cone of

confidence around the observed mean ( $\alpha_{95}$ ), which implies that the real mean of the direction lies with 95% probability within the cone (Buttler, 1992).

### 1.2.3. Paleointensity and Virtual Dipolar Moment

A complete understanding of the variations of the geomagnetic field through time requires knowledge of its direction and intensity. Paleointensity studies rely on the understanding of physical processes that cause rocks to acquire magnetization, as well as the ability to duplicate these processes at the laboratory level. Depending on the type of acquired remanent magnetization, thermal or detrital, absolute or relative measurements of the intensity of the magnetic field can be done, respectively. For low intensity fields, as with the Earth, the NRM of the rock will be approximately proportional to the applied field (Thellier and Thellier, 1959):

$$M_{NRM} = \vartheta H_{anc}, \quad (1.9)$$

where  $\vartheta$  is a proportionality constant.  $\vartheta$  can be determined by applying to the same sample a new remanent magnetization ( $M_{lab}$ ) in a known magnetic field,  $H_{lab}$ :

$$M_{lab} = \vartheta H_{lab}. \quad (1.10)$$

If the laboratory remanence has the same proportionality constant as the ancient one, we can relate the ancient magnetization with the applied laboratory field as:

$$H_{anc} = \frac{M_{NRM}}{M_{lab}} H_{lab}. \quad (1.11)$$

This relation implies that paleointensity can be easily determined by measuring the ancient NRM, and  $\vartheta$  can then be resolved by giving the rock a laboratory magnetization in a known magnetic field. The ratio of the two remanences multiplied by the know laboratory field would give the ancient magnetic field.

However, in practice, paleointensity determination is very difficult. The ferromagnetic particles carrying the magnetic information might suffer alterations during time and/or the experimental methods used to determine the remanent magnetization may produce physical or chemical changes in the rock, affecting the nature of the proportionality constant  $\vartheta$  (Tauxe et al. 2008).

Paleointensity experiments for rocks carrying TRM usually involve a series of heating steps to progressively higher temperatures. The idea is to replace the natural remanence of the sample with partial thermal remanent magnetization (pTRM) acquired in a known field. Three assumptions are required to perform the experiment and are known as: *Law of Independence*, *Law of Additivity*, and the *Law of Reciprocity* (Tauxe 2002):

- *Law of Independence*: The pTRM acquired by cooling between any two temperature steps are independent of those acquired between any other two temperatures.
- *Law of Additivity*: The total TRM is the sum of all the independent pTRMs
- *Law of Reciprocity*: A magnetization acquired by cooling from a given temperature is entirely replaced by re-heating to the same temperature.

Different methods can be used to replace the NRM with pTRM. The original technique was developed by Thellier (1941), and consists of heating up the sample to a given temperature  $T_1$  and then cooling it down in a field  $H_{lab}$ . The magnetic remanence will be given by what it is left of the NRM and the new pTRM:

$$M_1 = M_{NRM} + M_{pTRM}. \quad (1.12)$$

The second step consists of heating up the sample and cooling it in a field  $-H_{lab}$ . In this case, the measure remanence will be:

$$M_2 = M_{NRM} - M_{pTRM}. \quad (1.13)$$

Vector subtraction gives the value for the NRM remaining at each temperature step and the pTRM gained. This process is repeated at incremental heating steps until the Curie point is reached. To determine the final field, the NRM lost is plotted as a function of the acquired pTRM, in an “Arai” plot (Nagata, 1963; Figure 1.10). If no alteration occurs during the experiments and the remanence is carried by single domain particles, the relation between NRM lost and the pTRM gained is linear, the product of the slope with the laboratory applied field giving the ancient intensity.

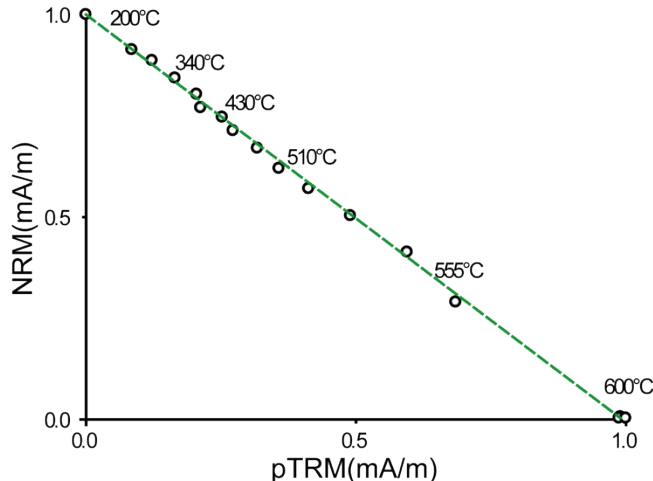


**Figure 1.10.** Typical Arai diagram.

With the development of more sensitive magnetometers, variations of the original method have been developed. In the most common variation (Coe, 1967), the first heating step is done in zero field, allowing the direct measurement of the NRM remaining in each step. In this case:

$$M_1 = M_{NRM}, \quad (1.14)$$

and

$$M_2 = M_{NRM} + M_{pTRM}, \quad (1.15)$$

$M_{pTRM}$  in this zero-field/in-field (ZI) method is calculated by vector subtraction. Furthermore, some variations (Aitken et al., 1988) of this technique, apply the first heating step in the laboratory field and the second one in zero field (in-field/zero-field, IZ).

The most powerful feature of this type of experimental method is the possibility to perform “checks” to determine if the capacity of the specimens to carry remanent magnetization has changed. The different checks that are usually applied in paleointensity studies are summarized in Table 1.2.

**Table 1.2.** Summary of the different checks applied in thermal paleointensity measurements.

Name	Characteristic
pTRM check	Consists of performing a lower temperature in-field cooling step to monitor alteration during the laboratory treatment. Differences between the first and second $M_{pTRM}$ at a given temperature indicate changes in the capacity of the specimen to acquire thermal remanence.
Multidomain (MD) tail check	After double (zero-field/in-field) heating to $T_i$ , a third heating to $T_i$ in zero laboratory field is applied. The tail check is the difference between the remanent magnetization of the two zero-field heatings (Riisager and Riisager, 2001) and provides information with respect to the presence of MD particles.
Additivity check	To determine if the law of additivity is fulfilled, a pTRM( $T_i, T_0$ ) is demagnetized up to $T_k$ ( $k < i$ ) and the remaining remanence is measured. In the case of pure single domain particles the measured remanence should be equal to the difference between $M_{pTRM}(T_i, T_0)$ and $M_{pTRM}(T_k, T_0)$ . If the remanence is carried by MD particles the measured remanence will be less than the difference (Krásá et al. 2003)

Defining the accuracy of experimental results is not an easy task and several statistical parameters have been defined to determine the goodness of fit (Coe et al. 1978; Selkin and Tauxe 2000; Tauxe 2002). Even though the paleointensity community has made a great effort to standardize the quality analysis, presently there is not a specific protocol that can be used to ensure the goodness of fit from the measurements. Table 1.3 summarizes the most important parameters. Usually the success rate of paleointensity experiments does not exceed 10–20% (Valet, 2003).

**Table 1.3** Statistical parameters to determine the goodness of the paleointensity determination.

Parameter	Name	Definition	Reference
B	Scatter parameter	Standard error of the slope over the slope of the best fitting line	Coe et al. 1978
f	Fraction of NRM	Fraction of the total extrapolated NRM spanned by the chosen segment of the NRM-TRM plot	Coe et al. 1978
q	Quality Factor	Combines several parameters	Coe et al. 1978
MAD	Maximum angle of deviation	Parameter used to monitor directional aspect of the demagnetized vector; is a qualitative indication of scatter about the principal component of demagnetization	Kirschvink 1980
DRAT	Difference ratio	Used to determine the quality of the pTRM checks; is determined by the normalization of the difference between repeated pTRM steps by the length of the selected NRM-TRM segment.	Selkin and Tauxe, 2000
DEV	Deviation of the pTRM check	The deviation expressed in percentage after normalizing the DEV value, defined as $DEV = \sum (p\text{TRM} - p\text{TRM}_{\text{check}})$ , with respect to the length of the TRM segment.	Valet et al. 1996

In order to compare geomagnetic intensity in different locations is often convenient to express the paleointensity values in terms of an equivalent geocentric dipole moment, which has been produced by the observed intensity at a specific paleolatitude, known as virtual dipole moment (VDM). If the inclination is known, a virtual dipolar moment can be determined:

$$VDM = \frac{4\pi r^3}{\mu_0} H_{anc} (1 + 3\cos^2 \theta_m)^{-1/2}, \quad (1.16)$$

where  $r$  is the radius of the Earth,  $\mu_0$  is the permeability of free space ( $4\pi \times 10^{-7}$  N/A<sup>2</sup>),  $H_{anc}$  is the paleointensity value and  $\theta_m$  is the magnetic co-latitude. Sometimes only information with respect to the site co-latitude is known (as opposed to the magnetic co-latitude), thus giving a virtual axial dipole moment (VADM).

The variations of Earth's VDM can be observed through the present international association of geomagnetism and aeronomy (IAGA) absolute paleointensity database (PINT, Biggins et al. 2010). Figure 1.11 presents the VDM and the

VADM versus time variation for the past 5 Ma, 300 Ma and 3500 Ma. For the past 800 kyr a mean value of  $5.9 \times 10^{22} \text{ Am}^2$  is estimated for the global dipole moments (Constable, 2005).

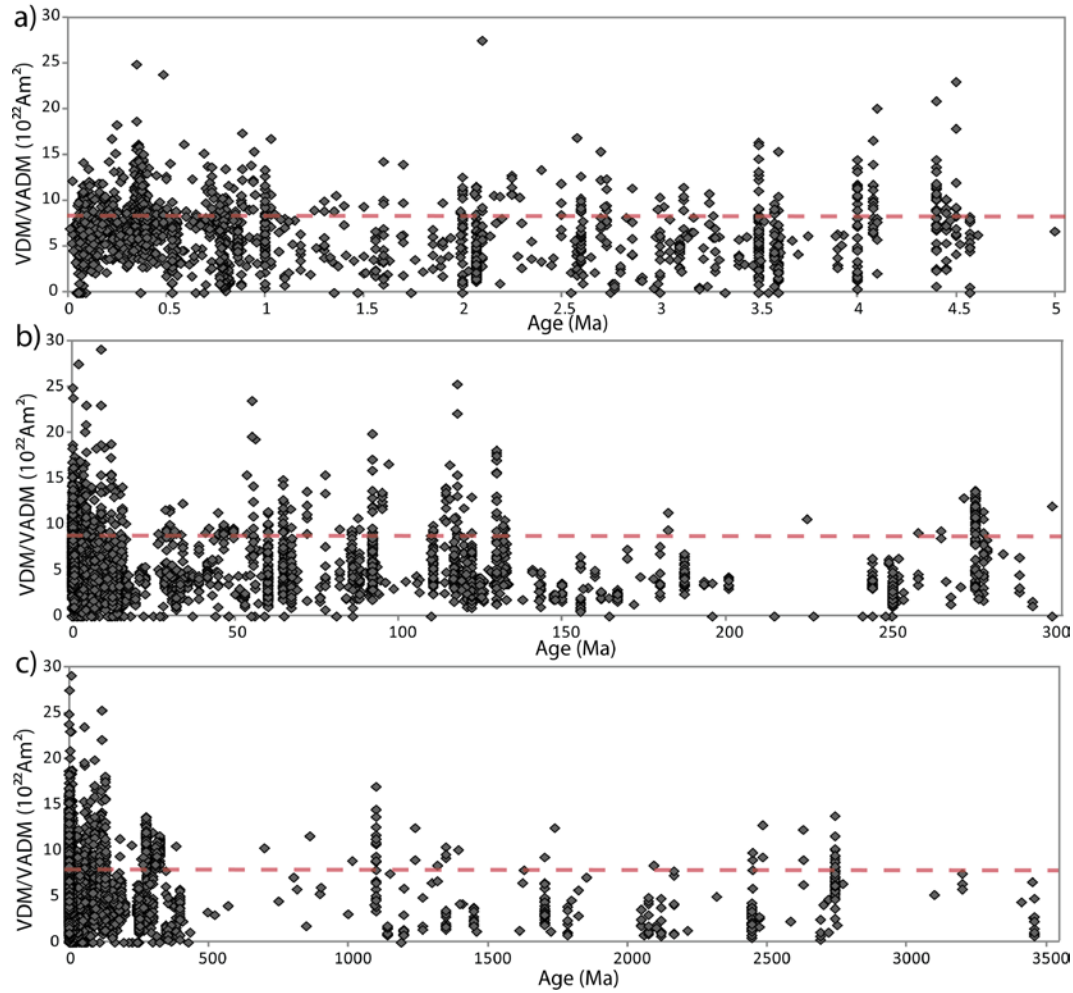


Figure 1.11. Variations of the VDM/VADM for the past a) 5 Ma, b) 300 Ma and c) 3500 Ma. Red dashed line represents the present value for Earth's dipolar moment ( $7.8 \times 10^{22} \text{ Am}^2$ ).

### 1.3 Geochronological Applications

One of the most important applications of paleomagnetism is the possibility to date events in Earth's history. For this purpose the understanding of the characteristic of the magnetic field and the assumption of a geocentric axial dipole are fundamental.

### 1.3.1 Geomagnetic Polarity Time Scale

Studies of Earth's magnetic field have shown that it has not remained constant. For example, when comparing magnetic directional maps from mariners in the seventeenth century with the present magnetic field, it is clear that the declinations and inclinations have changed more than a couple of degrees. Such changes in direction are known as *secular variations*, and have a typical period of 1yr to  $10^5$ yr, and are produced by non-dipolar and dipolar sources (Butler, 1992; McElhinny, 1973). Furthermore, on some occasions the field departs radically from what can be considered a normal secular variation, a feature related to axial dipole intensity known as *geomagnetic excursions*, which tends to have durations of the order of  $10^3$ – $10^4$ yr.

When the geomagnetic field is studied on longer time scales it has been observed to switch polarity. This phenomenon is known as *polarity reversals*. If the ancient magnetic field has the same configuration as the present dipole moment, the field is considered to have *normal polarity*; the opposite is identified as *reverse polarity*. The geomagnetic field changes direction by  $180^\circ$  when a reverse polarity occurs. The frequency of the reversals has changed considerably though time (Opdyke and Channell, 1996), and the interval between reversals can last  $\sim 10^5$ – $10^6$  yr; however, the reversal pattern is not predictable.

The study of secular variations, excursions and reversals of the geomagnetic field allows correlation of isochronous events between different sites. More importantly, with the development of high resolution rock dating, these characteristics allow the development of a geomagnetic polarity time scale (GPTS), which has been fundamental to estimating limits for the different geological times. Figure 1.11 shows the present GPTS for the past 5 million years. The polarity sequences are divided in times of normal and polarity zones, known as *chrons*.

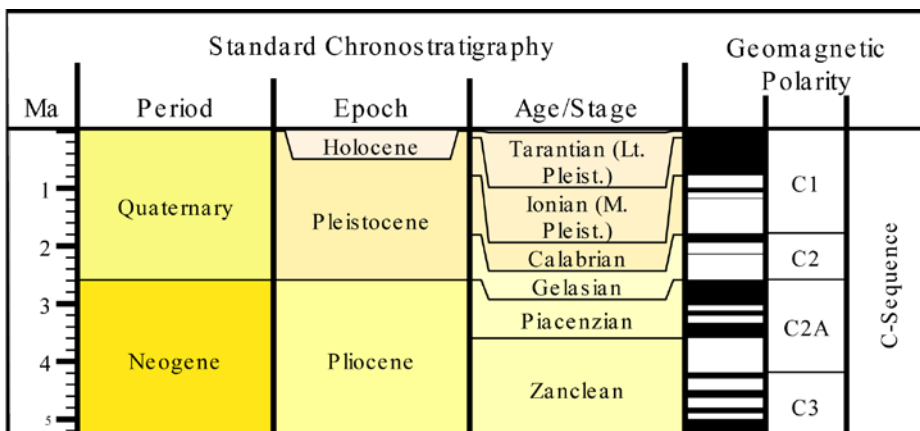


**Figure 1.12.** Geomagnetic polarity time scale and Chronostratigraphy scale for the Cenozoic Era.  
Time scale created TimeScale Creator online by Ogg et al. (<http://www.tscreator.com/>)

### 1.3.2 Magnetostratigraphy

One of the most broadly used geochronologic applications of paleomagnetism is the correlation between the polarization zones observed in geological sequences and the GPTS. This application is known as *magnetic polarity stratigraphy* or *magnetostratigraphy*. This technique uses the polarization variations as fingerprints to date and correlate sedimentary or volcanic sequences. In addition, it allows determination of the rate of processes, such as sea-floor spreading, sedimentary accumulation, extinctions and speciation, occurs (Tauxe 2002).

To ensure the accuracy of magnetostratigraphic studies, some basic principles need to be followed (Opdyke and Channell, 1996):

1. The primary characteristic of the magnetization has to be determined to ensure that the results are representative of Earth's magnetization.
2. Normal and reverse polarity directions should be clearly identified.
3. Sufficient stratigraphic coverage is required to ensure that the sequence delineates the polarity zonation. In addition, it is desirable to have several samples per horizon, to ensure that magnetization at a certain level is reproducible.

4. The average direction should be compared with the reference field expected for the age and location of the formation.
5. Independent age constraints, such as isotopic age determinations and/or biostratigraphy, are fundamental to ensure the correct correlation of the magnetic polarity zonation with the GPTS.

### **1.3.3 Dating using Apparent Polar Wander Paths**

Paleomagnetism provides information on the location of the sampling area at the moment the rock acquired its remanent magnetization. If several paleomagnetic poles are known for different times, an *apparent polar wander path* (APWP) can be created. Based on GAD hypothesis, an APWP represents the apparent motion of the geomagnetic pole with respect to the reference frame of the continent (Tauxe et al. 2008). Figure 1.12 shows the present APWP for North America between 40 Ma and 300 Ma (Torsvik et al. 2001). Further discussion of how APWPs are constructed will be given in the following section.

If the paleomagnetic pole of a locality is determined and no information on the age of the sample can be acquired, comparing the position of the pole to the dated APWP provide a good indication of the age of the sampled area. This method is not commonly used because of the uncertainties in the APWP construction, as well as the possible uncertainties in the paleomagnetic pole calculation. However, in some cases, for example dating kimberlites and ore deposits, this is a good technique to constrain the age of the samples.

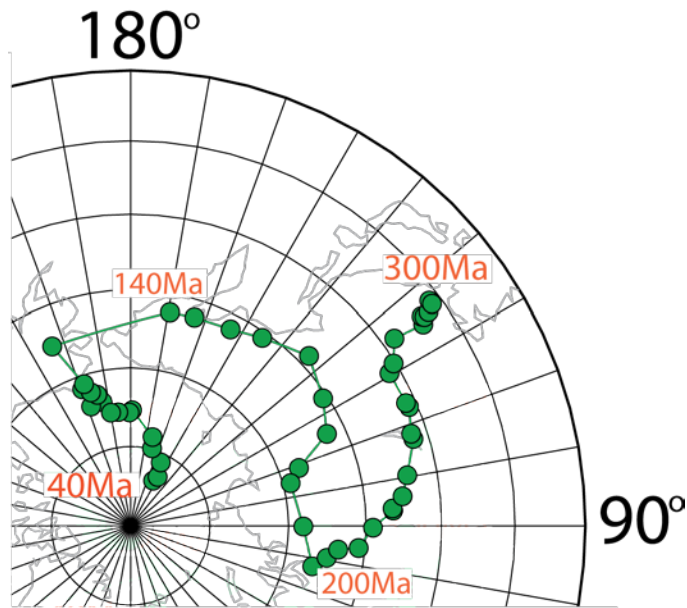


**Figure 1.13.** Apparent polar wander path for North America between 40Ma and 300Ma (data from Torsvik et al. 2001).

## 1.4 Construction of Apparent Polar Wander Paths

The apparent wandering of the poles can be interpreted as the relative motion of a continent with respect to a fixed pole, or, as the wandering of the pole with respect to a fixed continent (Figure 1.13). In paleomagnetism, it is convenient to analyze the wandering of the pole with respect to a fixed continent because the paleopole is a unique point (determined by D and I and the site location) and it is easier to create a graphical representation of the motion. Furthermore, the true polar wandering (TPW, the motion of the polar axis with respect to the whole Earth) has been found to be negligible in comparison to the drift velocities of the tectonic plates (Gordon, 1987; Van der Voo, 1993). If APWPs from several continents are analyzed and a dipolar geomagnetic field is assumed, it is possible to determine if the continents have moved relative to each other. For this reason, during the 1950's and 1960's paleomagnetism was fundamental to corroboration of the continental drift theory.

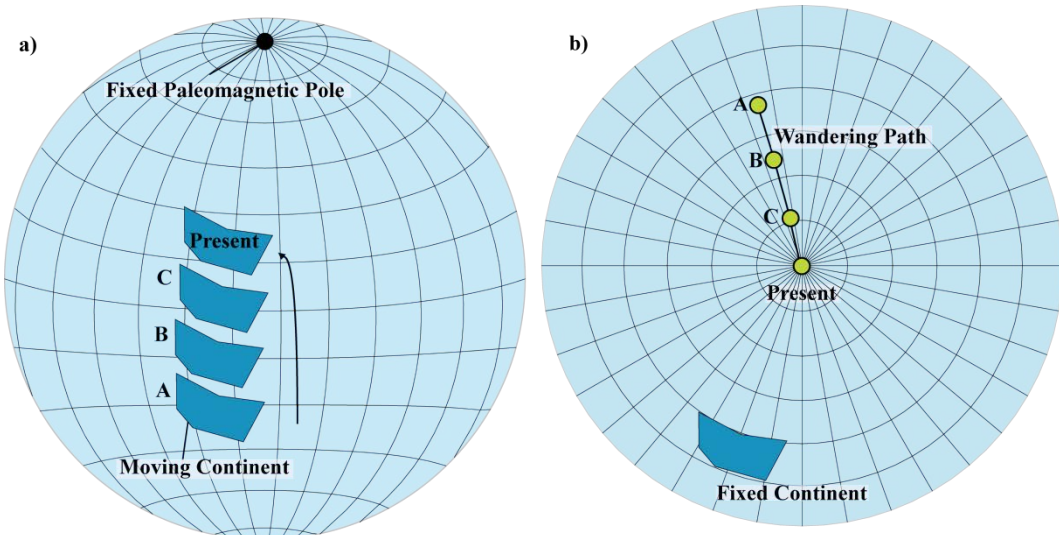


**Figure 1.14.** a) Moving continents with a fixed pole. The resulting path of pole position is the apparent polar wander path. b) Wandering pole with respect to a fixed continent. (Modified from Tauxe et al. 2008)

Selection criteria have been developed to guarantee the quality of the paleomagnetic data used to create the APWPs. The most commonly used are those developed by Van der Voo (1988, 1990, 1993) who proposes 7 reliability criteria:

1. The age of the formation should be accurately determined, so that the age of the magnetization can be assumed to be equal to the age of formation of the rock.
2. There must be sufficient samples to average the secular variation and appropriate use of Fisher (1953) statistic. Van der Voo 1990 recommends a minimum of 24 samples per site.
3. Appropriate demagnetization techniques and appropriate description of the experimental procedure.
4. Field tests (fold test, conglomerate test, backed contact test) must be applied to constrain the age of magnetization.
5. Agreement between pole positions from samples of similar age from an extended region should exist; knowledge of any structural correction is necessary.

6. Presence of polarity reversal; both normal and reverse pole should be antipodal.
7. Pole position should not resemble paleopoles of younger age.

Based on these criteria, Van der Voo (1990) defines the quality factor,  $Q$ . This factor takes into account the number of reliability criteria parameters fulfilled by the paleomagnetic study (Besse and Courtillot, 2002; Torsvik et al., 2008). A higher  $Q$  value represents a reliable study.

After the selection of data an appropriate curve fitting scheme has to be used to create an appropriated apparent polar wander path that describes the motion of the lithospheric region. Table 1.4 summaries different approaches used in modern paleomagnetism studies (Butler, 1992; Tauxe et al., 2008).

**Table 1.4.** Summary of the different methods used in the calculation of APW paths.

Method	Characteristic
Discrete Windows	Paleomagnetic poles from a specific region are separated into discrete time intervals, where poles for each time window are averaged. Each window is independent of the other, i.e. there is no overlap of poles between time windows. Using Fisher statistics the 95% confidence cone can be calculated for each mean pole. This method effectively averages out random noise. But if systematic errors are present, the method can reinforce them.
Key Poles	Construction of the APW path from the most reliable paleomagnetic poles, the so called “key poles”, without applying time averaging.
Moving Windows	Sliding time window technique uses the same approach as the discrete window technique but the time windows overlap and successive mean poles are not independent.
Spline Curve Fitting	Fits a smooth curve to the paleopoles which have different statistical weight.
Paleomagnetic Euler Pole	In this method, the APW path segments are analyzed as small circles around an Euler pole.
Master Path	If the rotation parameters between continents are well known as a function of time, the poles from one continent can be transferred to the coordinate system of another.

## 1.5 Major Goals of the Thesis

The major goals of my thesis and the description of the methods I have used to achieve them are described as follows:

- The Siberian trap basalts are the largest igneous continental province on Earth. They cover an area of  $\sim 3.7 \times 10^6 \text{ km}^2$  in the western part of the Siberian platform and were formed during a relatively short period of time ( $\sim 1 \text{ Ma}$ ) at the Permo-Triassic boundary. The study of the characteristics of the magnetic field during the formation of the traps is of great interest for their temporal relationship with the extension of the Mesozoic dipole low (MDL). This is a time interval characterized by a dipole intensity that is thought not to have exceeded about 30% of the present magnetic field (Prévot et al. 1990). Also, paleointensity studies at the Permo-Triassic boundary can provide insight into possible relationships between magnetic intensity variations during polarity reversals and the largest mass extinction of plants and animals of the planet, the Permian Extinction or Great Dying. The main objective of this research is to determine the characteristics of the geomagnetic field during the Permo-Triassic boundary. For this purpose, I performed an extensive paleointensity study on the Siberian trap basalts using a variation of the Thellier-Thellier experimental methodology on stable samples from 4 localities in the East and Northwest of the Siberian platform. Rock magnetization experiments will be also performed to ensure the primary remanent magnetization nature of the samples.
- Large magmatic events have been an important part of the geological history of Siberia. Some of them are well studied, as with the Siberian trap basalts, but others, such as several kimberlite intrusions along the platform are not. Dating is a problem because isotopic dating does not provide a

conclusive age. I used the Siberian APWP to unravel the age of four kimberlite pipes at the East of the Siberian platform, for which three main time intervals have been considered as possible candidates for their age of emplacement: the Devonian-Early Carboniferous, Triassic, and Cretaceous. Determining the correct age of these kimberlite pipes is fundamental to understanding the relationship between the Siberian platform kimberlite magmatism and the formation of the Permo-Triassic and Late Devonian large magmatic provinces.

- The evolution of the Western Canada Sedimentary Basin has been widely studied in the past. Although a great deal of knowledge has been acquired, the timing of formation for the different stratigraphic facies is not well understood because of the complex depositional environments. I used magnetostratigraphy as a tool to provide a magnetostratigraphic time frame for this sedimentary basin evolution. For this purpose, three cores that originate from Upper Cretaceous located in South of Alberta, Canada, were subject to paleomagnetic measurements. In addition, I aim to determine the presence of short normal polarity zones in the Chron 33r, usually believed to be of reverse polarity in its entire interval and to improve the Geomagnetic Polarity Times Scale.
- The Siberian APWP during the Phanerozoic Eon is fundamental for global tectonic reconstructions, because Siberia can be defined as an independent stable platform since the breakup of Rodinia (~800 Ma) until the end of the Paleozoic when it became part of Eurasia. Due to the sparse nature of the paleomagnetic data for Siberia, it is difficult to construct its APWP. Furthermore, for the Mesozoic Era two possible scenarios are discussed in the literature: Siberia as a consolidated component of Eurasia since the Triassic (Cocks and Torsvik, 2007; Torsvik et al., 2012; Pavlov, 2012), and Siberia as an independent continent (Metelkin et al., 2010) until late Cretaceous. I am interested in the development of a new fitting method

that provides accurate fitting paths for sparse data set. For this purpose I aim to use singular value decomposition to solve the least squares problem associated with the APWP construction. The present paleomagnetic data set needs to be up-dated and needs to follow Van der Voo's quality criteria. The methods I am using will be compared to the smoothing cubic spline technique, as well as the with the most recent version of the Siberian APWP created by Cock and Torsvik in 2007. Additionally, the two possible paths for Siberia during the Mesozoic will be discussed.

The research presented in this thesis has resulted in two manuscripts that have been published and one that is in the stage of submission to a peer reviewed journal. The publications associated with my Ph.D. program are presented below. The fourth manuscript was also prepared during my Ph.D. work and is planned to be submitted by December 2013.

1. **Blanco, D.**, Kravchinsky, V.A., Valet, J-P., Arfan, A., Potter, D.K., 2012. Does the Permo-Triassic geomagnetic dipole low exist? Physics of the Earth and Planetary Interiors, 204–205, 11-21.
2. **Blanco, D.**, Kravchinsky, V.A., Konstantinov, K.M., Kabin, K., 2013. Paleomagnetic dating of Phanerozoic kimberlites in Siberia. Journal of Applied Geophysics, 88, 139-153
3. **Blanco, D.**, Mumpy, A., Kravchinsky, V.A., Cataneanu, O. Upper Cretaceous magnetostratigraphy in Western Canada: Evidence for normal polarity zones in chron 33r and new genetic links between stratigraphic units. Submission journal: Geophysical Journal International.
4. Zhan, R., **Blanco, D.**, Kravchinsky, V.A., Yue, L. New paleomagnetic poles for the northern Junggar Basin, northwest China, about 40 and 20 Ma:

Evidence of tectonic rotations between Junggar and Siberia after 20 Ma.  
Submission journal: Geophysical Journal International.

In addition, I have presented my work in three international conferences:

1. **Blanco, D.**, Kravchinsky, V.A. Tectonic reconstructions of Siberian craton in Mesozoic era: combination of the hotspot trace and paleomagnetism; AGU Fall meeting, 2012. Poster presentation.
2. **Blanco, D.**, Kravchinsky, V.A., Kabin, K. Siberian Apparent Polar Wander Path for the Phanerozoic Eon: towards finding Siberian place on Earth; AGU Fall meeting, 2011. Poster presentation.
3. **Blanco, D.**, Kravchinsky, V.A. Valet, J-P., Arfan, A., Potter, D.K. Does the Permo-Triassic geomagnetic dipole low exist?. AGU Fall Meeting, 2010. Poster presentation.

## Bibliography

Aitken, M.J., Allsop, A.L., Bussel, G.D., Winter, M.B., 1988. Determination of the intensity of the Earth's magnetic field during archeological times: reliability of the Thellier technique. *Reviews of Geophysics*, 26, 3–12.

Besse, J., Courtillot, V., 2002. Apparent and true polar wander and the geometry of the geomagnetic field for the last 200 Myr. *Journal of Geophysical Research*, 107(B11), 2300, doi:10.1029/2000JB000050.

Biggin, A.J., McCormack, A., Roberts, A., 2010. Paleointensity database updated and upgraded. *EOS*, 91, 15.

Butler, R.F. 1992. Paleomagnetism: magnetic domains to geologic terranes. Blackwell Scientific Publications, Boston, MA. pp. 238.

Coe, R.S., 1967. Paleointensities of the Earth's magnetic field determined from tertiary and quaternary rocks. *Journal of Geophysical Research*, 72, 3247–3262.

Coe, R.S., Grommé, S., Mankinen, E.A., 1978. Geomagnetic paleointensities from radiocarbon-dated lava flows an Hawaii and the question of the Pacific non dipole low. *Journal of Geophysical Research*, 83, 1740–1756.

Cocks, L. R.M., Torsvik, T.H., 2007. Siberia, The wandering northern terrane, and its changing geography through the Paleozoic. *Earth-Science Reviews*, 82, 29–74.

Constable, C., 2005. Dipole moment variation. In: *Encyclopedia of Geomagnetism and Paleomagnetism*, Gubbins, D., Herrero-Bervera, E., eds., Springer, 1054 p.

Cox, A., Doell, R.R., 1960. Review of Paleomagnetism. *Geological Society of America Bulletin*, 71, 645-748.

Domeier, M., Van der Voo, R., Torsvik, T. H., 2012. Paleomagnetism and Pangea: The road to reconciliation. *Tectonophysics*, 514-517, 14–43. doi:10.1016/j.tecto.2011.10.021

Dunlop, D.J., Özdemir, Ö., 2007. Magnetization in rocks and minerals. *Treatise on Geophysics*, volume 5, pages 277-336.

Finlay, C.C., Maus, S., Beggan, C.D., Bondar, T. N., Chambodut, A., Chernova, T.A., Chulliat, A., Golovkov, V.P., Hamilton, B., Hamoudi, M., Holme, R., Hulot, G., Kuang, W., Langlais, B., Lesur, V., Lowes, F.J., Luhr, H., Macmillan, S., Mandea, M., McLean, S., Manoj, C., Menville, M., Michaelis, I., Olsen, N., Rauberg, J., Rother, M., Sabaka, T.J., Tangborn, A., Tøffner-Clausen, L., Thebault, E., Thomson, A.W.P., Wardinski, I., Wei Z., Zvereva, T.I., 2010. International geomagnetic reference field: the eleventh generation. *Geophysical Journal International*, 183, 1216-1230.

Fisher, R.A., 1953. Dispersion on a sphere. *Proceedings of the Royal Society London, Series A*, 217, 295-305.

Gordon, R.G., 1987, Polar wandering and paleomagnetism. *Annual Review of Earth and Planetary Sciences*, 15, 367-393.

Krása, D., Heunemann, C., Leonhardt, R., Petersen N., 2003. Experimental procedure to detect multidomain remanence during Thellier-Thellier experiments, *Physics and Chemistry of the Earth*, 28, 681-687.

Kearey, P., Klepjes, K.A., Vine, F.J., 2009. Global tectonics. Willey-Blackwell. Pp. 496.

Kirschvink, J.L., 1980. The least-squares line and plane and the analysis of paleomagnetic data. *Geophysical Journal of the Royal Astronomical Society*, 62, 699-718.

Lerbeckmo, J. F., Evans, M. E., 2012. Cryptochrons and tiny wiggles: New magnetostratigraphic evidence from chron 32 and 33 in Western Canada, *Physics of the Earth and Planetary Interiors*, 202-203, 8–13, doi:10.1016/j.pepi.2012.05.004

Metelkin, D.V., Vernikovsky, V.A., Kazansky, A.Y., Wingate, M.T.D., 2010. Late Mesozoic tectonics of Central Asia based on paleomagnetic evidence, *Gondwana Research*, 18, 400–419.

McElhinny, M.W., 1973. Paleomagnetism and plate tectonics. Cambridge University Press, London. pp. 358.

Nagata, T., Arai, Y., Momose, K., 1963. Secular variation of the geomagnetic total force during the last 5000 years. *Journal of Geophysical Research*, 68, 5277-5281.

Néel, L. 1955. Some theoretical aspects of rock magnetism. *Advances in Physics*, 4, 191-243.

Opdyke, N.D., Channell, 1996. Magnetic stratigraphy. Academic Press, San Diego, California. P. 341.

Pavlov, V., 2012. Siberian paleomagnetic data and the problem of rigidity of the Northern Eurasian Continent in the Post-Paleozoic. *Izvestiya, Physics of the Solid Earth*, 48, 721-737.

Prévot, M., El-Messaoud Derder, M., McWilliams, M., Thompson, J., 1990. Intensity of the Earth's magnetic field: Evidence for a Mesozoic dipole low, *Earth and Planetary Science Letters*, 97, 129–139.

Riisager, P., Riisager, J., 2001. Detecting multidomain magnetic grains in Thellier palaeointensity experiments. *Physics of the Earth and Planetary Interiors*, 125, 111–117.

Selkin, P.A., Tauxe, L., 2000. Long-term variations in paleointensity. *Philosophical Transactions of the Royal Society London*, 358, 1065–1088.

Tauxe, L., 2002. Paleomagnetism Principles and Practice. Kluwer Academic Publishers, The Netherlands, pp. 299.

Tauxe, L., Butler, R., Banerjee, S.K., van der Voo, R. 2008. Essentials of Rock and Paleomagnetism. University of California Press, USA, pp. 509.

Thellier, E., 1941. Sur la vérification d'une method permattant de determiner l'intensité du champ terrestre dans le Passé. *C.R. Hebd. Seances Acad. Sci.*, 212, 281-283.

Thellier, E., Thellier, O., 1959. Sur l'intensité du champ magnétique terrestre dans le passé historique et géologique, *Annales Geophysicae*, 15, 285–376.

Torsvik, T.H., Van der Voo, R., Meert, J.G., Mosar, J., Walderhaug, H.J., 2001. Reconstructions of the continents around the North Atlantic at about the 60th parallel, *Earth and Planetary Science Letters*, 187, 55–69.

Torsvik, T.H., Müller, R.D, Van der Voo, R., Steinberger, B., 2008. Global plate motion frames: toward a unified model. *Reviews of Geophysics*, 46, RG3004, doi:10.1029/2007RG000227.

Torvik, T.H., Van der Voo, R., Preeden, U., Mac Niocaill, C., Steinberger, B., Doubrovine, P.V., van Hinsbergen, D.J.J., Domeier, P., Gaina, C., Tohver, E., Meert, J.G., McCausland, P.J.A., Cocks, L.R.M., 2012. Phanerozoic polar wander, palaeogeography and dynamics. *Earth Science Reviews*, 144 (3-4), 325-368.

Valet, J. P., Brassart, J., Le Meur, I., Soler, V., Quidelleur, X., Tric, E., and Gillot, P., 1996. Absolute paleointensity and magnetomineralogical changes. *Journal of Geophysical Research*, 101(B11), 25029–25044.

Valet, J.P., 2003. Time variations in geomagnetic intensity. *Reviews of Geophysics*, 44: 4-1, 4-44.

Van der Voo, R., 1988. Paleozoic paleogeography of North America, Gondwana and intervening displaced terranes: Comparisons of paleomagnetism with paleoclimatology and biogeography. *Geological Society of America Buletin.*, 100, 311-324.

Van der Voo, R., 1990. Phanerozoic paleomagnetic poles from Europe and North-America and comparisons with continental reconstructions. *Reviews of Geophysics*, 28, 167-206.

Van der Voo, R., 1993. Paleomagnetism of the Atlantic, Tethys and Iapetus Oceans. Cambridge University Press, Cambridge, U.K., pp. 411.

Zijderveld, J.D.A., 1967. A.C. demagnetization of rocks, analysis of results. In: Methods in paleomagnetism, D.W. Collinson, K.M. Creer, and S.K. Runcorn, eds. Elsevier, Amsterdam, 254–286.

## **Chapter 2\***

# **Does the Permo-Triassic geomagnetic dipole low exist?**

### **2.1 Introduction**

Studies of absolute paleointensity provide important constraints to geodynamo models and a unique opportunity to document the evolution of the Earth's magnetic field over geological time. One of the best sources of magnetic paleointensity information comes from long sequences of continental flood basalts (CFB). As these geological formations involve massive lava flows that are produced over relatively short time periods, they have recorded detailed information regarding the evolution of the field vector (Vandamme and Courtillot, 1992). The largest CFB is located on the north-western margin of the Siberian platform and is known as the Siberian trap basalt (STB, Figure 2.1). Absolute dating indicates that the traps were intruded 250 Myr ago (Courtillot and Renne, 2003; Almukhamedov et al., 2004; Reichow et al., 2005, 2009, and references therein) and generated huge volcanic activity over a very short period of time. A direct consequence is that it may have triggered the most massive extinction of flora and fauna known so far in Earth's history (Courtillot and Renne, 2003).

The Permo-Triassic is also a period of particular interest concerning the characteristics of the dipolar field between 200 Ma and 300 Ma. The few paleointensity studies that have been published for this specific period of time (Senanayake and McElhinny, 1983; Bol'shakov et al., 1989; Perrin et al., 1991; Solodovnikov, 1992, 1995; Thomas et al., 1995, 1997; Harcombe-Smee et al., 1996; Heunemann et al., 2004; Shcherbakova et al., 2005; Garcia et al., 2006) have shown paleointensity values lower than the present-day field. Further

\* This chapter has been published in the journal of Physics of the Earth and Planetary Interiors, 204–205, 11–21, 2012.

paleointensity data is required to determine whether Earth's dipole was weak at that period of time. Moreover, late Jurassic dipolar characteristics can be linked with the extension of the Mesozoic dipole low (MDL), a time interval characterized by a dipole which is thought not to have exceeded about 30% of the present field according to the records of absolute paleointensity that have been obtained by Prévot et al. (1990). Some studies (Bol'shakov and Solodovnikov, 1983; Tanaka et al., 1995; Perrin and Shcherbakov, 1997; Kosterov et al., 1998; Selkin and Tauxe, 2000; Zhu et al., 2001, 2003; Heller et al., 2002; Biggin and Thomas, 2003; Pan et al., 2004; Tarduno and Cottrell, 2005; Tauxe, 2006; Garcia et al., 2006; Shcherbakova et al., 2009; Brandt et al., 2009) are consistent with this observation, while other results (Goguitchaichvili et al., 2002, 2008; Ruiz et al., 2006) report higher paleointensity values and consider that the field at that time seems to have a similar variability to that of the present field.

Detailed records of paleointensity during the Permo-Triassic boundary would provide valuable information regarding the actual extension and characteristics of the dipole low. Two previous studies of absolute paleointensity (Heunemann et al., 2004; Shcherbakova et al., 2005) have been conducted in the STB at the Permo-Triassic boundary. Heunemann et al. (2004) used specimens from transitional sections and Shcherbakova et al. (2005) applied paleointensity studies to non-oriented specimens belonging to a stable period of the Earth's magnetic field based on previous work. Both studies involved sections from the northwestern part of the formation, and have indicated low virtual dipolar moments ( $2.2 \pm 0.9 \times 10^{22}$  Am<sup>2</sup> and  $2.9 \pm 2.3 \times 10^{22}$  Am<sup>2</sup>, respectively). This new study presents the first paleointensity data from oriented and nontransitional sections at the eastern part of the STB, which enables to extend the paleointensity database for the Permo-Triassic boundary and verify if previous values are characteristic of the STB.

## 2.2 Geological Setting

Absolute dating suggests a very narrow age interval (about one million years) when the Siberian traps were intruded at ~250 Ma, which corresponds to the Permo-Triassic boundary (PTB). The traps are found in the western part of the Siberian platform and under the West Siberian sedimentary basin and occupy an area of  $\sim 3.7 \times 10^6$  km<sup>2</sup> with an approximate volcanic sequence thickness of 6.5 km and occupy a total volume of at least  $3.0 \times 10^6$  km<sup>3</sup> (Kravchinsky et al., 2002; Reichow et al., 2009; Kuzmin et al., 2010).

Several models have been proposed to explain the emplacement mechanism of the traps. Some authors (Basu et al., 1998; Griffin et al., 1999; Courtillot et al., 1999) suggested that an upwelling mantle plume could create the rift system that led to the formation of the Siberian Traps. The Siberian trap magmatism is thought to be related to lithospheric break up linked to the mantle plume and not to plate boundary dynamics (Almukhamedov et al., 1996; Courtillot et al., 1999; Saunders et al., 2005; Kuzmin et al., 2010). Others (Elkins Tanton and Hager, 2000) proposed melt intrusions as the trigger for the eruption of the STB.

Specimens from the eastern and northwestern part of the STB (Figure 2.1) were analyzed. In the eastern part ten extensive Permo-Triassic trap sills (5–20 m thick) have been studied in the areas of Sytikanskaya (66.11°N, 111.80°E), Yubileinaya (66.0°N, 111.7°E), and Aikhal (66.17°N, 111.33°E) kimberlite pipes. Paleomagnetic directions for three of the sills have been published by Kravchinsky et al. (2002). Sampling for both studies (Kravchinsky et al. (2002) and this study) was done in different parts of the kimberlite mine pit and outcrops nearby. The sampling locations were dependent upon mining progress and accessibility. It is common for smaller sills to branch out from the main sill intrusion and for the whole complex to occupy a few square kilometers. Although there are no absolute dates available for the Permo-Triassic traps, the sills cut through older, and are covered by younger, sediments. In some parts they also

contain inclusions or lenses of the older sediments and fossils. The stratigraphic and age relations between sills are still unclear and it is commonly considered from the field observations that there were a few phases of eruption in the area. It is therefore thought that sampling of the different sills will average the secular geomagnetic variations and paleointensity results.

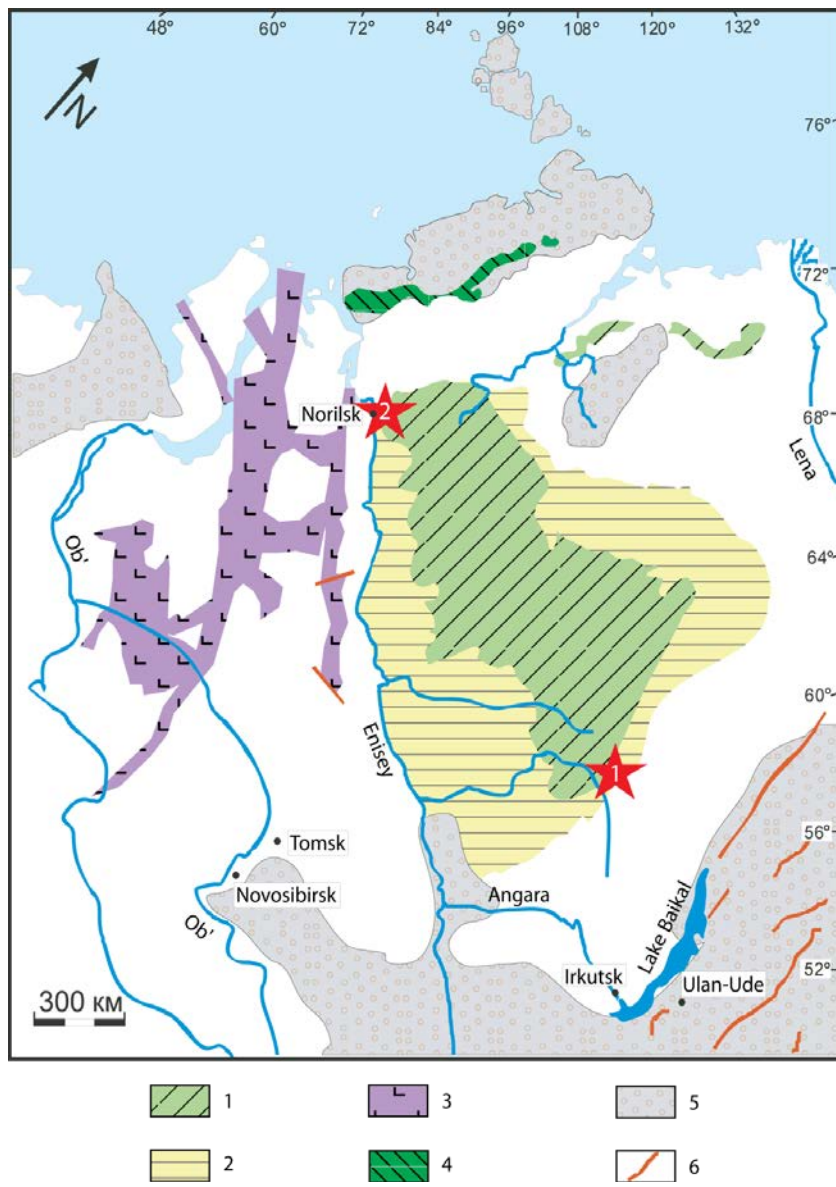


**Figure 2.1.** Occurrences of the Late Permian – Early Triassic magmatism in the structures of the Siberian platform and West Siberian plain (modified from Kuzmin et al., 2010). The study areas are shown as red stars (1 – East Siberian intrusives, 2 – Noril'sk intrusion). 1 – extrusive volcanic rock exposure; 2 – intrusive volcanic rock exposure; 3 – West Siberian Rift basalts, tuffs, and tuffites; 4 – Taimyr Early Triassic traps; 5 – folded surrounding; 6 – major tectonic dislocations.

One extrusive trap multi flow outcrop in the area of the Noril'sk-Talnakh copper-nickel ore-mining district ( $69.21^{\circ}\text{N}$ ,  $88.03^{\circ}\text{E}$ ), which is situated on the northwestern edge of the Siberian platform (Figure 2.1) was also studied. The district is located near the northwestern limit of the most extensive and relatively undisturbed exposures of STB. The basalt and dolerite specimens have been taken from six weakly mineralized and unmineralized more or less differentiated basalt sills south of Noril'sk. These intrusions have been correlated with stages of STB volcanism on the basis of cross-cutting relations, as well as geochemical and magnetic signatures (Dalrymple et al., 1995). Ergalakhsky type I, trachydolerite intrusions occur principally as shallow sills that were emplaced into friable sands and clays of the Upper Permian Tungusska Series (Dalrymple et al., 1995) in the central and southern parts of the Noril'sk area (location 2 on Figure 2.1). On the basis of geologic mapping, their geochemical characteristics, and the fact that all other intrusion types cut them, they are considered to be coeval with the alkali trachybasalt flows of the Lower Ivakinsky subsuite.

## 2.3 Methodology

### 2.3.1 Magnetic Mineralogy

The magnetic mineralogy of the specimens has been investigated by Curie point thermomagnetic experiments and thermal dependent magnetic susceptibility (MS) measurements. The thermomagnetic experiments were performed in air using a Variable Field Translation Balance (VFTB), in a dwell field of 100 mT up to 705 °C. Thermal dependent MS was measured in air up to 700 °C using a Bartington furnace and susceptibility meter.

In order to determine the size of the magnetic carriers, hysteresis measurements at room temperature were applied on powdered specimens (mass 0.5g) using the VFTB with a maximum applied field of 950 mT. Saturation magnetization ( $M_s$ ), remanent saturation magnetization ( $M_{rs}$ ), and coercive force ( $H_c$ ) were determined

after correcting for the paramagnetic contribution. The coercivity of remanence ( $H_{cr}$ ) was calculated from backfield coercivity experiments, up to 959 mT. The thermal dependent MS measurements were performed in the Laboratory of Paleomagnetism and Petromagnetism of the University of Alberta (Edmonton, Canada) and all the VFTB measurements were done in the Petrophysics Laboratory at Heriot-Watt University (Edinburgh, United Kingdom).

### **2.3.2 Directions**

Directional data for the STB has been previously studied by Kravchinsky et al. (2002) in the east of the province and by Pavlov et al. (2007) in the west of the province. In this study the paleomagnetic directions were obtained from thermal demagnetization in zero laboratory field during the paleointensity experiments described below. For both the directional analysis and paleointensity experiments any mineralogical changes were continuously monitored during the heating and cooling. Only a few specimens demonstrated such changes and therefore the directional analysis was reliable for most specimens. A total of 104 specimens from the northwestern locality and 237 specimens from the eastern localities were subject to this procedure up to a temperature of 580 °C.

The data were processed using Enkin (1996) and Cogné (2003) software. Demagnetization results were plotted on orthogonal vector endpoint diagrams (Zijderveld, 1967). Magnetization components were determined by principal component analysis (Kirschvink, 1980) and site-mean directions were calculated using Fisher (1953) statistics.

### **2.3.3. Absolute Paleointensity**

Measurements were carried out at the Laboratory of Paleomagnetism and Petromagnetism of the University of Alberta (Edmonton, Canada) and at the Institut de Physique du Globe de Paris (France). Data from one set of specimens

was acquired following the modified Coe version of the Thellier–Thellier technique (Coe, 1967). In this approach, the first heating step is then followed by cooling in zero magnetic field and the second heating step is followed by cooling in a known magnetic field, imparting a partial thermoremanent magnetization (pTRM) to the specimen (the so called ZI protocol). A slightly different protocol has been applied to another set of specimens. In this case pTRM was imparted before the demagnetization in zero field in order to test whether remagnetized components have been created in the presence of the field during the first heating (IZ protocol) (Aitken et al., 1988; Valet et al., 1998). Partial thermoremanent magnetization (pTRM) checks (Thellier and Thellier, 1959) were performed on all specimens and tail checks (McClelland and Briden, 1996; Riisager and Riisager, 2001) were applied only to specimens for which the intensity value was acquired following the standard Coe experimental protocol. In that case, after the double heating to  $T_i$  a third heating to  $T_i$  in zero laboratory field was performed. The tail check is the difference between the remanent magnetization of the two zero-field heatings.

The specimens were heated in a shielded ASC thermal demagnetizer (Edmonton) and a shielded Pyrox paleointensity furnace (Paris) and they were measured with 2G cryogenic magnetometers (both Edmonton and Paris). The field applied in the oven ranged between 20 and  $80\mu\text{T}$  and that the acquired TRM is linearly proportional to a low applied magnetic field (such as the Earth's) was assumed. The variation of TRM acquisition with applied field strength is beyond the scope of this study and the reader is refer to Selkin et al. (2007), Yu et al. (2007), and Shaar et al. (2010) for further discussion. However, the presented data do not present any evidence of a dependence of the average ancient field on the applied laboratory field. All specimens were heated and cooled in air. A total of 341 oriented cubic specimens with side length between 0.7 and 1 cm were subjected to paleointensity experiments.

The selection of appropriate specimens for the calculation of absolute paleointensity has been achieved using several successive steps, the more important ones are summarized below:

1. The quality of the demagnetization diagrams of the NRM was considered as a prerequisite to any interpretation. Only diagrams characterized by a linear decrease of the magnetic moment towards the origin have been considered. The specimens were always placed in the oven at exactly the same location with the same orientation relative to the applied magnetic field. This allowed monitoring of the presence or absence of remagnetization in the direction of the field within the oven when analyzing the directions.
2. The length of the linear segment (fraction of NRM, f) isolated from the Arai plots is critical to provide a suitable determination of absolute paleointensity. Recent results (Herrero–Bervera and Valet, 2009; Valet et al., 2010) have shown that specimens characterized by a sharp decrease of most of their NRM over a very narrow range of high temperatures are the most appropriate for successful determinations of paleointensity. Following the most recent suggestions on this matter (Valet et al., 2010) it is reasonable to consider that at least 60% of the magnetization should be incorporated in the segment defining the slope of the NRM–TRM plot.
3. Positive pTRM and tail checks indicate the absence of alteration and mineralogical changes produced during successive heatings. However, experimental uncertainties may affect the repeatability of the measurements so that quantitative factors are appropriate to determine a limit beyond which two successive measurements of pTRMs should be considered as being identical. For this reason the quality of the pTRM checks was defined from the mean of the deviations (DEV) between each initial pTRM and the corresponding check over the NRM–TRM segment selected for the calculation of the slope. Nevertheless, in contrast to the calculation of the difference ratio (DRAT) (Selkin and Tauxe,

2000) in this study any value of the NRM is incorporated in the calculation of DEV because the NRM is decoupled from the calculation of the pTRM check, which only involves the initial TRM and its repeated measurement. The deviation has been expressed in percentage after normalizing the DEV value, defined as  $DEV = \sum (pTRM - pTRM_{check})$ , with respect to the length of the TRM segment. Similarly, the largest deviation (maxDEV) obtained at all steps was also calculated. The slope of the plots was used to calculate a paleointensity when mean-DEV did not exceed 10%.

In accordance with the criteria described above, results have been divided in two categories, “A” and “B”. “A” category specimens correspond to results with  $meanDEV < 10\%$ ,  $pTRM$  tail check  $< 20\%$ , a linear segment  $f > 60\%$  incorporating at least four successive data points, a maximum angular deviation (MAD) of  $15^\circ$ , and  $\beta$  parameter  $< 0.1$  (as defined by Selkin and Tauxe, 2000). If one of the previous criteria is not fulfilled the result falls into a “B” category having as limits:  $10\% < meanDEV < 25\%$ ,  $20\% < pTRM$  tail check  $< 25\%$  and  $30\% < f < 60\%$ . In addition, the multiple-specimen reproducibility criterion, the ratio of the standard deviation of the field estimates to the average of the field for each of the sites,  $\sigma_B / \bar{B}$ , will be taken into account. This value should be less than 25%, otherwise the average is considered unreliable (Selkin and Tauxe, 2000).

## 2.4 Results

### 2.4.1 Thermomagnetic and Hysteresis Measurements

Results from Curie point and thermal dependent MS curves for the three eastern localities are presented in Figure 2.2. The heating and cooling thermomagnetic curves are very similar but not exactly identical. The deviations are unlikely to reflect large mineralogical changes, particularly for the second and third specimens (Figure 2.2). The first two specimens are characterized by Curie temperatures of  $\sim 560^{\circ}\text{C}$ , typical of magnetite with very low titanium content. The last specimen has a Curie temperature of  $500^{\circ}\text{C}$ , implying a larger amount of titanium. Specimens with non-reversible heating and cooling thermomagnetic curves or titanomagnetite with high titanium content have not been selected for the paleointensity experiments. Magnetic hysteresis curves are also shown in Figure 2.2. The hysteresis parameters are compatible with those of specimens containing predominantly pseudo-single domain (PSD) particles. The Mrs/Ms and Hcr/Hc ratios were plotted on a Day diagram in Figure 2.3 (Dunlop, 2002). Magnetite single domain (SD) and superparamagnetic (SP) and single domain and multidomain (MD) theoretical mixing lines of Dunlop (2002) are plotted as a reference. The magnetic grain size corresponds to the PSD region with specimens lying close to the mixing line of SD and MD grain sizes. For paleointensity experiments SD and PSD are the preferable grain sizes.

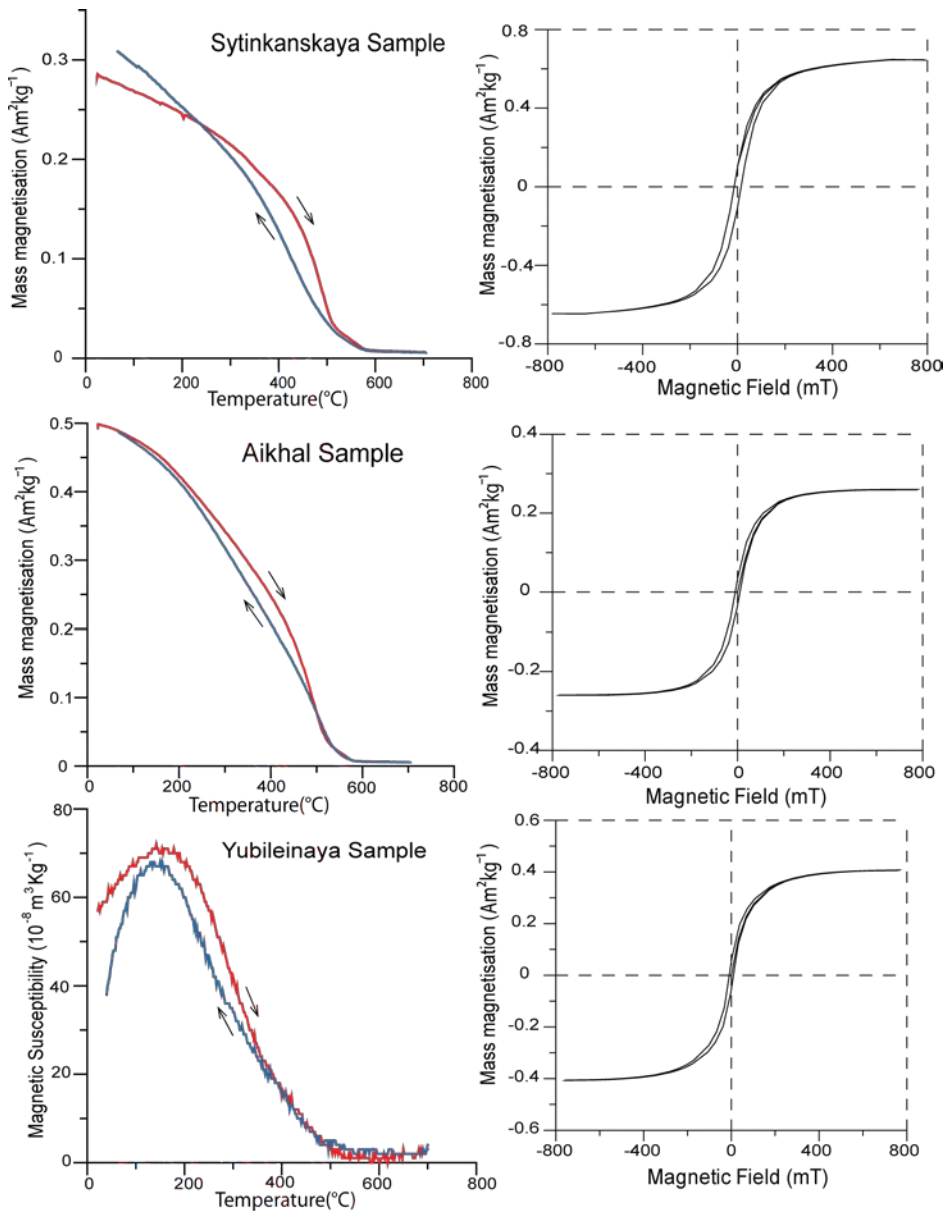


**Figure 2.2.** Results of the rock magnetic experiments for specimens from Sytikanskaya, Aikhal and Yubileinaya, respectively. Top row: thermomagnetic curves (using the VFTB) and thermal dependent magnetic susceptibility (using the Bartington susceptibility meter). The red (blue) curves represent the heating (cooling) curves. Bottom row: magnetic hysteresis loops (using the VFTB).

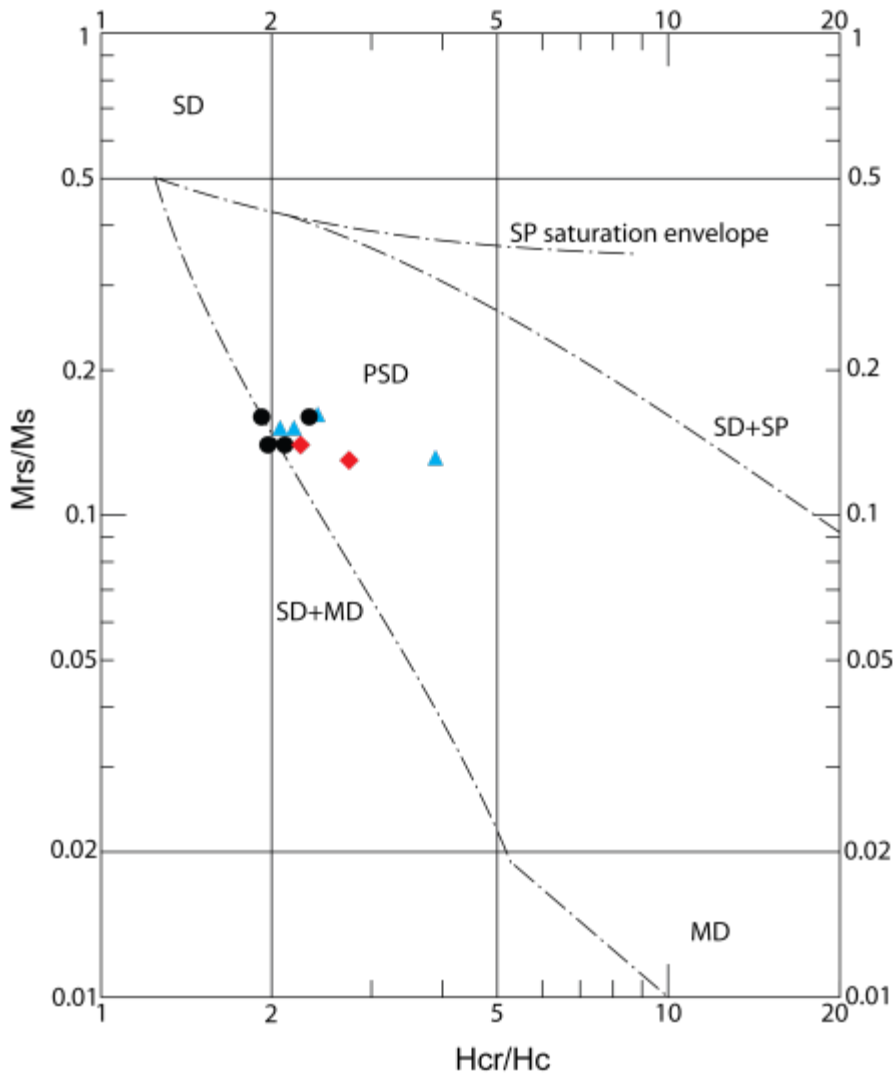


**Figure 2.3.** Modified day diagram (based on Dunlop, 2002) of the hysteresis parameters at room temperature for Sytikanskaya (triangles), Aikhal (diamonds) and Yubileinaya (circles) localities. Magnetite SD + SP and SD + MD theoretical mixing lines of Dunlop (2002) are also shown (the fainter lines).

#### 2.4.2. Directions

Typical vector end-point diagrams (Zijderveld, 1967) of specimens from 10 sills of the Aikhal, Sytikanskaya, Yubileinaya and four outcrops of the Noril'sk trap differential intrusion are shown in Figure 2.4. Secondary viscous components of magnetization were removed after 100°C for all basalts except Sytikanskaya where heating above 200–300°C is necessary to remove the secondary component. The mean direction of the high temperature (HT) primary stable

component of NRM for all four studied localities is plotted in Figure 2.5 and listed in Table 2.1.

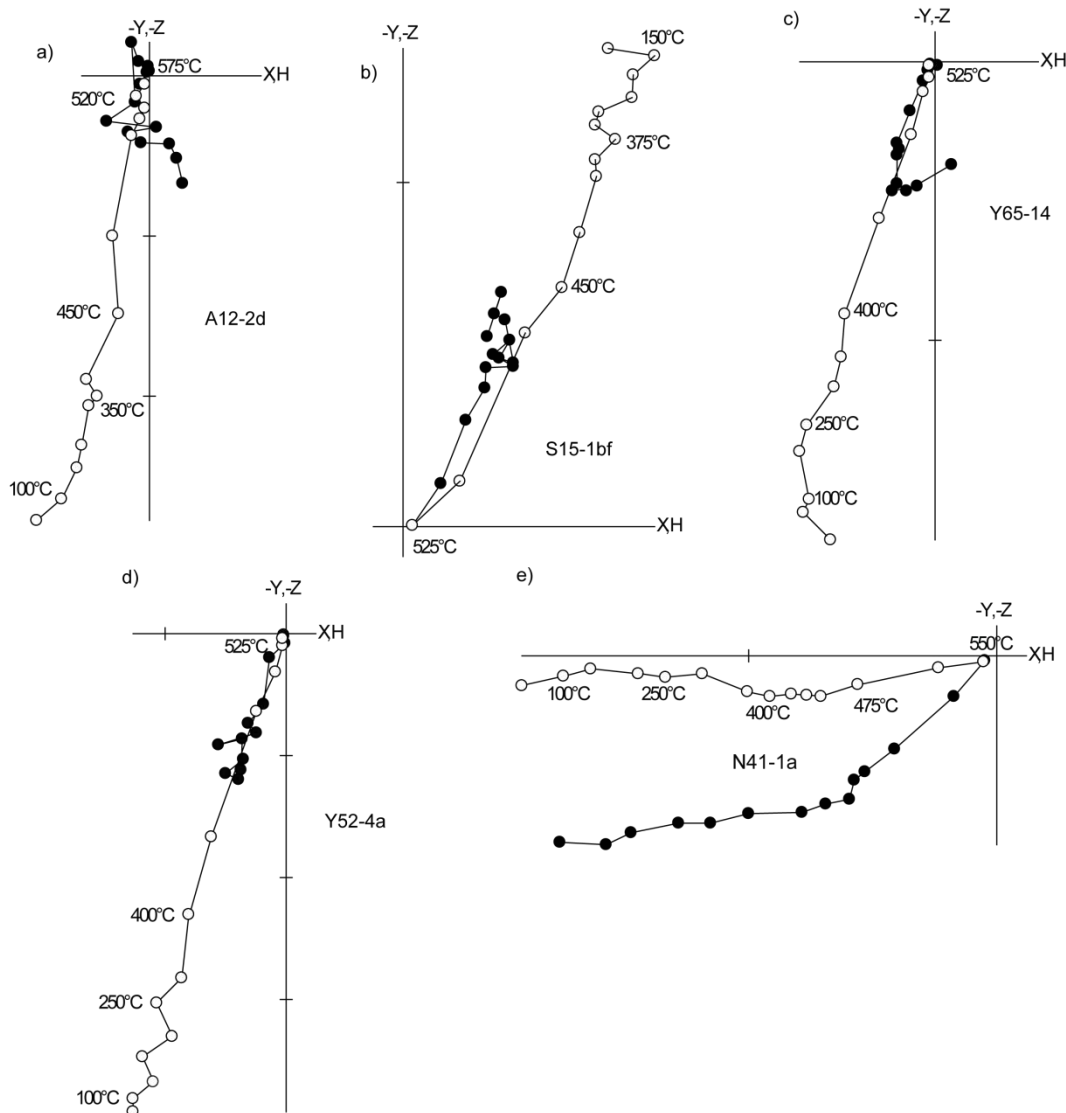


**Figure 2.4.** Representative vector end-point diagrams of stepwise thermal demagnetization of natural remanent magnetization for the studied localities. Demagnetization steps are in °C, open and solid circles represent vector endpoints projected onto the vertical and horizontal planes, respectively. (a) Aikhal, (b) Sytikanskaya, (c, d) Yubileinaya, and (e) Noril'sk.

The Aikhal, Yubileinaya and Noril'sk localities have a normal polarity and Sytikanskaya has a reverse polarity direction. Mean paleodirections for normal ( $D=110.0^\circ$ ,  $I=80.4^\circ$ ,  $k=338.0$ ,  $\alpha_{95}=3.3^\circ$ ,  $N=7$  sills) and reverse ( $D=285.3^\circ$ ,  $I=-64.1^\circ$ ,  $k=352.6$ ,  $\alpha_{95}=6.6^\circ$ ,  $N=3$  sills) sites were calculated and plotted in Figure

2.5. The confidence circles of individual sills overlap each other even when two sets of directions (normal and reverse polarity) exclude the mean of the other. The presence of two antipodal polarities confirms the result reported by Kravchinsky et al. (2002) and is an additional indication for the primary origin of the remanence. The mean directions from the eastern (normal and reverse polarities) ( $D=107.5^\circ$ ,  $I=75.5^\circ$ ,  $k=82.8$ ,  $\alpha_{95}=5.3^\circ$ ,  $N=10$  sills) and northwestern ( $D=96.1^\circ$ ,  $I=71.8^\circ$ ,  $k=35.2$ ,  $\alpha_{95}=15.7^\circ$ ,  $N=4$  outcrops) localities are in excellent agreement with the directions and range of uncertainties derived from the Pavlov et al. (2007) NSP3 paleomagnetic pole ( $57.0^\circ\text{N}$ ,  $148.1^\circ\text{E}$ ,  $N=6$ ,  $K=159$ ,  $A_{95}=5.3^\circ$ ) (estimated values are  $D = 100.6^\circ$ ,  $I = 80.1^\circ$ ,  $\alpha_{95} = 2.8^\circ$  for eastern localities and  $D = 84.7^\circ$ ,  $I = 74.9^\circ$ ,  $\alpha_{95} = 3.0^\circ$  for the northwestern locality). The good agreement between the paleomagnetic directions corroborate the  $\sim 250$  Ma ages of the specimens.

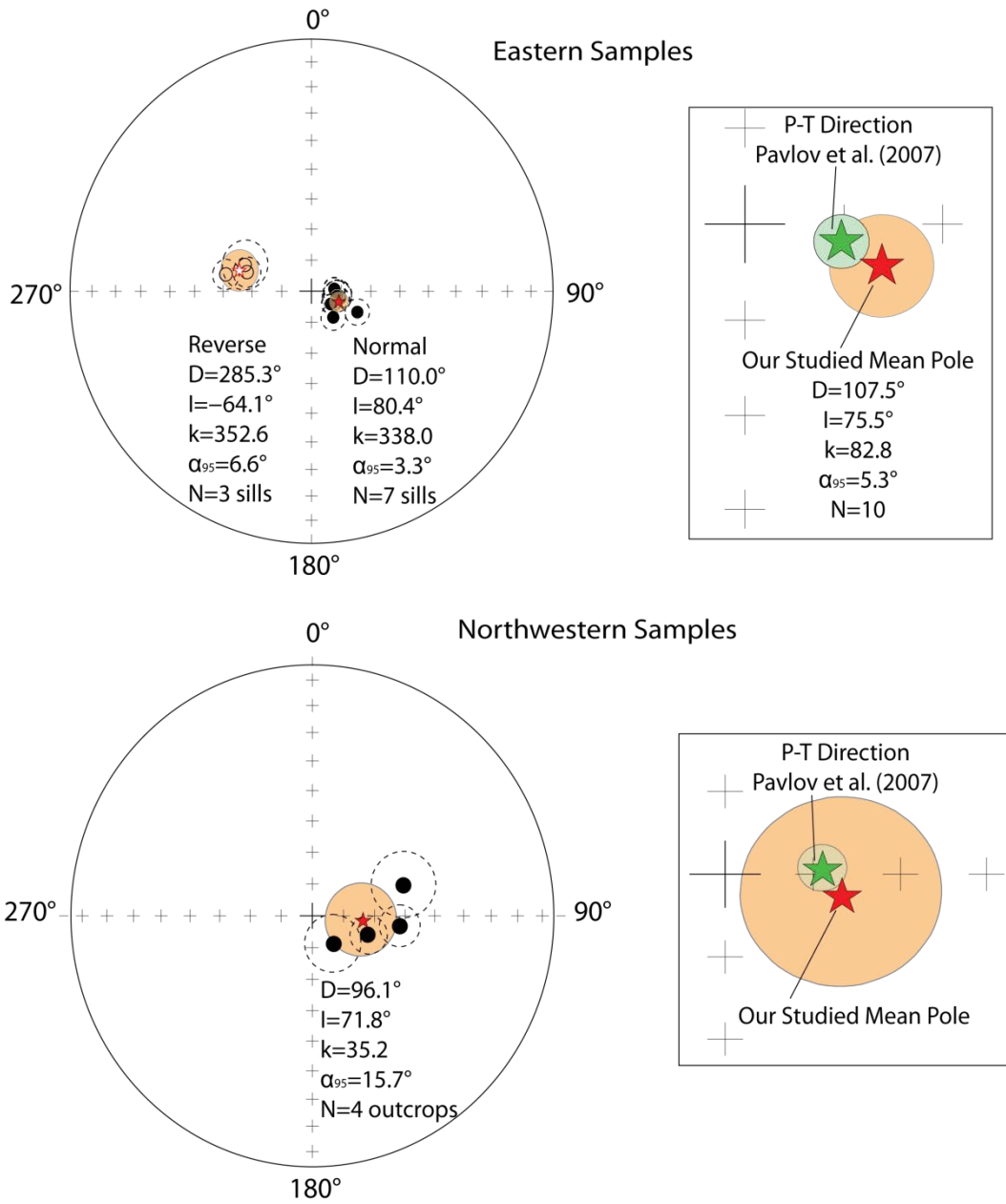


**Figure 2.5** Equal area projections of primary stable paleomagnetic directions for the eastern and northwestern specimens of the Siberian trap basalts. Closed (open) dots represent positive (negative) inclinations. The red star represents the mean direction for the studied localities. The green star corresponds to the expected mean direction calculated from the Permo-Triassic trap reference paleomagnetic poles from Pavlov et al. (2007). Circles around the directions represent the  $\alpha_{95}$  parameter for each sill/outcrop.

**Table 2.1.** Late Permian – Early Triassic basalt mean directions of the high temperature primary stable component of NRM for the Eastern Siberian traps (Aikhal (66.17°N, 111.33° E), Sytikanskaya (66.11°N, 111.80°E), Yubileinaya (66.0°N, 111.7°E) kimberlite mine pit areas) and northwestern Noril'sk sill intrusions (69.21°N, 88.03°E). N is the number of directions for specimens or sites accepted for calculation; D (I) is the declination (inclination) of the NRM in geographic (g) or stratigraphic (s) system of coordinates; k,  $\alpha_{95}$  - precision parameter and half angle radius of the 95% probability confidence cone.

Sill	N	Dg (°)	Ig (°)	Ds (°)	Is (°)	k	$\alpha_{95}$ (°)	Notes
<b>Aikhal</b>								
A1	26	113.3	73.2	-	-	46.0	4.2	Sill near Aikhal kimberlite mine pit
A2	27	102.9	80.2	-	-	78.4	3.2	Aikhal kimberlite mine pit (already published by Kravchinsky et al., 2002)
A3	12	139.1	79.0	-	-	109.2	4.2	Sill near Aikhal kimberlite mine pit
<i>Average</i>	65	118.1	77.8	-	-	236.1	8.0	
<b>Yubileinaya</b>								
Y1	22	97.4	81.2	-	-	42.7	4.8	Sill near Yubileinaya kimberlite mine pit
Y2	21	84.0	82.4	-	-	75.8	3.7	Yubileinaya kimberlite mine pit (already published by Kravchinsky et al., 2002)
Y3	15	100.2	81.4	-	-	58.4	5.0	Sill near Yubileinaya kimberlite mine pit
Y4	15	122.4	82.5	-	-	155.5	3.1	Sill near Yubileinaya kimberlite mine pit
<i>Average</i>	73	100.7	82.1	-	-	1298.8	2.6	
Mean for normal polarity sites	7 sills	110.0	80.4	-	-	338.0	3.3	Aikhal and Yubileinaya sites combined
<b>Sytikanskaya</b>								
S1	16	280.6	-59.8	-	-	61.5	4.7	Sytikanskaya kimberlite mine pit (already published by Kravchinsky et al., 2002)
S2	8	290.5	-65.4	-	-	50.1	7.9	Sill near Sytikanskaya kimberlite mine pit
S3	20	285.7	-66.8	-	-	46.4	4.8	Sill near Sytikanskaya kimberlite mine pit
<i>Average</i>	44	285.3	-64.1	-	-	352.6	6.6	
Mean for reverse polarity sites	3 sills	285.3	-64.1	-	-	352.6	6.6	Sytikanskaya sites combined
<b>Mean for Aikhal, Yubileinaya and Sytikanskaya sills</b>								
	10 sills	107.5	75.5	-	-	82.8	5.3	
<b>Noril'sk</b>								
N1	14	160.6	80.7	291.9	84.3	11.5	12.3	
N2	7	92.7	67.9	44.1	88.0	47.4	8.9	
N3	11	73.6	58.6	101.3	73.9	14.2	12.6	
N4	4	110.4	72.0	162.7	75.4	144.8	7.7	
Mean for Noril'sk intrusion	4 out-crops	96.1	71.8	-	-	35.2	15.7	

### **2.4.3. Absolute Paleointensity**

Typical accepted Arai plots are shown in Figure 2.6 along with the variations of the NRM intensity as a function of temperature, for specimens that met the criteria described in the methodology section.

In accordance with recent studies conducted on historical lava flows (Valet et al., 2010) the suitable specimens are characterized by a sharp decrease of the NRM at high temperatures, which defines the length of the NRM-TRM segment that has been used to calculate the slope. The results of absolute paleointensity have been summarized in Table 2.2 and Table 2.3. Twenty-three out of 341 specimens (82 Aikhal, 104 Noril'sk, 73 Sytikanskaya and 82 Yubileinaya) were characterized by acceptable Arai diagrams, but only eight specimens strictly satisfy the criteria in terms of deviations of their pTRM checks with a mean DEV lower than 10%. Northwestern specimens (Noril'sk) did not meet the reliability criteria described above and have been rejected from the final results. All the accepted sites had a parameter  $\sigma_B/B$  less than 25% (Aikhal: 9.67%, Sytikanskaya: 13.29%, Yubileinaya: 6.00%). The mean geomagnetic field intensity for the three eastern sites obtained from “A” category specimens is  $38.43 \pm 3.01 \mu\text{T}$ , a result that agrees within the error with the value of  $44.93 \pm 4.05 \mu\text{T}$  derived from the “B” category specimens. Both categories agree within error and thus the category B specimens have not been biased by significant changes in magnetic mineralogy during the experiments. The mean paleointensity for the whole category A and B dataset is  $42.62 \pm 3.69 \mu\text{T}$ , which corresponds to a mean virtual dipole moment (VDM) of  $6.01 \pm 1.45 \times 10^{22} \text{ Am}^2$ .

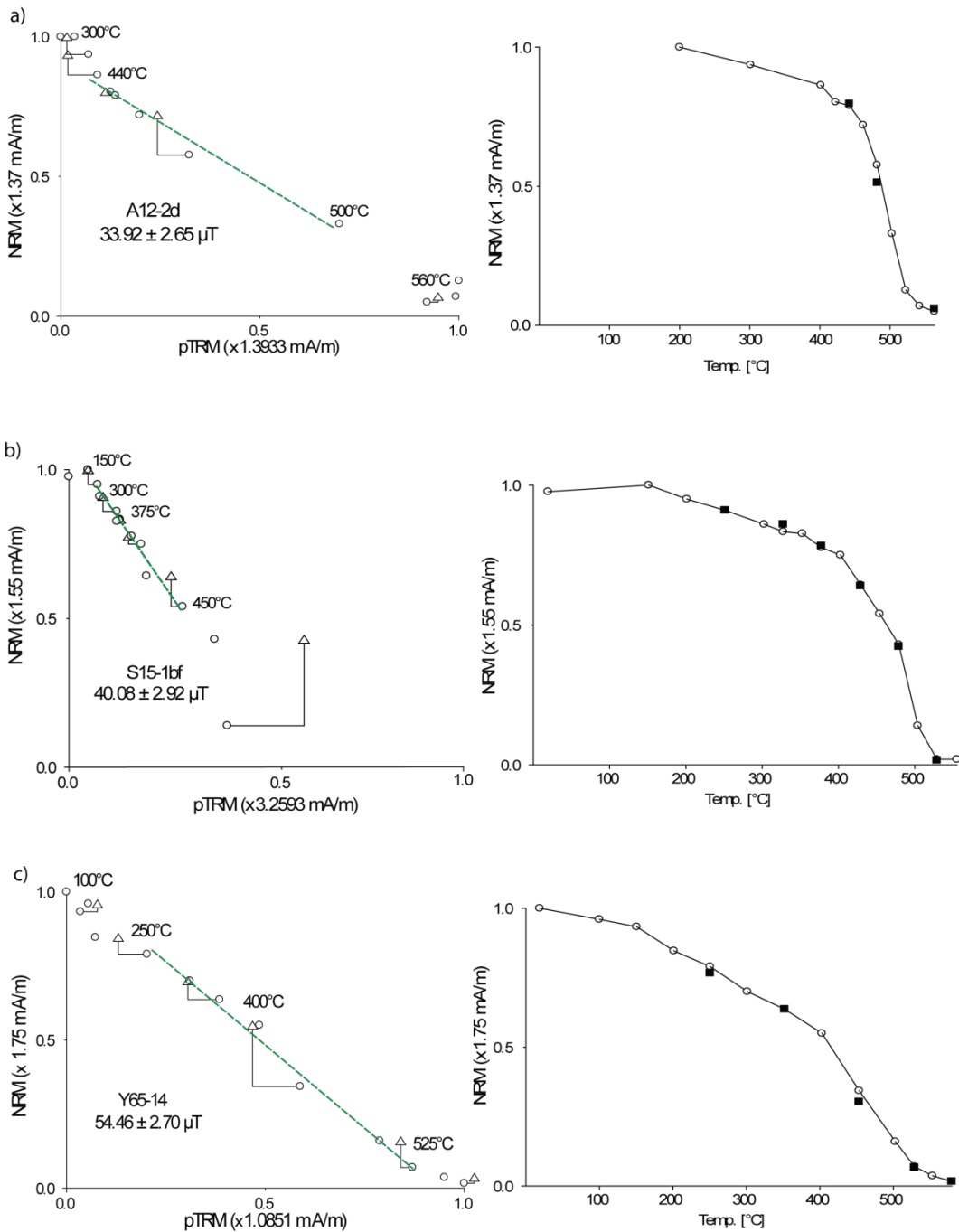


**Figure 2.6.** Typical examples of the paleointensity results for some specimens that met the three criteria listed in the methodology section. NRM vs. pTRM (left hand figures) and NRM as a function of temperature (right hand figures) are shown. Triangles on the NRM vs pTRM plots represent pTRM checks and the faint straight lines represent the temperature interval used for estimating the intensity. Squares on the NRM as a function of temperature plots represent the tail check measurements. (a) Aikhal specimen. (b) Sytikanskaya specimen. (c) Yubileinaya specimens. Noril'sk specimens are not presented because they did not fulfill the paleointensity selection criteria.

## 2.5 Discussion

The average paleointensity from this study for eastern localities is approximately 50% larger than previous studies obtained at the northwest of the province ( $19.3 \pm 7.2 \mu\text{T}$  by Heunemann et al. (2004), and  $14.5 \pm 1.1 \mu\text{T}$  by Shcherbakova et al. (2005)). This result imply that the magnetic field intensity during the Permo-Triassic boundary is similar to the present day variability and that the Mesozoic dipole low could not be straight forwardly extended to the Permo-Triassic boundary.

The suitability of the determinations is constrained by the selection of specimens with high unblocking temperatures. The NRM–TRM diagrams (Figure 2.6) do not show any curvature in the analyzed segments which represent at least 60% of the magnetization and more than 80% for the A category specimens, confirming that the specimens are not influenced by MD grains. Furthermore, all specimens that exhibited mineralogical changes during the heating and cooling curves were rejected from the analysis. In addition, 13 of the accepted results follow the ZI protocol and 10 the IZ protocol (Table 2.2). The results do not present any significant difference between the two protocols; on the contrary they consistently agree within each other. Moreover, the paleomagnetic directions were stable and corresponded to the expected mean values from Kravchinsky et al. (2002) and Pavlov et al. (2007), confirming that the observed vectors represent the primary magnetization.

The possible presence of MD grains in the northwestern specimens might help to explain the differences in the new and previous paleointensity results for the STB. Shcherbakova et al. (2005) provide evidence for the presence of MD grains indicated by the low temperature segments of the Arai plot of specimens from the Noril'sk area (Table 2, Figure 4 and the analysis description in their article). Such features might lead to underestimations of the paleointensity values by 10% (Shcherbakova et al., 2005).

**Table 2.2.** Statistical parameters of the paleointensity results. Site: Nomenclature for each of the studied sites. Class: Category for each of the samples as defined in the text.  $\Delta T$ : Temperature range of the linear segment. Prot: paleointensity protocol applied: ZI, Coe protocol; IZ, Atkin protocol.  $B_{lab}$ : Applied laboratory magnetic field. N: Number of successive data points used for paleointensity calculations.  $\beta$ : measure of linearity (Selkin and Tauxe, 2000). f, is the fraction of the NRM, as defined by Coe et al. (1978) and Prévot et al. (1985). MAD: maximum angular deviation.

Site	Class	$\Delta T(^{\circ}C)$	Prot	$B_{lab}$ ( $\mu$ T)	N	$\beta$	f	MAD( $^{\circ}$ )	Mean DEV (%)
<b>Aikhal</b>									
A2-15c	B	250-525	ZI	25	7	0.05	0.84	1.12	23.0
A03-8a	B	200-475	IZ	50	7	0.08	0.55	5.15	10.0
A04-7a	A	300-520	IZ	50	8	0.05	0.77	7.81	4.4
A08-1B	B	400-550	ZI	30	5	0.1	0.57	2.09	14.0
A10-3a	B	400-525	ZI	35	4	0.08	0.82	0.85	12.0
A12-2a	B	200-475	IZ	50	7	0.1	0.55	5.44	13.0
A12-2d	A	400-520	ZI	40	7	0.05	0.82	1.44	9.5
A17-7a	B	200-475	IZ	50	7	0.1	0.57	5.65	9.0
<b>Sytika-nskaya</b>									
S8-9a	A	450-575	ZI	30	5	0.1	0.95	2.36	7.0
S15-1bf	B	200-450	IZ	40	9	0.07	0.38	2.71	11.0
S28-5b2	B	350-575	ZI	25	7	0.07	0.86	1.99	18.0
S32-4b	B	375-475	ZI	40	5	0.1	0.32	4.86	19.0
S32-4bf	B	375-500	IZ	40	6	0.1	0.49	2.35	9.5
<b>Yubilei-naya</b>									
Y51-3b	A	250-550	ZI	80	7	0.02	0.87	3.36	4.2
Y52-3a	A	300-525	IZ	40	10	0.1	0.89	2.82	3.2
Y52-4a	B	250-525	ZI	35	7	0.04	0.82	2.42	20.0
Y57-6b	B	200-525	ZI	35	8	0.04	0.93	1.78	12.0
Y57-6c	B	200-500	ZI	30	7	0.04	0.89	208	16.0
Y58-2a	A	150-475	IZ	40	11	0.09	0.84	4.81	7.0
Y58-1b	B	150-525	ZI	35	9	0.03	0.86	2.25	13.0
Y65-14	B	100-575	ZI	30	12	0.03	0.96	2.25	12.0
Y71-3aa	A	100-525	IZ	50	13	0.06	0.86	3.23	8.0
Y71-3b	A	200-550	IZ	40	13	0.08	0.78	3.87	5.0

**Table 2.3.** Paleointensity results. Site: Nomenclature for each of the studied sites.  $B \pm \sigma_b$ : paleointensity result with its associated standard deviation.  $VDM \pm \sigma_{VDM}$ : Virtual dipolar moment and its associated standard deviation.

Site	$B \pm \sigma_b$ ( $\mu\text{T}$ )	$VDM \pm \sigma_{VDM}$ ( $\times 10^{22} \text{ Am}^2$ )
<b><i>Aikhal</i></b>		
A2-15c	49.47±2.53	6.81±0.63
A03-8a	47.09±3.83	6.48±0.72
A04-7a	34.77±1.65	4.79±0.43
A08-1B	54.75±10.4	7.54±0.15
A10-3a	28.93±2.24	3.98±0.43
A12-2a	61.40±6.41	8.46±0.11
A12-2d	31.27±1.65	4.31±0.40
A17-7a	53.21±6.13	7.33±0.10
<i>Average</i>	45.11±4.36	6.21±0.78
<b><i>Sytikanskaya</i></b>		
S8-9a	17.96±2.21	2.91±0.44
S15-1bf	40.08±2.92	6.50±0.73
S28-5b2	27.98±2.04	4.54±0.51
S32-4b	40.78±6.77	6.61±0.12
S32-4bf	49.28±9.46	7.99±0.17
<i>Average</i>	35.22±4.68	5.71±0.92
<b><i>Yubileinaya</i></b>		
Y51-3b	36.25±0.98	4.82±0.16
Y52-3a	44.90±7.14	5.97±0.95
Y52-4a	44.70±1.83	5.94±0.26
Y57-6b	41.03±1.67	5.45±0.24
Y57-6c	40.33±1.69	5.36±0.24
Y58-2a	39.48±3.4	5.25±0.46
Y58-1b	44.88±1.18	5.97±0.19
Y65-14	48.98±1.69	6.51±0.25
Y71-3aa	60.82±3.54	8.08±0.49
Y71-3b	42.02±3.47	5.59±0.47
<i>Average</i>	44.34±2.66	5.89±0.37
<i>Total Ave.</i>	42.62±3.69	6.01±1.45

Theory and experiments suggest that longer cooling periods for specimens with PSD or MD grains could yield underestimated paleointensity values (Brown, 1984; Winklhofer et al., 1997; Yu, 2011). Differences in cooling rate would only explain the discrepancy between paleointensity results from this study for the

eastern localities and the previous results for the northwestern localities if the cooling rate of the specimens was faster than that of the northwestern specimens in the previous studies. However, the cooling rate for the studied specimens was either similar or slower than that of the northwestern specimens in the previous studies. The specimens come from near surface intrusions (the studied volcanic area preserves the conical structures of the kimberlite pipes which are typical near surface kimberlite structures), whereas the northwestern specimens in the previous studies are extrusive basalts. Thus higher paleointensity values in this study are real. Moreover, the paleointensity results from the three studied localities are fairly consistent with each other. Significantly, the paleointensity results for both the normal (Aikhal and Yubileinaya) and reverse (Sytikanskaya) polarity localities are higher than those for previous studies, which adds support to the argument that the geomagnetic dipole low is not characteristic of the STB.

## 2.6 Conclusions

In this study the first paleointensity results for the eastern part of the Siberian trap basalt province are reported. Paleomagnetic directions from the eastern ( $D=107.5^\circ$ ,  $I=75.5^\circ$ ,  $k=82.8$ ,  $\alpha_{95}=5.3^\circ$ ,  $N=10$  sills) and northwestern ( $D=95.1^\circ$ ,  $I=71.8^\circ$ ,  $k=35.2$ ,  $\alpha_{95}=15.7^\circ$ ,  $N=4$  outcrops) localities are in excellent agreement with the expected directions calculated from the reference paleomagnetic poles of Pavlov et al. (2007) ( $D=100.6^\circ$ ,  $I=80.1^\circ$ ,  $\alpha_{95}=2.8^\circ$  for the eastern localities and  $D=84.7^\circ$ ,  $I=74.9^\circ$ ,  $\alpha_{95}=3.0^\circ$  for the northwestern locality), confirming that the age interval of the studied specimens correspond to the Permo-Triassic boundary. The northwestern specimens did not meet the reliability criteria for paleointensity and were not used for further analysis. The eastern locality results have distinctly higher VDM values ( $6.01\pm1.45\times10^{22}$  Am $^2$ ) compared to previous studies (Heunemann et al., 2004; Shcherbakova et al., 2005) suggesting: (1) a low intensity of the magnetic field is not characteristic during the Permo-Triassic boundary; and (2) the Mesozoic dipole low cannot be extended until this period of

time. Discrepancies between the present results and previous studies could possibly be explained by the existence of multidomain grains in the northwestern specimens of the previous studies. The mineralogical experiments did not reveal the presence of multidomain grains in the selected specimens for paleointensity analysis. These results suggest that the geomagnetic field intensity at the Permo-Triassic boundary was very close to the observed present-day values.

## Bibliography

- Aitken, M.J., Allsop, A.L., Bussel, G.D., Winter, M.B., 1988. Determination of the intensity of the Earth's magnetic field during archeological times: reliability of the Thellier technique. *Reviews of Geophysics* 26, 3–12.
- Almukhamedov, A.I., Medvedev, A.Ya., Mitchell, C., Zolotukhin, V.V., 1996. Flood basalts in the core of the Tunguska synclinorium: comparative geochemistry. *Russian Geology and Geophysics Novosibirsk*, 37, 3–16 (in Russian).
- Almukhamedov, A.I., Medvedev, A.Ya., Zolotukhin, V.V., 2004. Compositional evolution of the Permian–Triassic basalts of the Siberian Platform in time and space. *Petrology*, 2 (4), 339–353 (in Russian).
- Basu, A.R., Hannigan, R.E., Jacobsen, S.B., 1998. Melting of the Siberian mantle plume. *Geophysical Research Letters*, 25, 2209–2212.
- Biggin, A.J., Thomas, D.N., 2003. Analysis of long-term variations in the geomagnetic poloidal field intensity and evaluation of their relationship with global geodynamics. *Geophysical Journal International*, 152, 392–415.
- Bol'shakov, A.S., Solodovnikov, G.M., 1983. Geomagnetic field intensity in the Late Jurassic and Early Cretaceous. *Izvestiya Academy of Science Physics*. 19, 976–982.
- Bol'shakov, A.S., Solodovnikov, G.M., Vinogradov, Y.K., 1989. Paleointensity of the geomagnetic field in the early Permian. *Izvestiya., Earth Physics (Eng. Trans.)* 25, 70–78.
- Brandt, D., Hartmann, G.A., Yokoyama, E., Catelani, E.L., Trindade, R.I.F., 2009. Paleointensity data from Early Cretaceous Ponta Grossa dikes (Brazil) using a multispecimen method. *Earth, Planets and Space*, 61, 41–49.
- Brown, E.M., 1984. Experiments on TRM intensity dependence on cooling rate. *Geophysical Research Letters*, 3, 205–208.

Coe, R.S., 1967. Paleointensities of the Earth's magnetic field determined from tertiary and quaternary rocks. *Journal of Geophysical Research*, 72, 3247–3262.  
Coe, R.S., Grommé, S., Mankinen, E.A., 1978. Geomagnetic paleointensities from radiocarbon-dated lava flows an Hawaii and the question of the Pacific nondipole low. *Journal of Geophysical Research*, 83, 1740–1756.

Cogné, J.-P., 2003. PaleoMac: a Macintosh™ application for treating paleomagnetic data and making plate reconstructions. *Geochemistry, Geophysics, Geosystems*, 4 (1), 1007. doi:10.1029/2001GC000227.

Courtillot, V., Jaupart, C., Manighetti, I., Tapponnier, P., Besse, J., 1999. On causal links between flood basalts and continental breakup. *Earth and Planetary Scientific Letters*, 166, 177–195.

Courtillot, V., Renne, P.R., 2003. On the ages of flood basalt events. *Comptes Rendus Geoscience*, 335, 113–140.

Dalrymple, G.B., Czamanske, G.K., Fedorenki, V.A., Simonov, O.N., Lanphere, M.A., Likhachev, A.P., 1995. A reconnaissance  $40\text{Ar}/39\text{Ar}$  geochronologic study of orebearing and related rocks, Siberian Russia. *Geochimica et Cosmochimica Acta*, 59, 2071–2083.

Dunlop, D.J., 2002. Theory and application of the Day plot ( $\text{Mrs/Ms}$  vs  $\text{Hcr/Hc}$ ) 1. Theoretical curves and test using titanomagnetite data. *Journal of Geophysical Research*, 107, 4–22.

Enkin, R.J., 1996. A computer program package for analysis and presentation of paleomagnetic data, Pacific Geoscience Center, Geological Survey of Canada.

Elkins Tanton, L.T., Hager, B.H., 2000. Melt intrusion as a trigger for lithospheric foundering and the eruption of the Siberian flood basalts. *Geophysical Research Letters*, 27, 3937–3940.

Fisher, R., 1953. Dispersion on a sphere. *Proceedings Royal Society of London. Series A*. 217, 295–305.

Garcia, A., Thomas, N., Liss, D., Shaw, J., 2006. Low geomagnetic field intensity

during the Kiaman superchron: Thellier and microwave results from the Great Whin Sill intrusive complex, northern United Kingdom. *Geophysical Research Letters*, 33. doi: 10.1029/2006GL026729

Goguitchaichvili, A., Alva-Valdivia, L.M., Urrutia, J., Morales, J., 2002. On the reliability of Mesozoic Dipole Low: New absolute paleointensity results from Parana flood basalts (Brazil). *Geophysical Research Letters*, 29, doi: 10.1029/2002GL015242.

Goguitchaichvili, A., Cejudo Ruiz, R., Sanchez Bettucci, L., Aguilar Reyes, B., Alva- Valdivia, L.M., Urrutia-Fucugauchi, J., Morales, J., Calvo Rathert, M., 2008. New absolute paleointensity results from the Parana Magmatic Province (Uruguay) and the Early Cretaceous geomagnetic paleofield. *Geochemistry, Geophysics, Geosystems*, 9, doi: 10.1029/2008GC002102.

Griffin, W.L., Ryan, C.G., Kaminsky, F.V., O'Reilly, S.Y., Natapov, L.M., Win, T.T., Kinny, P.D., Ilupin, I.P., 1999. The Siberian lithosphere traverse, mantle terranes and the assembly of the Siberian Craton. *Tectonophysics*, 310, 1–35.

Harcombe-Smee, B.J., Piper, J.D.A., Rolph, T.C., Thomas, D.N., 1996. A palaeomagnetic and palaeointensity study of the Mauchline lavas, south-west Scotland. *Physics of the Earth and Planetary Interiors*, 94, 63–73.

Heller, R., Merrill, R.T., McFadden, P.L., 2002. The variation of intensity of earth's magnetic field with time. *Physics of the Earth and Planetary Interiors*, 131, 237–249.

Herrero\_Bervera, E., Valet, J.-P., 2009. Testing determinations of absolute paleointensity from the 1955 and 1960 Hawaiian flows. *Earth and Planetary Scientific Letters*, 287, 420–433.

Heunemann, C., Krupa, D., Soffel, H.C., Gurevitch, E., Bachtadse, V., 2004. Directions and intensities of the Earth's magnetic field during a reversal: results from the Permo-Triassic Siberian trap basalts, Russia. *Earth and Planetary Scientific Letters*, 218, 197– 213.

Kirschvink, J.L., 1980. The least-squares line and plane and the analysis of paleomagnetic data. *Geophysical Journal of the Royal Astronomical Society*, 62, 699–718.

Kosterov, A., Perrin, M., Glen, J.M., Coe, R.S., 1998. Paleointensity of the Earth's magnetic field in early Cretaceous time: The Paraná Basalt. Brazil. *Journal of Geophysical Research*, 103, 9739–9753.

Kravchinsky, V.A., Konstantinov, K.M., Courtillot, V., Savrasov, J.I., Valet, J.P., Cherniy, S.D., Mishenin, S.G., Parasotka, S., 2002. Palaeomagnetism of the east Siberian traps and kimberlites: two new poles and palaeogeographic reconstruction at about 360 and 250 Ma. *Geophysical Journal International*, 148, 1–33.

Kuzmin, M.I., Yarmolyuk, V.V., Kravchinsky, V.A., 2010. Phanerozoic hot spot traces and paleogeographic reconstruction of the Siberian continent based on interaction with the African large low shear velocity province. *Earth Science Reviews*, 102, 29–59.

McClelland, E., Briden, J.C., 1996. An improved methodology for Thellier-type paleointensity determination in igneous rocks and its usefulness for verifying primary thermoremanence. *Journal of Geophysical Research*, 101, 21995–22013.

Pan, Y., Hill, M., Zhu, R., Shaw, J., 2004. Further evidence for low intensity of the geomagnetic field during the early Cretaceous time: using the modified Shaw method and microwave technique. *Geophysical Journal International*, 157, 553–564.

Pavlov, V.E., Courtillot, V., Bazhenov, M.L., Veselovsky, R.V., 2007. Paleomagnetism of the Siberian traps: new data and new overall 250 Ma pole of Siberia. *Tectonophysics*, 443, 72–92.

Prévet, M., Mankinen, E.A., Coe, R.S., Grommé, C.S., 1985. The Steens mountain (Oregon) geomagnetic polarity transition. 2. Field intensity variations and discussion of reversal models. *Journal of Geophysical Research*, 90, 10417–10448.

Prévet, M., El\_Messaoud Derder, M., McWilliams, M., Thompson, J., 1990. Intensity of the Earth's magnetic field: evidence for a Mesozoic dipole low. *Earth and Planetary Science Letter*, 97, 129–139.

Perrin, M., Prevot, M., Mankinen, E.A., 1991. Low intensity of the geomagnetic field in early Jurassic time. *Journal of Geophysical Research*, 96, 14197–14210.

Perrin, M., Shcherbakov, V., 1997. Paleointensity of the Earth's magnetic field for the past 400 Ma: evidence for a dipole structure during the mesozoic low. *Journal of Geomagnetism and Geoelectricity*, 49, 601–614.

Reichow, M.K., Saunders, A.D., White, R.V., Almukhamedov, A.I., Medvedev, A.Ya., 2005. Geochemistry and petrogenesis of basalts from the West Siberian Basin: an extension of Permo-Triassic Siberian Traps, Russia. *Lithos*, 79, 425–452.

Reichow, M.K., Pringle, M.S., Al'Mukhamedov, A.I., Allen, M.B., Andreichev, V.L., Buslov, M.M., Davies, C.E., Fedoseer, G.S., Fitton, J.G., Inger, S., Medvedev, A.Ya., Mitchell, C., Puchkov, V.N., Safonava, I.Yu., Scoot, R.A., Saunders, A.D., 2009. The timing and the extent of the eruption of the Siberian traps large igneous province. Implications for the end-Permian environmental crisis. *Earth and Planetary Science Letters*, 227, 9–20.

Riisager, P., Riisager, J., 2001. Detecting multidomain magnetic grains in Thellier palaeointensity experiments. *Physics of the Earth and Planetary Interiors*, 125, 111–117.

Ruiz, R.C., Goguitchaichvili, A., Geuna, S.E., Alva-Valdivia, L.M., Sole, J., Morales, J., 2006. Early cretaceous absolute geomagnetic paleointensities from Cordoba Province (Argentina). *Earth, Planets and Space*, 58, 1333–1339.

Saunders, A.D., Englend, R.W., Reichow, M.K., White, R.W., 2005. A mantle plume origin for the Siberian traps: uplift and extension in the West Siberian Basin, Russia. *Lithos*, 79, 407–424.

Senanayake, W.E., McElhinny, M.W., 1983. A paleointensity method for use with highly oxidized basalts, and application to some Permian volcanics. *Journal of Geophysics*, 52, 85–96.

Selkin, P.A., Tauxe, L., 2000. Long-term variations in paleointensity. *Philosophical Transactions of the Royal Society of London*, 358, 1065–1088.

Selkin, P.A., Gee, J.S., Tauxe, L., 2007. Nonlinear thermoremanence acquisition and implications for paleointensity data. *Earth and Planetary Science Letters*, 256, 81–89.

Shaar, R., Ron, H., Tauxe, L., Kessel, R., Agnon, A., Ben-Yosef, E., Feinberg, J.M., 2010. Testing the accuracy of absolute intensity estimates of the ancient geomagnetic field using copper slag material. *Earth and Planetary Science Letters*, 290, 201–213.

Shcherbakova, V.V., Shcherbakov, V.P., Vodovozov, V.V., Sycheva, N.K., 2005. Paleointensity at the Permian-Triassic boundary and in the late Permian. *Izvestiya, Physics of the Solid Earth*, 41, 931–944.

Shcherbakova, V.V., Perrin, M., Shcherbakov, V.P., Pavlov, V.E., Ayvaz'yan, A., Zhidkov, G.V., 2009. Rock Magnetic and paleointensity results from Mesozoic baked contacts of Armenia. *Earth, Planets and Space*, 61, 23–39.

Solodovnikov, G.M., 1992. Paleointensity of the geomagnetic field in the lower Permian. *Izvestiya, Earth Physics (Eng. Trans.)*, 28, 718–722.

Solodovnikov, G.M., 1995. Paleointensity of the early Triassic geomagnetic field. *Izvestiya, Earth Physics (Eng. Trans.)*, 30, 815–821.

Tanaka, H., Kono, M., Uchimura, H., 1995. Some global features of paleointensity in geological time. *Geophysical Journal International*, 120, 97–102.

Tarduno, J.A., Cottrell, R.D., 2005. Dipole strength and variation of the time-averaged reversing and nonreversing geodynamo based on Thellier analyses of single plagioclase crystals. *Journal of Geophysical Research*, 110, doi:10.1029/2005JB003970

Tauxe, L., 2006. Long-term trends in paleointensity: The contribution of DSDP/ODP submarine basaltic glass collections. *Physics of the Earth and Planetary Interiors*, 156, 223–241.

Thellier, E., Thellier, O., 1959. Sur l'intensité du champ magnétique terrestre dans le passé historique et géologique. *Annales Geophysicae*, 15, 285–376.

Thomas, D.N., Rolph, T.C., Shaw, J., 1995. Palaeointensity results from the Permo-Carboniferous (Kiaman) reversed superchron: the Great Whin and Midland Valley sills of the northern United Kingdom. *Geophysical Journal International*, 123, 798–816.

Thomas, D.N., Rolph, T.C., Friel, D.F., 1997. Permo-Carboniferous (Kiaman) paleointensity results from the western Bohemian Massif Germany. *Geophysical Journal International*, 130, 257–265.

Valet, J.P., Tric, E., Herrero-Bervera, E., Meynadier, L., Lockwood, J.P., 1998. Absolute paleointensity from Hawaiian lavas younger than 35 ka. *Earth and Planetary Science Letters*, 161, 19–32.

Valet, J.-P., Herrero-Bervera, E., Carlut, J., Kondopoulou, D., 2010. A selective procedure for absolute paleointensity in lava flows. *Geophysical Research Letters*, 37. doi:10.1029/2010GL044100

Vandamme, D., Courtillot, V., 1992. Paleomagnetic constraints on the structure of the Deccan traps. *Physics of the Earth and Planetary Interiors*, 74, 241–261.

Winklhofer, M., Fabian, K., Heider, F., 1997. Magnetic blocking temperatures of magnetite calculated with a three-dimensional micromagnetic model. *Journal of Geophysical Research*, 102, 22,695–22,709.

Yu, Y., Tauxe, L., Gee, J.S., 2007. A linear field dependence of thermoremanence in low magnetic fields. *Physics of the Earth and Planetary Interiors*, 162, 244–248.

Yu, Y., 2011. Importance of cooling rate dependence of thermoremanence in paleointensity determination. *Journal of Geophysical Research*, 116, B09101. doi:10.1029/2011JB008388.

Zhu, R., Pan, Y., Shaw, J., Li, D., Li, Q., 2001. Geomagnetic palaeointensity just prior to the Cretaceous normal superchron. *Physics of the Earth and Planetary Interiors*, 128, 207–222.

Zhu, R., Hoffman, K.A., Pan, Y., Shi, R., Li, D., 2003. Evidence for weak geomagnetic field intensity prior to the Cretaceous normal superchron. *Physics of the Earth and Planetary Interiors*, 136, 187–199.

Zijderveld, J.D.A., 1967. A.C. demagnetization of rocks, analysis of results. In: Methods in paleomagnetism, D.W. Collinson, K.M. Creer, and S.K. Runcorn, eds., Elsevier, Amsterdam, 254–286.

## **Chapter 3\***

# **Paleomagnetic dating of Phanerozoic kimberlites in Siberia**

### **3.1 Introduction**

Paleomagnetic data have often been used to estimate the ages of ore deposits and kimberlite fields over the world (Gregory et al., 2006; Hargraves and Onstott, 1980; Jones, 1968; Jones and McElhinny, 1966; Konstantinov and Stegnitskii, 2012; Kravchinsky et al., 2009; Malone et al., 2008; Symons and Arne, 2005; Symons et al., 1999; Wynne et al., 1992; among other studies). The aim in this contribution is to date four Siberian kimberlite pipes for which radiometric age dating has not provided reliable age estimates. This paper also introduces a quantitative method to estate a paleopole paleomagnetic age with respect to an assumed apparent polar wander path (APWP). Previous studies (Kravchinsky et al., 2002) reported high quality paleomagnetic data from Siberian kimberlites and confirmed that the magmatism coincided with Late Devonian and Permo-Triassic rifting events. The ages of the kimberlite intrusions are important for the origin of large-scale magmatic events in Siberia and will help industry to search for prospective areas for future diamond exploration.

### **3.2 Geological Settings**

A chain of Paleozoic to Mesozoic age kimberlites stretches for 1000 km in a SW–NE direction across the north-central part of the Siberian platform, and other trail of Mesozoic kimberlites extends for ~320 km to the northwest from the center of the platform along the eastern boundary of the Anabar Shield (Figure

\* This chapter has been published in the Journal of Applied Geophysics, 88, 139-153, 2013.

3.1). The Siberian kimberlites are thought to be emplaced during three main epochs: the Devonian–Early Carboniferous, the Triassic, and the Cretaceous (Brakhfogel, 1984). On the eastern side of the Siberian platform, the Devonian Viluy and Kyutungda aulacogens extend into the platform from the ancient passive margin. All Devonian to Early Carboniferous kimberlite exposures are situated between these aulacogens. The Devonian and Triassic kimberlites are associated with Late Devonian–Lower Carboniferous and Permo-Triassic intraplate mafic volcanism (Kravchinsky et al., 2002). Cretaceous kimberlites are exposed in the north Siberian platform on the slopes of the Olenek uplift. They are likely connected with intraplate magmatism in the arctic area as described in Kuzmin et al. (2010). The Viluy aulacogen (Figure 3.1) includes 7–8 km of Upper Devonian–Lower Carboniferous evaporite sedimentary rocks and bimodal volcanic rocks. The ~50 km wide Kyutungde aulacogen is filled with Upper Devonian–Lower Carboniferous evaporite rocks (Masaitis et al., 1975; Oleinikov, 1979; Shpount and Oleinikov, 1987).

Isotopic age data and geologic age estimates for the kimberlites have been summarized by Brakhfogel (1984), Krivonos (1997), Griffin et al. (1999), and Agashev et al. (2004). However, there are major differences among age estimates for a given kimberlite pipe obtained by different methods. Griffin et al. (1999) emphasized this problem for several kimberlite fields. For instance, the authors noted that some age estimates based on K–Ar data were significantly older than estimates by other methods and in several cases they contradicted stratigraphic and paleontologic age estimates, which suggested the presence of excess argon in the K–Ar method. Currently, it is not possible to date every kimberlite pipe because of differences between geologic and absolute age determination methods.

The Udachnaya kimberlite pipes ( $66^{\circ}26'N$ ,  $112^{\circ}19'E$ ) are located in the Daldyn kimberlite field (Figure 3.1). The field includes a broad band of diamondiferous Devonian to Carboniferous kimberlites that extends from the central to north-central part of the Siberian platform (Ashchepkov et al., 2010). The Udachnaya

kimberlite consists of two intersecting intrusions, the smaller eastern and larger western pipes. These pipes cut Cambrian and Ordovician limestones, dolomites, and siltites. Kinny et al. (1997) and Griffin et al. (1999) reported high resolution ion-microprobe U–Pb perovskite ages of  $367 \pm 5$  Ma for the Eastern Udachnaya pipe and  $361 \pm 4$  and  $353 \pm 5$  Ma for the Western Udachnaya pipe. Other absolute dating methods on various kimberlite pipes in the region yield dates of 364–461 Ma (fission track zircon), 344–358 Ma (U–Pb zircon),  $350 \pm 13$  Ma (Rb–Sr, Svetlaya pipe), and 335–365 Ma (K–Ar, Moskvichka pipe). Recently, Maas et al. (2005) obtained an age estimate of  $347 \pm 5$  Ma using U–Pb isotope dating for the Eastern Udachnaya pipe. Carbonate rock xenoliths with faunas including brachiopods, tetracorallians, tabulates, ostracods, tentaculites, and trilobites of Middle–Late Devonian age were found in the neighboring Alakit–Markha kimberlite field and this age was extrapolated to the Daldyn kimberlite field (Krivonos, 1997). Thus the age of the whole kimberlite field is considered to be Late Devonian–Early Carboniferous.

The Eastern Udachnaya pipe consists of massive kimberlite and kimberlite breccias and contains the freshest and most abundant mantle xenoliths from Siberia (Ionov et al., 2010). A recent excavation exposed exceptionally fresh kimberlites at deeper levels in the pit, which is nearly 600 m deep. The kimberlite is free of serpentine, and it contains fresh olivine and “exotic” volatile-bearing minerals (chlorides, carbonates) of inferred magmatic origin (Ionov et al., 2010; Kamenetsky et al., 2009). The Western Udachnaya pipe is composed of altered kimberlite that does not contain fresh minerals.

The Malo-Botuoba kimberlite field consists of several pipes, including Mir, Trubka-1, Amakinskaya, International, and Taezhnaya (Figure 3.1). The Paleozoic basement sedimentary rocks of this kimberlite province are exposed close to the Viluy autogen in the center of the Siberian platform around the southern Anabar Shield. The subvertical oval-shaped International kimberlite pipe (coordinates:  $62.5^\circ\text{N}$ ,  $113.0^\circ\text{E}$ ) was sampled at different levels of a quarry that

had reached a depth of 284 m when its excavation was halted in 1980. The gem quality of the International pipe's diamonds is unique in the global market. The pit boundaries of the kimberlite pipe are 90×55 m.

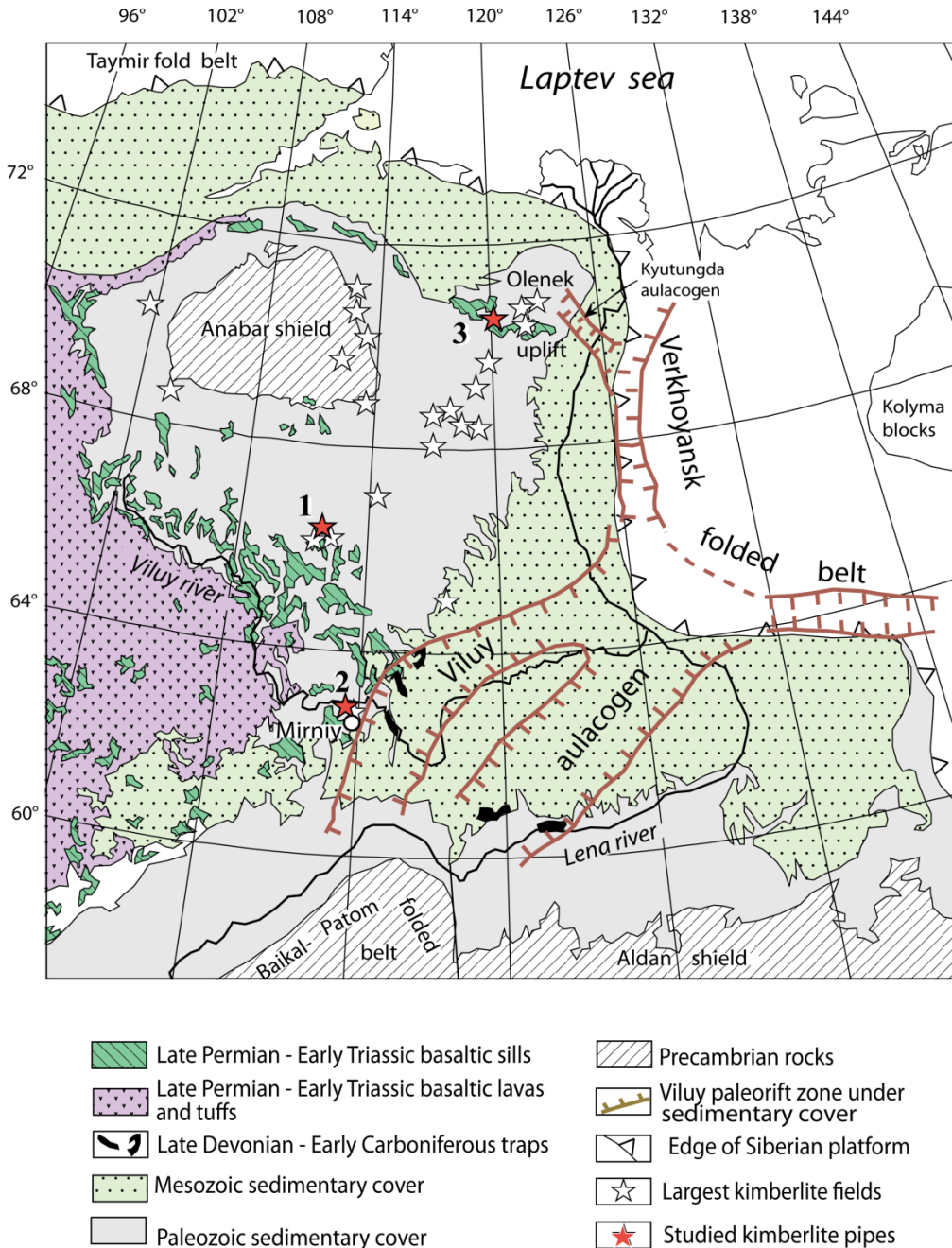


**Figure 3.1.** Simplified equal area projection geological map of the northeastern part of the Siberian platform (Kravchinsky et al., 2002). Sampling localities are as follows: 1 — Daldyn kimberlite pipe field (Eastern and Western Udachnaya pipes); 2 — Malo-Botuoba kimberlite pipe field (International pipe); 3 — Kuoika kimberlite pipe field (Obnazhennaya pipe).

Isotopic age data for the Malo-Botuoba kimberlite field are inconsistent (Griffin et al., 1999; Krivonos, 1997). Fission track zircon dates are mainly between 358 and 397 Ma. U–Pb zircon dating gives dates from 344 to 403 Ma. For the Mir pipe the K–Ar age estimate is  $403 \pm 15$  Ma and the Rb–Sr age estimate is  $324 \pm 11$  Ma. Mafic rocks of Late Devonian age are xenoliths (Krivonos, 1997). The pipe cuts across a Late Devonian mafic sill and contains its xenoliths. Conglomerate clasts from these pipes have been found in Carboniferous and Jurassic rocks of the region. Thus, the Late Devonian–Early Carboniferous age of this field is about 340–400 Ma. Kravchinsky et al. (2002) demonstrated that the magnetization of the Mir kimberlite pipe was reset in Permo-Triassic time due to Siberian trap volcanism at the Permo-Triassic boundary.

The Obnazhennaya kimberlite pipe belongs to the Kuoyka kimberlite field. The pipe contains mantle xenoliths of eclogite, pyrope, peridotite, Permo-Triassic flood basalts, Vendian and Cambrian limestones and dolomites as well as Jurassic fossils including a belemnite rostra from the Late Jurassic (Malkov, 2008). Some of the kimberlite pipes of the Kuoyka kimberlite field such as the Piatnitsa and Slyudianka pipes cut Permian sedimentary rocks and contain xenoliths of Jurassic sediments with poorly preserved fragments of leaves and of Permo-Triassic mafic lavas (Malkov, 2008). U–Pb perovskite age determinations of Kuoyka kimberlites has given 147.7 Ma (Slyudianka pipe), 150.9 Ma (Muse pipe), 151.2 Ma (Tokur pipe), 149.9 Ma (Irina pipe) (Brakhfogel, 1984) and 157 Ma (D'yanga pipe) (Agashev et al., 2004). Zircon has not been detected in the Obnazhennaya pipe. Its age has been determined to be 135 Ma using Rb–Sr whole rock and to range between 128 and 170 Ma using U–Pb method on perovskites nearby picrite bodies (Kinny et al., 1997). Overall, the age of the Kuoyka kimberlite field, including the Obnazhennaya pipe, is commonly considered to be Middle–Late Jurassic.

### **3.3 Methods**

#### **3.3.1 Laboratory Techniques**

Kimberlites as oriented blocks were sampled from 58 sites and 17 localities, from which two to five oriented  $8\text{ cm}^3$  cubic specimens were cut, giving a total of four hundred specimens. All samples are oriented in *in-situ* only coordinate because of the absence of any folding in the central parts of the Siberian platform. Stepwise thermal demagnetizations and magnetic measurements of the specimens were carried out in the paleomagnetic laboratories at the Physics Department of the University of Alberta, Canada, and at the Russian Academy of Sciences, at Irkutsk, Rusia.

Thermal demagnetization was performed using an ASC thermal demagnetizer oven, model TD48-SC, housed in three concentric  $\mu$ -metal shields. The residual field was about 10 nT in the center of the oven. The samples were demagnetized in 10–50 °C steps up to 600–650 °C, and the remanent magnetization was measured with a 2-G Enterprise cryogenic magnetometer (model 755-1.65) and a JR-4 spinner magnetometer. All the measurements were done in a shielded room. Magnetic susceptibility was measured with a Bartington MS2 magnetic susceptibility meter. Data were processed using Enkin (1996) and Cogné (2003) PaleoMac paleomagnetic software. Zijderveld (1967) diagrams were constructed for each sample, and the results were analyzed using principal component analysis (Kirschvink, 1980). The site mean directions were calculated using Fisher (1953) statistics. The combined analysis technique of McFadden and McElhinny (1988) was used when dealing with mixed populations of directions and remagnetization great circles with sector constraints (Halls, 1976; McFadden and McElhinny, 1988).

Isothermal remanent magnetization (IRM) experiments, thermomagnetic curves (Curie point measurements), and hysteresis loop measurements were performed using a Variable Field Translation Balance (VFTB) in the paleomagnetic

laboratory at the University of Alberta and at the Munich Institute of Applied Geophysics.

### 3.3.2. Paleomagnetic Dating Techniques

To determine the age of the kimberlites, the estimated pipe mean paleomagnetic poles were compared to the Siberian APWP reported in Cocks and Torsvik (2007). Their APWP spline without the 275 Ma pole of Pisarevsky et al. (2006), i.e., their alternative model B, was used. Cocks and Torsvik (2007) considered model B to be the most probable path. To ensure the quality of the age determination, the angular distance between the resultant pole and every point on the APWP was calculated. The age was estimated based on the minimum angular distance between the analyzed point and the APWP. To perform the calculation, two unit vectors were defined,  $\mathbf{S}$  for the obtained paleomagnetic pole:

$$\begin{aligned} S_x &= \cos(\lambda_s) \times \cos(\varphi_s), \\ S_y &= \cos(\lambda_s) \times \sin(\varphi_s), \\ S_z &= \sin(\lambda_s), \end{aligned} \quad (3.1)$$

and  $\mathbf{P}$  for the points on the reference APWP:

$$\begin{aligned} P_x &= \cos(\lambda_p) \times \cos(\varphi_p), \\ P_y &= \cos(\lambda_p) \times \sin(\varphi_p), \\ P_z &= \sin(\lambda_p), \end{aligned} \quad (3.2)$$

where  $\lambda_s$  and  $\varphi_s$  represent the latitude and the longitude of the obtained paleomagnetic pole and  $\lambda_p$  and  $\varphi_p$  the latitude and longitude of the APWP points. The angular distance  $\psi$  is given by the dot product between the two vectors:

$$\psi = \cos^{-1}(\mathbf{S} \cdot \mathbf{P}). \quad (3.3)$$

To improve the fit of the age determination, the sampling rate of the APWP was increased to 2 Myr by applying a linear interpolation between the points of the path. To calculate the uncertainty in age, the confidence cone angle  $A_{95}$  for each

of the studied sites was projected at the minimum distance point on the APWP (Figure 3.2). The uncertainty is equal to the intersection between the confidence circle and the APWP path and was calculated as:

$$E = \{(i_1 - m) + (m - i_2)\}/2. \quad (3.4)$$

where  $i_1$  and  $i_2$  are the intersection ages and  $m$  is the minimum point age.

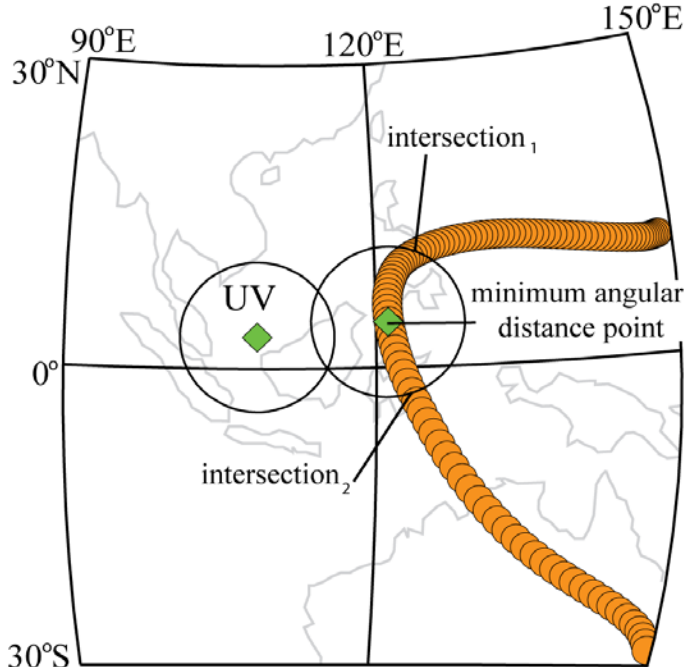


**Figure 3.2.** Procedure used to determine the error in the paleomagnetic age determination. The pole and the circle of confidence are projected over the minimum distance point on the APWP. The intersection points will constrain the error in age. The final uncertainty is given by an average of the two intersection points.

## 3.4 Paleomagnetic Results

### 3.4.1 Rock-magnetic Properties of the Studied Kimberlites

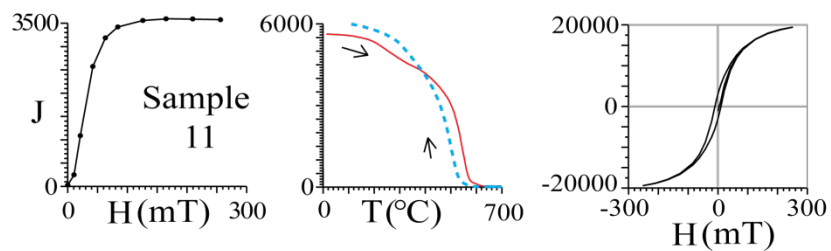
Three different behaviors (A, B, C) were defined by rock-magnetic experiments (Figure 3.3). Behaviors A and B were obtained for all four studied kimberlite pipes. Behavior (C) was observed only in the International pipe. In the first case (sample 11), saturation of IRM was attained at 100–120 mT. The thermomagnetic curves are almost reversible with a Curie temperature of 580 °C. The shape of the

hysteresis curve is compatible with a relatively narrow distribution of single or pseudosingle domain magnetite grains. It can be inferred that this sample was dominated by magnetite or low-titanium titanomagnetite. The magnetization of sample 3 (type B) is saturated in a relatively high field (250 mT). In contrast, sample 11 showed a marked increase of magnetization beyond 400 °C, which is typical of titanomagnetite being transformed into magnetite. Titanomagnetite is identified in Eastern Udachaya by mineralogical studies (Kamenetsky et al., 2004). During transformation, the parent spinel breaks down into magnetite and the Curie point rises (Dunlop and Özdemir, 1997), explaining the increase of magnetization on sample 11.

Saturation isothermal remanent magnetization (SIRM) acquisition of type C (sample 9) indicated the presence of two components with medium and high coercitivity, these could be related to the presence of sulfides like pyrrhotite. The thermomagnetic results show the formation of a strongly magnetic component, presumably magnetite, during cooling. Because the primary magnetization may not be carried by magnetite, the natural remanent magnetization (NRM) results from the International pipe must be considered with caution.

### Type A

Western  
Udachnaya  
pipe



Eastern  
Udachnaya  
pipe

### Type B

Obnazhennaya  
pipe

Obnazhennaya  
pipe

### Type C

International  
pipe

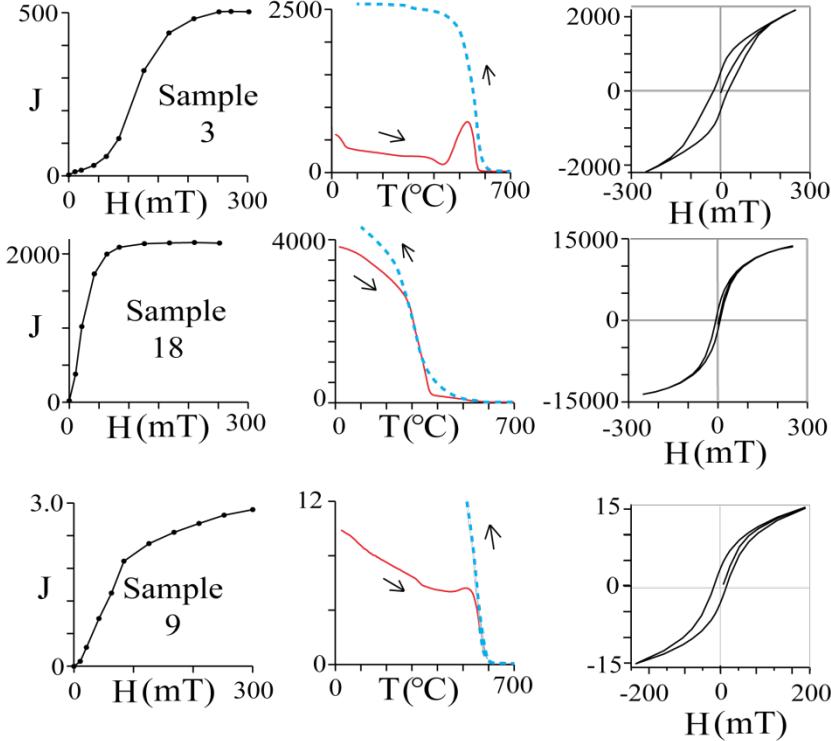


**Figure 3.3.** Typical results of rock magnetic experiments for kimberlite samples from the Eastern Vostochnaya, Western Udachnaya, International, and Obnazhennaya pipes. Isothermal remanent magnetization (IRM) acquisition curves (left), Curie point thermomagnetic curves  $J_s(T)$  (center), and hysteresis loop (right).  $J$  is the isothermal remanence intensity ( $10^{-4} \text{ Am}^2 \times \text{m}^3/\text{kg}$ ),  $H$  is the magnetizing field intensity in millitesla,  $T$  is the temperature in Celsius degrees, respectively.

### **3.4.2 Kimberlites from the Eastern Udachnaya Pipe**

Two characteristic components were identified in the 14 sites from the Eastern Udachnaya kimberlite pipe (Figure 3.4). The low temperature component (LTC), isolated between room temperature and 300 °C, has an average direction of: D=356.9°, I=72.2° (k=65.9, α95=5.1°, N=13 sites) (Table 3.1). This direction is close to the Earth's present field direction in the region (D=352°, I=81.8°), which is interpreted to be a present-day viscous magnetization overprint. The high temperature component (HTC) was isolated between 200–300 °C and 550 °C and converged toward the origin of orthogonal demagnetization diagrams. Most of the samples demonstrated behavior identical to 22T2UV and 26T13UV during demagnetization (Figure 3.4). Only a few samples did not display long linear segments at high temperatures and for them the HTC was evaluated using remagnetization circle analysis. The mean direction of the HTC is D=4.3°, I=−44.5° (k=29.4, α95=7.4° N=14 sites) (Figure 3.4, Table 3.1). There is no folding in the central part of the Siberian platform, and therefore no fold test could be applied.

## Eastern Udachnaya kimberlite pipe

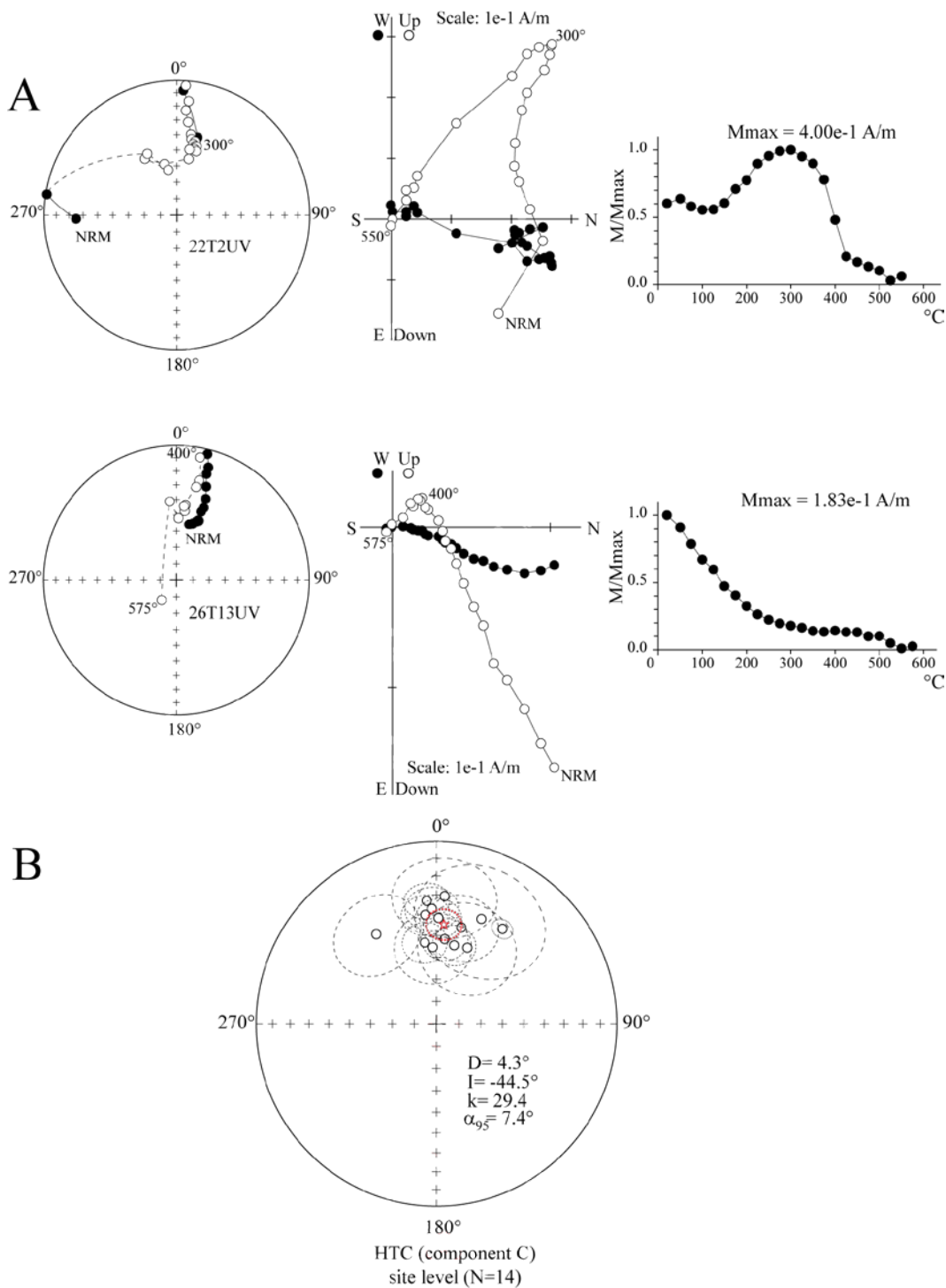


**Figure 3.4.** (A) Typical equal-area projections illustrating demagnetization paths during experiments, and thermal demagnetization orthogonal vector plots in-situ coordinates (Zijderveld, 1967) for samples from the Eastern Udachnaya pipe. Closed (open) symbols in orthogonal plots represent projections onto the horizontal (vertical) plane; temperature steps are indicated in Celsius degrees ( $^{\circ}\text{C}$ ). NRM: natural remanent magnetization. M/Max: ratio of the measured

magnetization respect to the maximum magnetization value (in amperes per meter). (B) Equal-area projections of site-mean directions of high temperature (HTC) component, with circles of 95% confidence. Open symbols: upward inclinations. Star: mean formation direction D: declination, I: inclination, k: precision parameter,  $\alpha_{95}$ : radius of the 95% probability confidence circle, N: number of specimens at site level.

**Table 3.1.** Site mean paleomagnetic directions for the high temperature components for the Eastern Udachnaya pipe (66.9°N, 112.5°E); the Western Udachnaya pipe (66.9°N, 112.5°E); and the host sediments and sediments from the baked contact zone.

Site/Unit	n	D(°)	I(°)	k	$\alpha_{95}$ (°)	Notes
<i>Eastern</i>						
<i>Udachnaya pipe</i>						
UV_01	11	355.4	-32.8	28.7	9.1	3d+8cc
UV_02	3	35.1	-36.5	741.6	4.5	3d
UV_03	5	5.6	-51.4	59.0	10.0	5d
UV_04	8	325.8	-40.3	10.0	18.8	5d+3cc
UV_05	7	14.6	-44.6	15.3	15.9	7d
UV_06	6	12.8	-53.6	51.6	9.4	6d
UV_07	5	22.3	-52.8	14.3	21.5	4d+1cc
UV_08	6	357.2	-55.4	17.0	16.7	6d
UV_09	11	23.4	-37.4	3.6	27.5	5d+6cc
UV_10	5	3.7	-30.5	15.4	20.7	4d+1cc
UV_11	10	357.7	-36.9	20.9	10.9	8d+2cc
UV_12	9	354.1	-39.7	29.6	9.9	5d+4cc
UV_13	9	1.1	-41.5	30.7	9.5	8d+1cc
UV_14	10	351.7	-52.8	26.1	9.6	10d
UV mean	14 sites	4.3	-44.5	29.4	7.4	
<i>Western</i>						
<i>Udachnaya pipe</i>						
UZ-1	7	7.9	-75.1	25.5	12.2	7d
UZ-2	6	31.9	-76.1	17.3	16.6	6d
UZ-3	8	8.7	-63.4	13.2	15.9	7d+1cc
UZ-4	9	358.9	-62.8	15.7	13.8	5d+4c
UZ-5	9	312.1	-65.5	22.1	11.2	9d
UZ-6	6	308.5	-28.8	15.9	17.7	1d+5cc
UZ mean	6 sites	340.5	-65.6	12.9	19.4	
<i>Host Sediments</i>	21 samples	6.1	-12.4	26.6	6.3	14d + 7cc
<i>Baked Contact zone</i>	7 sites	29.3	-28.3	15.8	15.7	

n: number of directions for samples or sites accepted for calculation; D (I): declination (inclination) of the characteristic component of NRM in geographic coordinates; k: precision parameter;  $\alpha_{95}$ : radius of the 95 per cent probability confidence circle. Entry d or cc in Notes means number of directions or great circles accepted for calculations; if there is no entry this means that only directions were accepted for the calculation.

### 3.4.3 Sediments Near the Eastern Udachnaya Kimberlite Pipe

The Eastern Udachnaya pipe intrudes through the carbonate and fine sandstone sediments of the Early Ordovician Oldondinskaya Formation with a Tremadocian–Arenigian age of 505–478 Ma. The Oldondinskaya samples were taken 500 m away from the contact of  $400 \times 350$  m<sup>2</sup> kimberlite pipe. The formation's bedding is horizontal, and the kimberlite pipe cuts the horizontal strata. The LTC component calculated for 21 samples ( $D=342.3^\circ$ ,  $I=77.3^\circ$ ,  $k=255.6$ ,  $\alpha_{95}=2.0^\circ$ ; Figure 3.5, Table 3.1) was easily removed below to 300 °C and coincided with the present-day Earth's geomagnetic field, therefore, it is interpreted to be the present day overprint.

Although the magnetization of the host sedimentary rocks is four orders of magnitude weaker than that of the kimberlites, about 65% of the samples studied revealed a high temperature component between 300 °C and 400–450 °C. Above this temperature oxidation occurred during heating and magnetic susceptibility increased radically, indicating severe mineralogical changes. The brownish color of the sedimentary rocks that appeared during heating likely indicates the transformation of magnetite to hematite. The mean direction for the high temperature component, calculated from 21 samples, is  $D=6.1^\circ$ ,  $I=-12.4^\circ$  ( $k=26.6$ ,  $\alpha_{95}=6.3^\circ$ ; Figure 3.5, Table 3.1). This direction differs radically from that of the Eastern Udachnaya kimberlite and, therefore, we conclude that the area was not reheated by metamorphism related to the Permo-Triassic traps. Therefore, both the kimberlites and sedimentary rocks most likely preserve a primary magnetization associated with kimberlite emplacement.

## Host sediments near the kimberlite pipe Udachnaya (Late Cambrian)

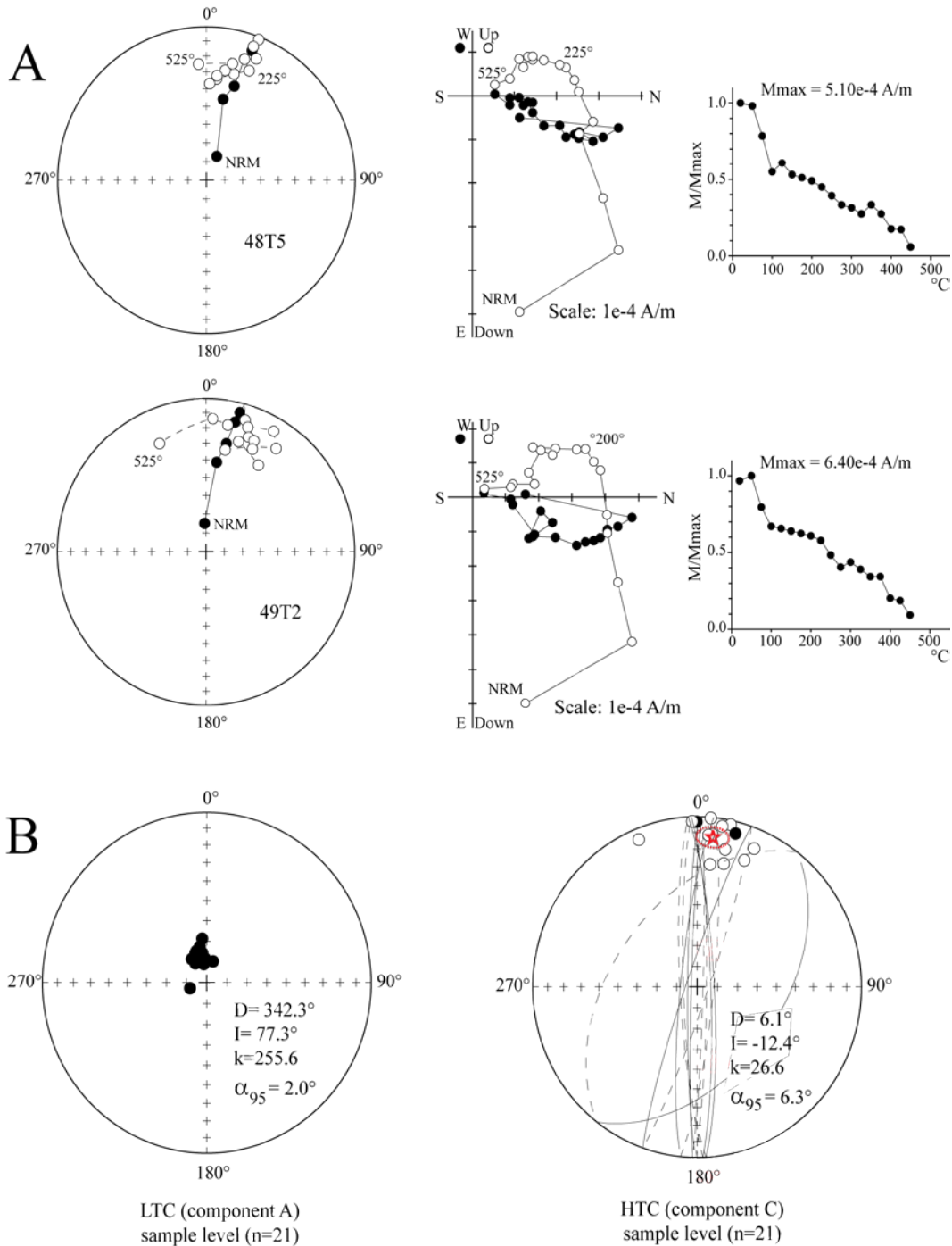


**Figure 3.5.** (A) Typical equal-area projections, orthogonal vector plots and remanence intensity decay plots for the host sediments near the kimberlite pipe Udachnaya. Plotting conventions as in Figure 3.4A. (B) Equal-area projections of the low temperature component (LTC) and high temperature component (HTC) for the host sediments. Plotting conventions as in Figure 3.4B, except n: number of specimens at sample level.

### **3.4.4 Kimberlites from the Western Udachnaya Pipe**

The Western Udachnaya pipe is situated beside the Eastern Udachnaya kimberlite pipe. The LTC from  $<300^{\circ}\text{C}$  gives a direction of  $D=325.5^{\circ}$ ,  $I=73.8^{\circ}$  ( $k=25.0$ ,  $\alpha_{95}=5.0^{\circ}$ ,  $n=34$  samples) (Table 3.1, Figure 3.6). The HTC demagnetization response is very similar to that of the Eastern Udachnaya kimberlite. The mean direction isolated between  $300^{\circ}\text{C}$  and  $550\text{--}580^{\circ}\text{C}$  is  $D=340.5^{\circ}$ ,  $I=-65.6^{\circ}$  ( $k=12.9$ ,  $\alpha_{95}=19.4^{\circ}$ ,  $N=6$  sites) (Table 3.1, Figure 3.6). The direction differs noticeably from the mean value of the Eastern Udachnaya kimberlite, which may indicate a different age of magnetization for Eastern and Western kimberlite pipes.

## Western Udachnaya kimberlite pipe

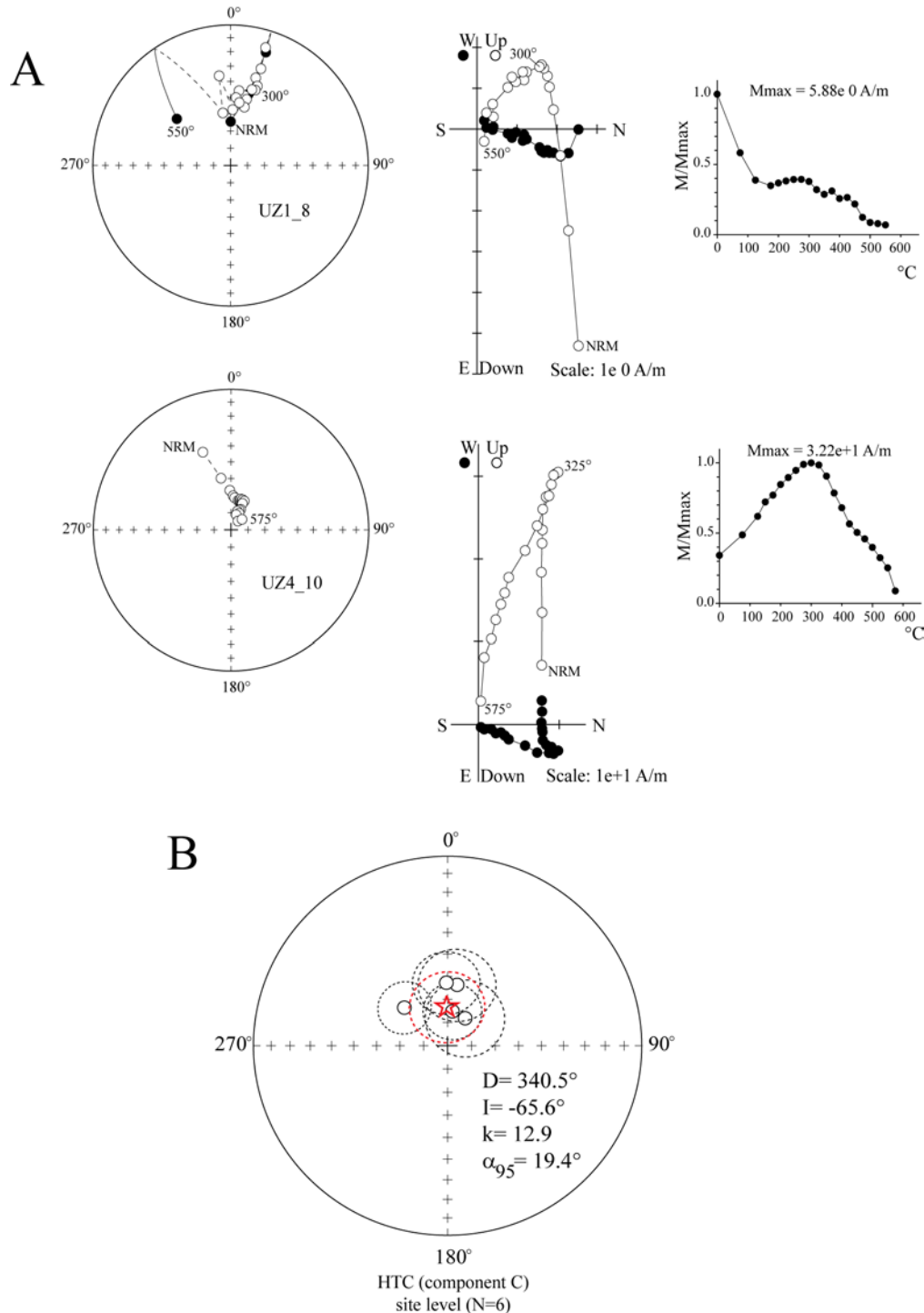


**Figure 3.6** (A) Typical equal-area projections, orthogonal vector plots and remanence intensity decay plots for the Western Udachnaya pipe. Plotting conventions as in Figure 3.4A. (B) Equal-area projections of the high temperature component (HTC) for the pipe. Plotting conventions as in Figure 3.4B.

### **3.4.5 Sedimentary Rocks from the Baked Contact of the Western Udachnaya Kimberlite Pipe**

Sedimentary rocks along a perpendicular profile to the Western Udachnaya kimberlite pipe's contact were sampled to perform a baked contact test. The agreement between the primary magnetization direction of the pipe and the adjacent baked rocks provides confidence with respect to the stability of the primary natural remanent magnetization of the intrusive body (Butler, 1998). Sediments from the contact are harder and visibly metamorphosed. Only the HTC is well-preserved from room temperature to 380–440 °C (Figure 3.7). Magnetic susceptibility and NRM intensity increased rapidly. When the samples were heated above 440 °C the heating was accompanied by a change in color towards red, indicating the likely transformation of magnetite to hematite. Mean HTC directions for the seven sites are scattered, ranging from shallow to steeper inclinations. The mean site direction is as follows:  $D=29.3^\circ$ ,  $I=-28.3^\circ$  ( $k=15.8$ ,  $\alpha_{95}=15.7^\circ$ ,  $N=7$  sites) (Table 3.1). This direction is very different from those of the kimberlites and host sedimentary rocks. The result implies that regional remagnetization did not occur in either the sediments or kimberlites by Permo-Triassic traps because they all possessed different HTC directions. The mean direction from the baked contact sedimentary rocks is likely the unresolved superposition of the primary magnetization of the host rocks by partial remagnetization caused by the kimberlite intrusion.

## Remagnetised Sediments from the baked contact zone

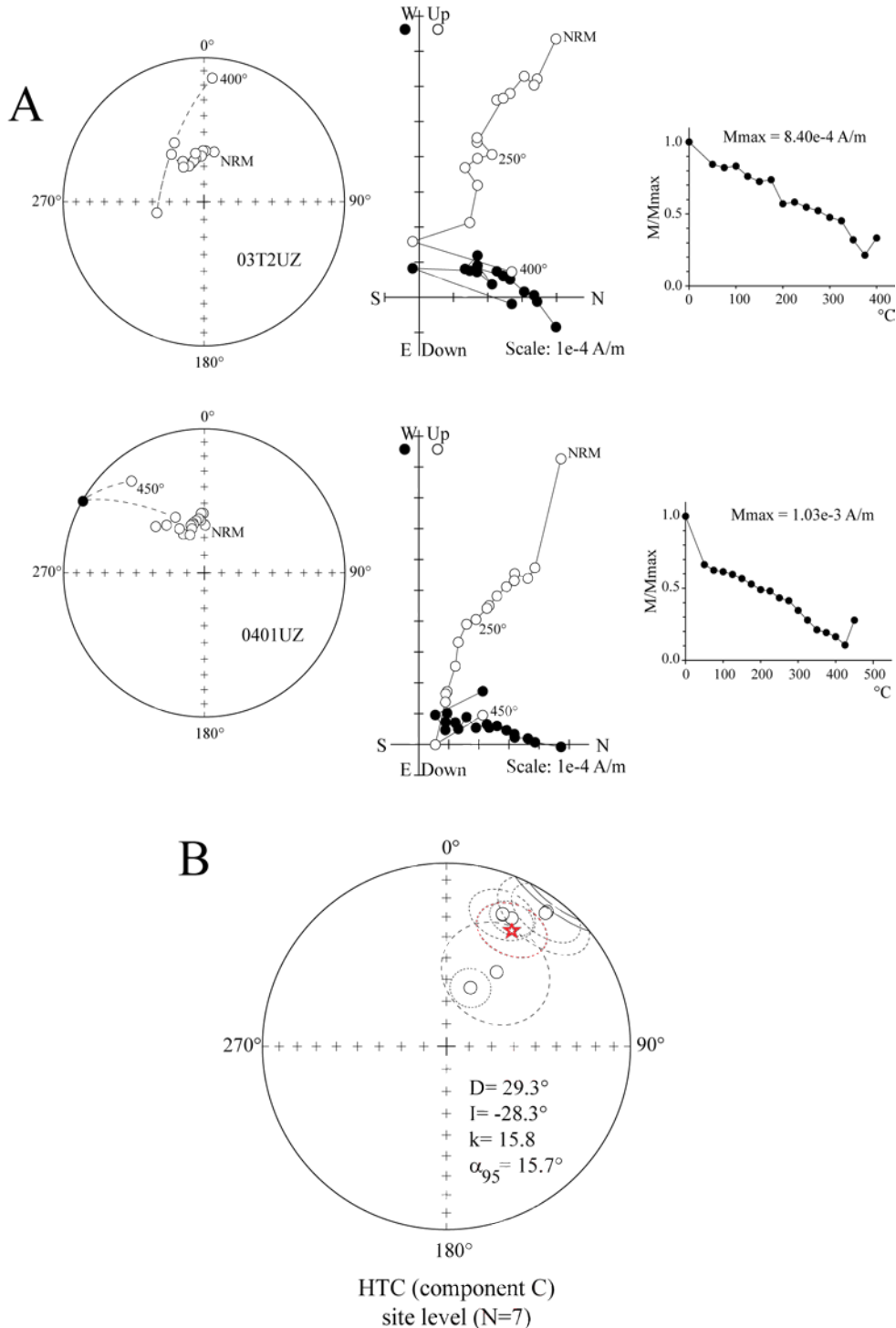


**Figure 3.7** (A) Typical equal-area projections, orthogonal vector plots and remanence intensity decay plots for the remagnetized sediments from the baked contact zone. Plotting conventions as in Figure 3.4A. (B) Equal-area projections of high temperature component (HTC) for the remagnetized sediments. Plotting conventions as in Figure 3.4B.

### **3.4.6 International Kimberlite Pipe**

Twenty-two samples from 14 sites were subjected to progressive thermal demagnetization. The LTC, unblocked below 200°C, has a mean direction of D=17.3°, I=83.8° ( $k=56.7$ ,  $\alpha_{95}=4.2^\circ$ ,  $n=22$  samples) (Table 3.2, Figure 3.8), which is close to the present magnetic field of the region of D=350.7°, I=78.9°. Therefore the LTC is deemed to be a present-day overprint. The HTC is unblocked between almost 130°C and 658°C. As expected from the rock-magnetic experiments, the primary components of magnetization were not well defined and often did not trend to the origin of the Zijderveld diagrams, thus requiring the use of remagnetization circles for several samples. The average HTC direction, obtained from combining the directions and great circles, at the site level is as follows: D=291.1°, I=-78.1° ( $k=27.5$ ,  $\alpha_{95}= 14.9^\circ$ ,  $N=5$ ) (Table 3.2). However, because of the mineralogy characteristic of the samples, this result should be considered with caution.

## International kimberlite pipe

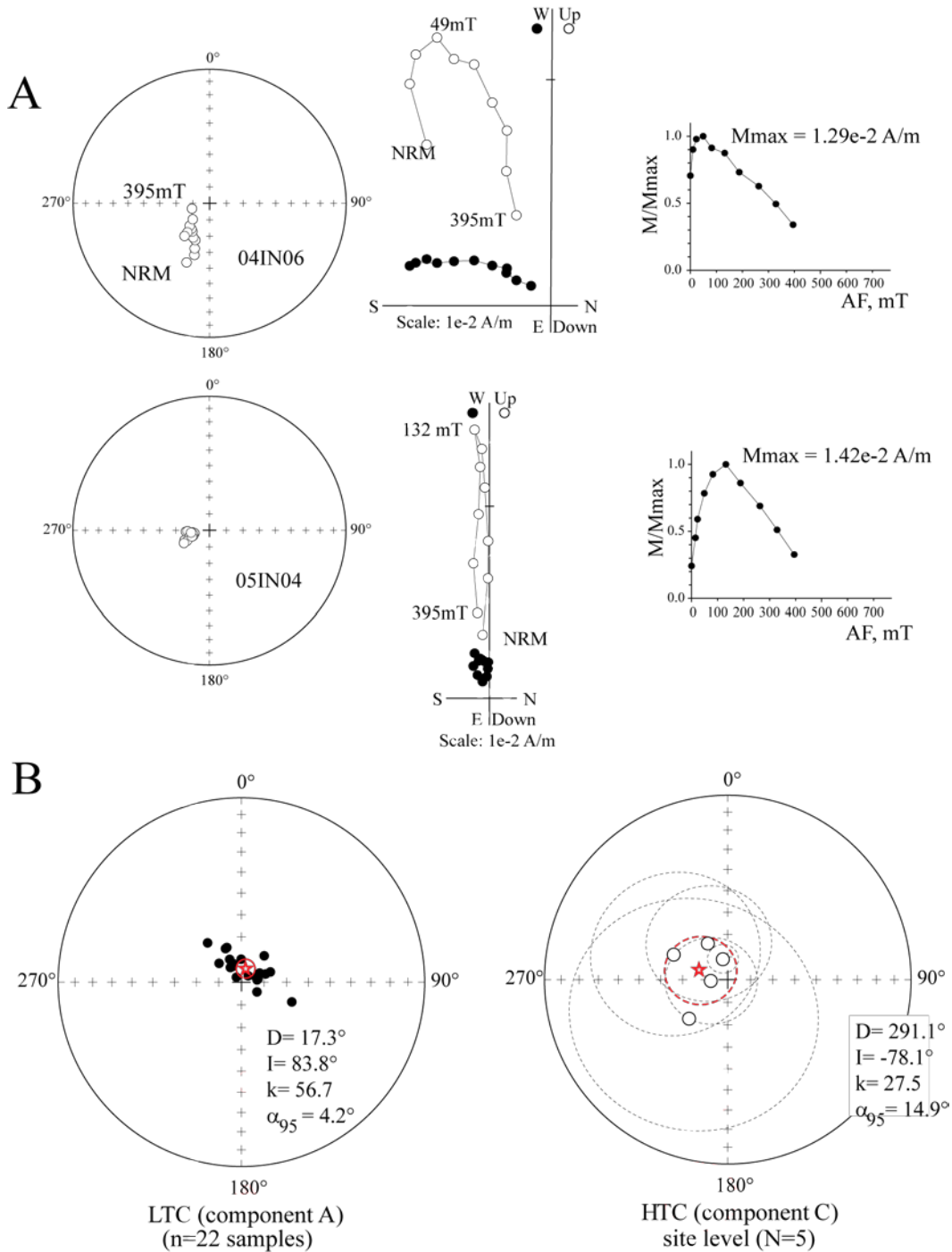


**Figure 3.8** (A) Typical equal-area projections, orthogonal vector plots and remanence intensity decay plots for the International pipe. Plotting conventions as in Figure 3.4A. (B) Equal-area projections of the low temperature component (LTC) and high temperature component (HTC) for the pipe. Plotting conventions as in Figure 3.4B, except n: number of specimens at sample level.

**Table 3.2.** Paleomagnetic high temperature components mean directions for the International Pipe ( $62.4^{\circ}\text{N}$ ,  $113.7^{\circ}\text{E}$ ) and the Obnazhennaya Pipe ( $70.5^{\circ}\text{N}$ ,  $120.5^{\circ}\text{E}$ ).

Site Number	n	D ( $^{\circ}$ )	I ( $^{\circ}$ )	k	$\alpha_{95} (^{\circ})$	Com- ment
<b><i>International Pipe</i></b>						
IN-1	5	267.8	-83.2	17.1	19.0	5d
IN-2	4	298.3	-64.3	9.7	35.8	2d+2cc
IN-3	4	222.7	-67.0	4.9	52.7	2d+2cc
IN-4	4	348.5	-80.4	783.1	6.3	4cc
IN-5	4	334.4	-71.7	18.0	25.7	2d+2cc
IN mean	5 sites	291.1	-78.1	27.5	14.9	
<b><i>Obnazhennaya Pipe</i></b>						
Obn-02	9	2.8	-76.6	7.4	20.6	5d+4cc
Obn-04	4	156.3	-77.7	144.9	7.7	4d
Obn-06	11	70.1	-85.8	36.8	7.6	11d
Obn-08	12	281.4	-78.1	60.8	5.6	10d+2c c
Obn-10	12	153.3	-79.4	7.8	16.7	11d+1c c
Obn-12	10	319.7	-82.2	27.6	9.4	10d
Obn-14	6	302.6	-71.1	72.4	7.9	6d
Obn-16	10	31.4	-82.1	59.7	6.3	10d
Obn-18	3	326.5	-71.7	78.5	14.0	3d
Obn-20	5	317.3	-73.5	154.2	6.2	5d
Obn-22	6	119.4	-86.0	68.8	8.1	6d
Obn-24	8	336.4	-78.5	52.6	7.7	8d
Obn-26	6	256.8	-71.9	21.9	14.6	6d
Obn-28	8	322.0	-66.1	28.3	10.6	8d
Obn-30	5	38.7	-82.7	28.1	14.7	5d
Obn-32	6	304.0	-75.3	33.4	11.6	6d
Obn-34	5	248.8	-63.9	25.6	15.4	5d
Obn Mean	17 sites	306.7	-82.6	38.4	5.8	all sites

Same abbreviations as in Table 1.

### 3.4.7 Obnazhennaya Kimberlite Pipe

Thermal and alternating field (AF) demagnetization was applied to samples from 17 sites in the Obnazhennaya kimberlite pipe (Table 3.2, Figure 3.9). Two magnetization components were isolated in most of the samples. The LTC is completely removed above  $250^{\circ}\text{C}$  and by 50 mT, giving an average direction of  $D=302.5^{\circ}$ ,  $I=87.0^{\circ}$  ( $k=110.9$ ,  $\alpha_{95}=3.4^{\circ}$ ,  $N=17$  sites). This direction is close to the present field direction in the region ( $D=347.0^{\circ}$ ,  $I=83.1^{\circ}$ ) and is interpreted to be a present-day overprint. The high temperature/high AF component is isolated between  $350^{\circ}\text{C}$  and  $575^{\circ}\text{C}$  and 125 mT and 350 mT. During heating to higher

temperatures, some samples demonstrate a substantial increase in magnetic susceptibility, indicating thereby a possible oxidation of titanomagnetite. For this reason, using a combination of the stable end point directions and great circle analysis (McFadden and McElhinny, 1988), an average HTC direction of  $D=306.7^\circ$ ,  $I=-82.6^\circ$  ( $k=38.4$ ,  $\alpha_{95}=5.8^\circ$ ,  $N=17$  sites) (Table 3.2) was determined.

### Obnazhennaya kimberlite pipe

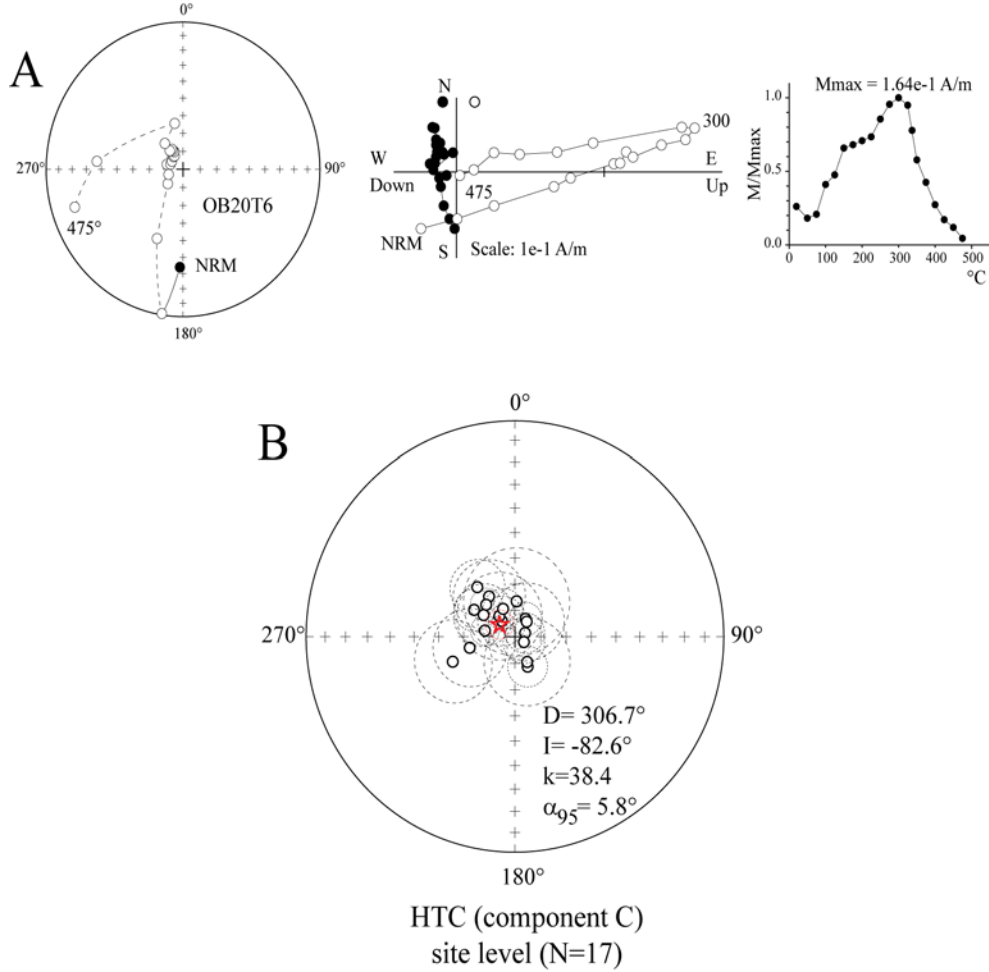


**Figure 3.9** (A) Typical equal-area projections, orthogonal vector plots and remanence intensity decay plots for the Obnazhennaya kimberlite pipe. Plotting conventions as in Figure 3.4A. (B) Equal-area projections of the high temperature component (HTC) for the pipe. Plotting conventions as in Figure 3.4B.

### 3.5 Discussion

Both low and high laboratory unblocking temperature magnetization components have been identified in the studied kimberlite pipes and sedimentary rocks. HTC directions for the pipes are summarized in Figure 3.10. Only high temperature components were found in the contact zone sedimentary rocks of the Western Udachnaya pipe. In all other cases the LTC can be interpreted as either a present day or a Cenozoic geomagnetic field overprint. The individual HTC paleomagnetic poles for the kimberlite pipes and sedimentary rocks are listed in Table 3.3 and plotted in Figure 3.11. The pole locations do not exactly match the current APWP for Siberia because the reliable poles used by Cocks and Torsvik (2007) to construct the APWP are few in number and paleomagnetic data are not available for many geologic time periods.

Cooling rates of kimbelite magma depend on the magma emplacement temperature, size of the body and depth of the sampling level. McFadden and Jones (1977) and McFadden (1977) found that cooling of some small South African kimberlite bodies took place over on the order of a few hundreds to first few thousands of years from the maximum temperature of 350°C. Fontana et al. (2011) estimated from thermomagnetic analysis done on Southern Africa kimberlite pipes that the basaltic clasts in the layered and massive vent-filling pyroclastic deposits in the center of the pipe were emplaced at >570 °C (some even >760–920 °C), and the temperatures near the edges were as low as 200–440 °C. Van Fossen and Kent (1993) reported a polarity reversal recorded in one kimberlite dyke in the US. They estimated an emplacement temperature of ~700 °C and cooling rates between 103 and 107 years. The sizes of the kimberlite pipes studied in the present contribution are in the order of 100 m in diameter and the present day sampling surface is estimated to be at least few hundred meters below the ancient surface. The preliminary estimate of the cooling temperature rate using the method of Van Fossen and Kent (1993) is at least 104 and 107 years in the center of the kimberlite bodies. Samples were acquired from different levels

across the kimberlite pipes and therefore it can be consider that geomagnetic secular variations are most likely averaged in this study.

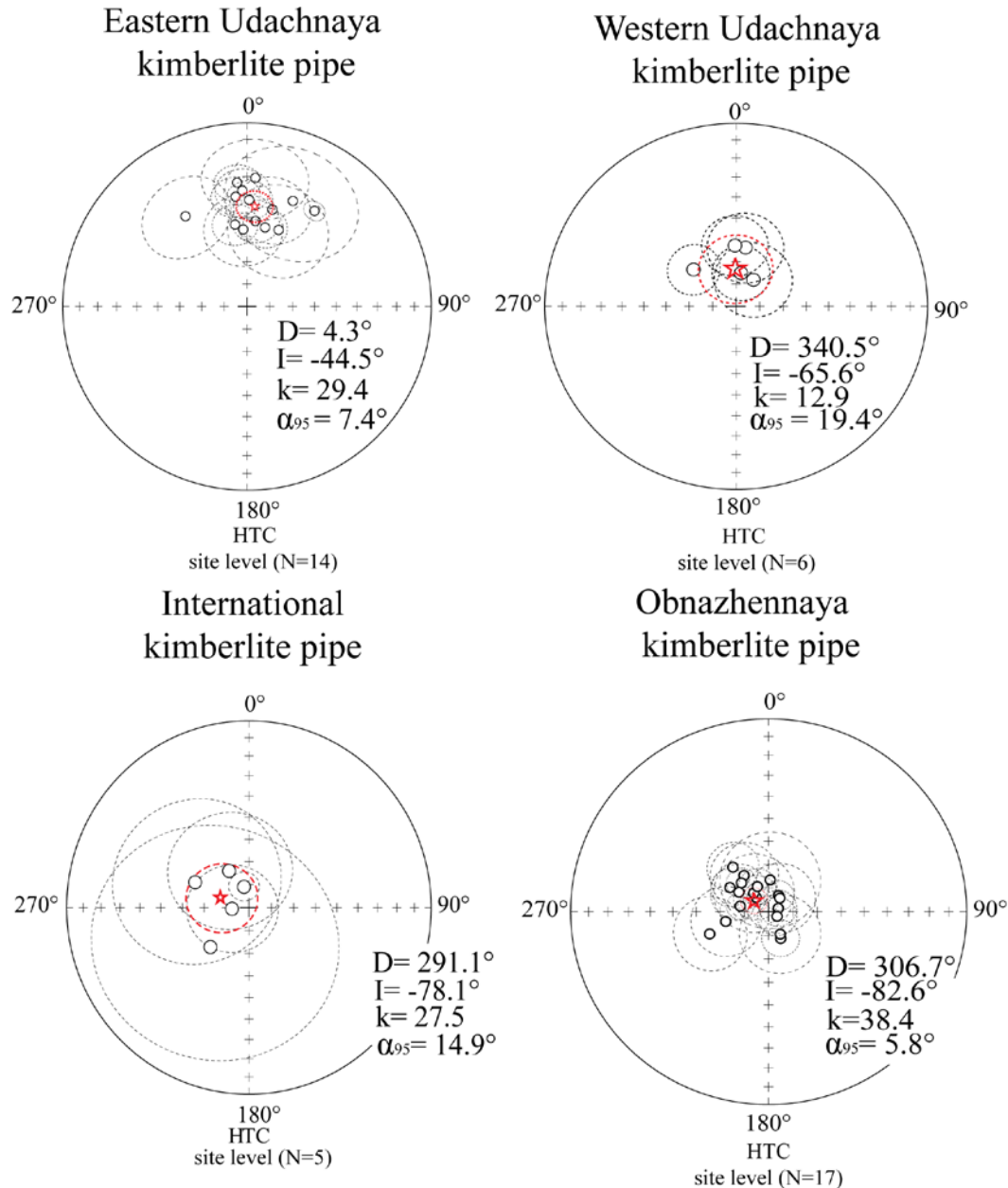


**Figure 3.10.** Equal-area projections of site-mean directions of high temperature (HTC) components for each studied pipe, with circles of 95% confidence. Open (close) symbols: upward (downward) inclinations. Star: mean formation direction. D: declination, I: inclination, k: precision parameter,  $\alpha_{95}$ : radius of the 95% probability confidence circle, N: number of specimens at site level.

The poles for the Eastern Udachnaya and Western Udachnaya kimberlites are situated far apart from each other at  $3.1^{\circ}\text{N}/108.6^{\circ}\text{E}$  and  $25.6^{\circ}\text{N}/126.9^{\circ}\text{E}$ ,

respectively (Figure 3.11). The Eastern Udachnaya kimberlite pole lies among the group of the Late Ordovician–Early Silurian Siberian poles, and gives a paleomagnetic age of  $428\pm13$  Ma (Figure 3.11). This pole is close to the paleomagnetic pole for the host Early Ordovician sedimentary rocks. The pole for the host sedimentary rocks at  $16.7^\circ\text{S}/106.2^\circ\text{E}$  with  $\text{A}95=4.6^\circ$  is very well defined, although no fold test or reversal test could be applied, and gives an Early Silurian paleomagnetic age of  $441\pm3$  Ma that is situated near the Late Ordovician Siberian pole of 450 Ma. The age of the sedimentary rocks is well defined paleontologically as Early Ordovician; therefore it can be interpreted that the pole recorded either an overprint of the host sedimentary rocks of the Udachnaya area by the Eastern Udachnaya kimberlite magmatic event or to record secular variation that was not averaged out during magnetization acquisition.

The primary nature of the HTC was inferred based on the proximity of the pole's position to the Ordovician group of poles and the result of the baked contact test. The pole calculated for the baked sedimentary rocks is notably different from the kimberlite or sediment poles and is situated farther west in the center of the Indian Ocean at  $5.2^\circ\text{S}/84.2^\circ\text{E}$ ,  $\text{A}95=12.7^\circ$  (Figure 3.11). This pole is interpreted to record the partial overprinting of the original remanence in the Early Ordovician sedimentary rocks by a thermoremanent magnetization from the intrusion of the Udachnaya kimberlite pipes.

The Early Silurian paleomagnetic age of the Eastern Udachnaya kimberlite differs radically from the inferred Late Devonian age inferred from radiometric dating (Griffin et al., 1999; Kinny et al., 1997; Maas et al., 2005). This discrepancy may be caused by several factors. Although the Siberian APWP has the most poles from the Ordovician period, these poles are very scattered. The Silurian is poorly represented, and there are no poles with ages between 435 and 365 Myr. The APWP for this time interval has been reconstructed by interpolation. The low resolution and precision of the Siberian APWP invite speculation and undoubtedly affect the accuracy of the paleomagnetic dating attempted in this

study substantially. However, if the inferred paleomagnetic age is assumed to be reasonable, it can conclude that kimberlite magmatism in the Siberian platform started much earlier than the Late Devonian. Kravchinsky et al. (2002) discussed the then available radiometric ages and paleomagnetic data, and suggested that the Alakit–Markha kimberlite field magmatism located south of the Anabar Shield was associated with the eruption of the Late Devonian–Early Carboniferous Viluy traps. The Eastern Udachnaya pipe is from the Daldyn kimberlite field, which appears to be older than the Alakit–Markha kimberlite field. Kuzmin et al. (2010) discussed the early Paleozoic large scale magmatism to the south of the present

**Table 3.3.** Paleomagnetic poles and estimated ages for the studied pipes. Lat (Long): Latitude (Longitude) of the sampling sites of paleomagnetic pole. dp/dm: semi-axes of the oval of 95% confidence of the paleomagnetic pole;  $A_{95}$ : radius of the 95% confidence circle.

Studied Object	Site coordinates		Paleomagnetic pole coordinates		dp/dm ( $A_{95}$ )	N	Paleo-latitude (°)	Paleomagnetic age (Ma)
	Lat °N	Long °E	Lat °N	Long °E				
Udachnaya Eastern kimberlite pipe	66.9	112.5	3.1	108.6	9.3/5.9 (7.4)	14 sites	26.2±9. 3	428±13
Udachnaya Western kimberlite pipe	66.9	112.5	25.6	126.9	31.6/25.7 (28.5)	6 sites		Remagnetized
Baked contact test (BCT)	66.9	112.5	-5.2	84.2	17.2/9.4 (12.7)	7 sites		
Early Ordovician host sediments	66.9	112.5	-16.7	106.2	6.4/3.3 (4.6)	21 samples	6.3±6.4	Remagnetized
International kimberlite pipe	62.4	113.7	48.8	147.0	28.1/26.4 (27.2)	5 sites		251±30
Obnazhennaya kimberlite pipe	70.5	120.5	59.6	143.9	11.3/11.1 (11.2)	17 sites	75.4±1 1.3	168±11* 151±14**

\* Age determined using APWP of Besse and Courtillot (2002)

\*\* Age determined using APWP of Torsvik et al. (2008).

day Siberian platform in the Altay–Sayan terrane and the Viluy rift. They found that Siberia was located above the large African low shear wave velocity zone throughout the Paleozoic. The earliest igneous rocks in the Viluy rift are tephrites, trachybasalts, trachytes, phonolites, and ultrabasic alkali rocks with carbonatites

(Gaiduk, 1987), which corresponds to the earliest arch-uplift stage of development of the Viluy rift. The intrusion of the Eastern Udachnaya kimberlite pipe could be provisionally associated with this early arch uplift.

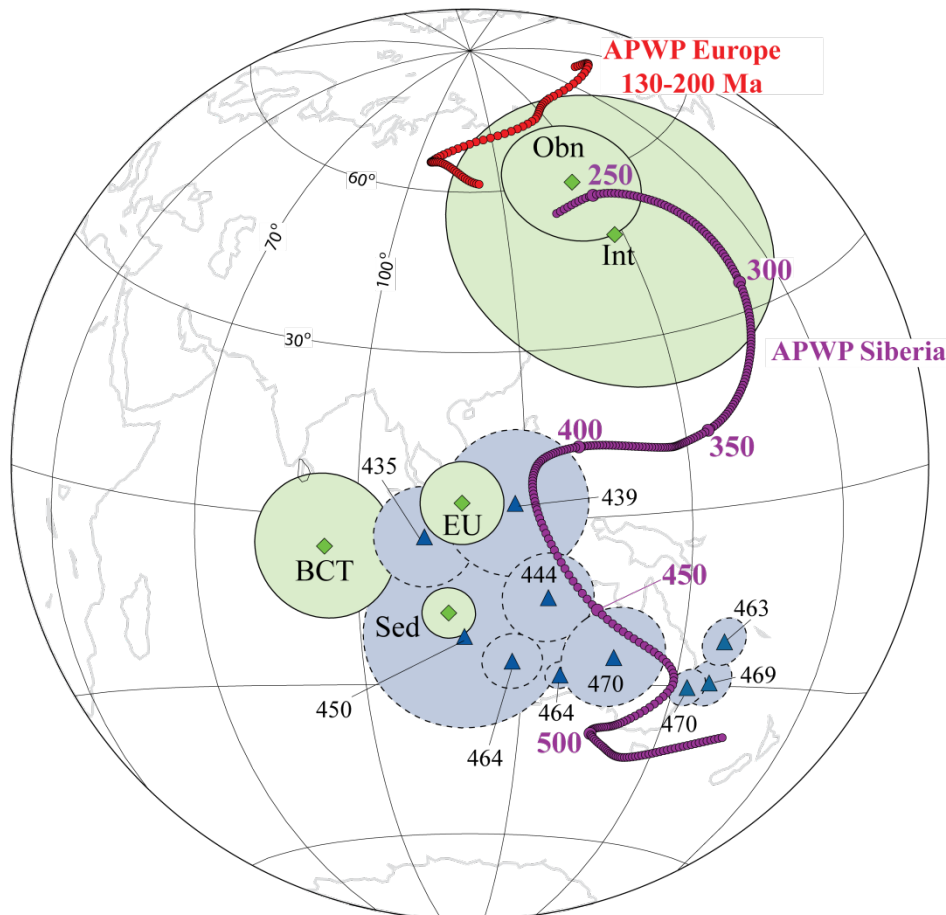


**Figure 3.11** Equal area projection of paleomagnetic poles from kimberlites pipes and sediments (diamonds) with ellipses of 95% confidence (shadow areas). Triangles represent the Siberian platform poles between 430 and 470 Myr with their corresponding 95% confidence ellipses (dashed ellipses). Circles represent the Siberian APWP of Cocks and Torsvik (2007) interpolated to 2 Myr intervals and the European APWP of Besse and Courtillot (2002) between 130 and 200 Ma interpolated to 2 Myr intervals. Obn: Obnazhennay pipe paleomagnetic pole; Int: International pipe paleomagnetic poles; EU: Eastern Udachnaya pipe paleomagnetic pole; BCT: baked contact test paleomagnetic pole; Sed: sediments near the Eastern Udachnaya kimberlite pipe paleomagnetic pole. The Western Udachnaya paleomagnetic pole is not included in this figure.

The Western Udachnaya kimberlite pole at  $25.6^{\circ}\text{N}/126.9^{\circ}\text{E}$ ,  $\text{A}95=28.5^{\circ}$  is distinct from all other poles obtained in this study and from the Siberian APWP. The anomalous location of this pole can be interpreted to be a result of remagnetization during later alteration. The Western Udachnaya pipe is composed

of altered kimberlite; such alteration could have take place either gradually or quickly at any time after kimberlite intrusion. The pipe's paleomagnetic pole is located between the Early Paleozoic and Mesozoic segments of the APWP but does not match well with any specific poles. Most likely the HTC is a combination of a primary and a viscous magnetization, which could be related to gradual alteration processes related to hydrothermal fluids. The regional remagnetization by the Permo-Triassic trap magmatic event is unlikely because the host sedimentary rocks and the Eastern Udachnaya pipe paleopoles coincide with the early Paleozoic segment of the APWP.

The paleomagnetic pole for the International kimberlite pipe is located at  $48.8^{\circ}\text{N}/147^{\circ}\text{E}$  ( $\text{A95}=27.2^{\circ}$ ; Table 3.3, Figure 3.11). This pole agrees with the Permo-Triassic NSP3 paleomagnetic pole for the Siberian traps of  $57.0^{\circ}\text{N}/148.1^{\circ}\text{E}$ ,  $\text{A95}=5.3^{\circ}$  as reported by Pavlov et al. (2007). The rock-magnetic data showed that the initial primary magnetization is not carried by magnetite and could be associated with secondary minerals. The magnetizations from four of the five sites did not preserve linear segments of the high temperature component and they could be evaluated only by using remagnetization circle analysis. The paleomagnetic age is determined as  $251\pm30$  Ma. The HTC magnetization in these rocks is secondary and likely corresponds to the age of the major remagnetization event in the area — the Siberian traps eruption.

The paleomagnetic pole for the Obnazhennaya kimberlite pipe at  $59.6^{\circ}\text{N}/143.9^{\circ}\text{E}$  ( $\text{A95}=11.2^{\circ}$ ; Table 3.3, Figure 3.11) is also located near the Permo-Triassic NSP3 paleomagnetic pole of Pavlov et al. (2007) for Siberian traps at  $57.0^{\circ}\text{N}/148.1^{\circ}\text{E}$ ,  $\text{A95}=5.3^{\circ}$ . The pipe's mean direction is based on HTC directions and some remagnetization circles. The kimberlite is fresh and rock-magnetic data suggest that magnetite/titanomagnetite are the major carriers of what it is assume a primary thermoremanent magnetization. Radiometric, paleontological, and stratigraphic ages for this pipe suggest Middle–Late Jurassic. For this period of time, the Siberian APWP is not well defined and the Eurasian APWP is used to

describe the motion of Siberia (Besse and Courtillot, 2002; Schettino and Scotese, 2005). For this reason the Eurasian APWP of Besse and Courtillot (2002) and the most recent Eurasian APWP of Torsvik et al. (2008) for the past 200 Ma is used. A paleomagnetic age of  $168 \pm 11$  Ma with the APWP of Besse and Courtillot (2002) and  $151 \pm 14$  Ma with the APWP of Torsvik et al. (2008) was estimated. Both results agree within error and the difference might be related to the data selection of Besse and Courtillot (2002) and Torsvik et al. (2008) for the APWP construction, different Euler rotation parameters, and degree of smoothing used to construct the APWP (Torsvik et al., 2008). The Obnazhennaya age results are consistent with the geologic constraints and with the published radiometric dating data; thus the Middle–Late Jurassic age of the Obnazhennaya pipe can be confirmed.

### 3.6 Conclusions

New paleomagnetic poles for the Eastern Udachnaya, Western Udachnaya, International, and Obnazhennaya kimberlite pipes of the Siberian platform have been obtained. The poles are compared to the Siberian APWP (Cocks and Torsvik, 2007) for the Paleozoic interval and to Besse and Courtillot (2002) and Torsvik et al. (2008) for the Mesozoic interval to estimate the ages of the studied pipes. The ages of the kimberlites fall into three groups spanning the Early Silurian to the Late Jurassic.

1. Two kimberlite pipes were studied from the Udachnaya field. The Western Udachnaya pipe has been remagnetized by post-intrusion alteration so that no clear age could be determined. The Eastern Udachnaya pipe provides a well-defined, most likely primary, thermoremanent magnetization that gives an Early Silurian age of  $428 \pm 13$  Ma. Magmatism can be considered to correspond to the earliest stage of the Viluy rift formation. This age contradicts previously published Late Devonian radiometric ages. An alternative interpretation is that the paleomagnetic age could be inaccurate because of the imprecision of the

Paleozoic segment of the Siberian APWP that was used as the reference path for the age estimates.

2. For the International kimberlite pipe, magnetic mineralogy and paleomagnetic data provide evidence that the samples have been remagnetized. The estimated paleomagnetic age of  $251 \pm 30$  Ma is likely related to the Permo-Triassic trap magmatism that was a major remagnetization event affecting the Malo-Botuoba kimberlite field. The previously studied Mir kimberlite pipe was remagnetized by the same magmatic event (Kravchinsky et al., 2002).

3. Comparison of the Obnazhennya paleomagnetic pole with the Eurasian APWP (Besse and Courtillot, 2002; Torsvik et al., 2008) yields a Middle–Late Jurassic age for the kimberlite, which corresponds to previously reported radiometric, paleontologic, and stratigraphic age estimates.

Paleomagnetic techniques applied to dating Siberian kimberlite magmatism reveal a large span of kimberlite ages, from the Early Silurian to Middle–Late Jurassic. Early Silurian to Late Devonian ages are most likely related to magmatism during the early and main stages of formation of the Viluy rift. Middle–Late Jurassic magmatism could be associated with subduction processes that took place on the present day northeast margin of the Siberian platform during this time period, associated with the accretion of the Omolon, Kolyma, and surrounding terranes. The Omolon block accreted to the Siberian platform in the post–Late Jurassic (Savostin et al., 1993). Recent numerical models have demonstrated that low-angle subduction can result from high plate convergence velocities and can trigger partial melting and kimberlite/lamproite magmatism far into North American continent by more than 1200 km from the subduction trench (Currie and Beaumont, 2011). Geochemical studies on some kimberlite pipes in Siberia also suggest that subduction is involved in the formation of some kimberlite fields (Ashchepkov et al., 2010).

## Bibliography

Agashev, A.M., Pokhilenko, N.P., Tolstov, A.V., Polyanichko, V.V., Mal'kovets, V.G., Sobolev, N.V., 2004. New age data on kimberlites from the Yakutian diamondiferous province. *Doklady Earth Sciences*, 399 (8), 1142–1145.

Ashchepkov, I.V., Pokhilenko, N.P., Vladynova, A.M., Afanasiev, V.P., Pokhilenko, L.N., Kuligin, S.S., Malygina, E.V., Alyanova, N.A., Kostrovitsky, S.I., Rotman, A.Y., Mityukhin, S.I., Karpenko, M.A., Stegnitsky, Y.V., Khemelnikova, O.S., 2010. Structure and evolution of the lithospheric mantle beneath Siberian craton, thermobarometric study. *Tectonophysics*, 485 (1), 17–41.

Besse, J., Courtillot, V., 2002. Apparent and true polar wander and the geometry of the geomagnetic field over the last 200 Myrs. *Journal of Geophysical Research*, 107, 1–31.

Brakhfogel, F.F., 1984. Geological Aspects of Kimberlite Magmatism in the Northeastern Siberian Platform. Publication of the Yakutian Institute of Geology, Russian Academy of Sciences, Yakutsk . (in Russian).

Butler, R.F., 1998. Paleomagnetism: Magnetic Domains to Geologic Terrains, Electronic Ed. Blackwell Scientific Publications.

Cocks, L.R.M., Torsvik, T.H., 2007. Siberia, the wandering northern terrane, and its changing geography through the Paleozoic. *Earth-Science Reviews*, 82, 29–74.

Cogné, J.-P., 2003. PaleoMac: a Macintosh™application for treating paleomagnetic data and making plate reconstructions. *Geochemistry, Geophysics, Geosystems*, 4 (1), 1007. doi:10.1029/2001GC000227

Currie, C.A., Beaumont, C., 2011. Are diamond-bearing Cretaceous kimberlites related to low-angle subduction beneath western North America? *Earth and Planetary Science Letters* 303, 59–70.

Dunlop, D.J., Özdemir, Ö., 1997. Rock Magnetism: Fundamentals and Frontiers. (573 pp.) Cambridge University Press, New York, London and Cambridge.

Enkin, R.J., 1996. A computer program package for analysis and presentation of paleomagnetic data. Pacific Geoscience Centre, Geological Survey of Canada.

Fisher, R., 1953. Dispersion on a sphere. *Proceedings of the Royal Society of London Series A* 217, 295–305.

Fontana, G., Niocaill, C.M., Brown, R.J., Sparks, R.S.J., Field, M., 2011. Emplacement temperatures of pyroclastic and volcanoclastic deposits in kimberlite pipes in southern Africa. *Bulletin of Volcanology*, 73, 1063–1083.

Gaiduk, V.V., 1987. ViluyMiddle Paleozoic Rift System. *Geotectonics*, 3, 66–76 (in Russian).

Gregory, L.C., Meert, J.G., Pradhan, V., Pandit, M.K., Tamrat, E., Malone, S.J., 2006. A paleomagnetic and geochronologic study of the Majhgawan kimberlites, India: implications for the age of the Upper Vindhyan Supergroup. *Precambrian Research*, 149, 65–75.

Griffin, W.L., Ryan, C.G., Kaminsky, F.V., O'Reilly, S.Y., Natapov, L.M., Win, T.T., Kinny, P.D., Ilupin, I.P., 1999. The Siberian lithosphere traverse, mantle terranes and the assembly of the Siberian Craton. *Tectonophysics*, 310 (1–4), 1–35.

Halls, H.C., 1976. A least-squares method to find a remanence direction from converging remanence circles. *Geophysical Journal of the Royal Astronomical Society*, 45, 297–304.

Hargraves, R.B., Onstott, T.C., 1980. Paleomagnetic results from some southern African kimberlites, and their tectonic significance. *Journal of Geophysical Research*, 85 (B7), 3587–3596.

Ionov, D.A., Doucet, L.S., Ashchepkov, I.V., 2010. Composition of the lithospheric mantle in the Siberian craton: new constraints from fresh peridotites in the Udachnaya–East kimberlite. *Journal of Petrology*, 51 (11), 2177–2210.

Jones, D.L., 1968. Paleomagnetism of premier mine kimberlite. *Journal of Geophysical Research*, 73 (22), 6937–6945.

Jones, D.L., McElhinny, 1966. Paleomagnetic correlation of basic intrusions in the Precambrian of Southern Africa. *Journal of Geophysical Research*, 71 (2), 543–552.

Kamenetsky, M.B., Sobolev, A.V., Kamenetsky, V.S., Maas, R., Danyushevsky, L.V., Thomas, R., Pokhilenko, N.P., Sobolev, N.V., 2004. Kimberlite melts rich in alkali chlorides and carbonates: a potent metasomatic agent in the mantle. *Geology*, 32 (10), 845–848.

Kamenetsky, V.S., Maas, R., Kamenetsky, M.B., Paton, C., Phillips, D., Golovin, A.V., Gornova, M.A., 2009. Chlorine from the mantle: magmatic halides in the Udachnaya–East kimberlite, Siberia. *Earth and Planetary Science Letters*, 285, 96–104.

Kinny, P.D., Griffin, B.J., Heaman, L.M., Brakhfogel, F.F., Spetzius, Z.V., 1997. SHRIMP U–Pb ages of perovskite from Yakutian kimberlites. *Russian Geology and Geophysics*, 38, 97–105 (in Russian).

Kirschvink, J.L., 1980. The least-squares line and plane and the analysis of paleomagnetic data. *Geophysical Journal of the Royal Astronomical Society*, 62, 699–718.

Konstantinov, K.M., Stegnitskii, B., 2012. The Late Silurian–Early Devonian natural remanentmagnetization of kimberlites and traps in the Yakutian diamondiferous province. *Doklady Earth Sciences*, 442 (1), 152–158.

Kravchinsky, V.A., Konstantinov, K.M., Courtillot, V., Valet, J.-P., Savrasov, J.I., Cherniy, S.D., Mishenin, S.G., Parasotka, B.S., 2002. Palaeomagnetism of East Siberian traps and kimberlites: two new poles and palaeogeographic reconstructions at about 360 and 250 Ma. *Geophysical Journal International*, 148, 1–33.

Kravchinsky, V.A., Eccles, D.R., Zhang, R., Cannon, M., 2009. Paleomagnetic dating of the Northern Alberta kimberlites. *Canadian Journal of Earth Sciences*, 46, 231–245.

Krivonos, V.F., 1997. Relative and absolute age of kimberlites. *Otechestvennaya Geologiya*, 1, 41–51 (in Russian).

Kuzmin, M.I., Yarmolyuk, V.V., Kravchinsky, V.A., 2010. Phanerozoic hot spot traces and paleogeographic reconstructions of the Siberian continent based on interaction with the African large low shear velocity province. *Earth-Science Reviews*, 102, 29–59.

Maas, R., Kamenetsky, M.B., Sobolev, A.V., Kamenetsky, V.S., Sobolev, N.V., 2005. Sr, Nd and Pb isotope evidence for a mantle origin of alkali chlorides and carbonates in the Udachnaya kimberlites, Siberia. *Geology*, 33, 549–552.

Malkov, B.A., 2008. Belemnites and eclogites of the Obnazhennaya kimberlite pipe (Olenek Uplift, Yakutia). *Vestnik*, 6, 12–14 (in Russian).

Malone, S.J., Meert, J.G., Banerjee, D.M., Pandit, M.K., Tamrat, E., Kamenov, G.D., Pradhan, V.R., Sohl, L.E., 2008. Paleomagnetism and detrital zircon geochronology of the Upper Vindhyan Sequence, Son Valley and Rajasthan, India: a ca. 1000 Ma closure age for the Purana Basins? *Precambrian Research*, 164, 137–159.

Masaitis, V.L., Milhailov, M.V., Selivanovskya, T.V., 1975. The Popigai Meteorite Crater. Nauka Press, Moscow, Russia. (124 pp. (In Russian)).

McFadden, P.L., 1977. A palaeomagnetic determination of the emplacement temperature of some South African kimberlites. *Geophysical Journal of the Royal Astronomical Society*, 50, 587–604.

McFadden, P.L., Jones, D.L., 1977. The palaeomagnetismof some upper Cretaceous kimberlite occurrences in South Africa. *Earth and Planetary Science Letters*, 34, 125–135.

McFadden, P.L., McElhinny,M.W., 1988. The combined analysis of remagnetization and direct observation in paleomagnetism. *Earth and Planetary Science Letters*, 87, 161–172.

Oleinikov, B.V., 1979. Geokhimiya i rudogenet platformennykh bazitov (Geochemistry and Ore Genesis in Platform Basic Rocks). Nauka, Novosibirsk. (in Russian).

Pavlov, V.E., Courtillot, V., Bazhenov, M.L., Veselovsky, R.V., 2007. Paleomagnetism of the Siberian traps: new data and new overall 250 Ma pole of Siberia. *Tectonophysics*, 443, 72–92.

Pisarevsky, S.A., Gladkochub, D.P., Donskaya, T.A., De Waele, B., Mazukagzov, A.M., 2006. Palaeomagnetism and geochronology of mafic dykes in south Siberia, Russia: the first precisely dated Early Permian palaeomagnetic pole from the Siberian craton. *Geophysical Journal International*, 167, 649–658.

Savostin, L.A., Pavlov, V.E., Safonov, V.G., Bondarenko, G.E., 1993. Lower and Middle Jurassic deposits in the Western Zone of the Omolon Block (Northeastern Russia): conditions of formation and paleomagnetism. *Doklady Akademii Nauk of the USSR*, 333, 481–486 (in Russian).

Schettino, A., Scotese, C.R., 2005. Apparent polar wander paths for the major continents (200 Ma to the present day): a palaeomagnetic reference frame for global tectonic reconstructions. *Geophysical Journal International*, 163, 727–759.

Shpount, B.R., Oleinikov, A., 1987. A comparison of mafic dike swarm from the Siberian and Russian platforms. In: Halls, H.C., Fahrig, W.F. (Eds.), *Mafic Dyke Swarms*, Special Paper, 34. Geological Association of Canada, Toronto, ON, pp. 393–400.

Symons, D.T.A., Arne, D.C., 2005. Paleomagnetic constraints on Zn–Pn ore genesis of the Pillara Mine, Lennard Shelf, Western Australia. *Mineralium eposita* 39, 944–959.

Symons, D.T.A., Enkin, R.J., Cioppa, M.T., 1999. Paleomagnetism in the Western Canada sedimentary basin; dating and fluid flow and deformation events. *Bulletin of Canadian Petroleum Geology*, 47, 534–547.

Torsvik, T.H., Muller, D.R., Van Der Voo, R., Steinberger, B., Gaina, C., 2008. Global plate motion frames: toward a unified model. *Reviews of Geophysics*, 46, 1–44.

Van Fossen, M.C., Kent, D.V., 1993. A palaeomagnetic study of 143 Ma kimberlite dikes in central New York State. *Geophysical Journal International*, 113, 175–185.

Wynne, P.J., Irving, E., Schulze, D.L., Hall, D.C., Helmstaedt, H.H., 1992. Paleomagnetism and age of three Canadian Rocky-Mountain diatremes. *Canadian Journal of Earth Sciences*, 29 (1), 35–47.

Zijderveld, J.D.A., 1967. A.C. demagnetization of rocks, analysis of results. In: Methods in paleomagnetism, D.W. Collinson, K.M. Creer, and S.K. Runcorn, eds., Elsevier, Amsterdam, 254–286.

## **Chapter 4\***

# **Upper Cretaceous magnetostratigraphy in Western Canada: Evidence for normal polarity zones in chron 33r and high resolution age correlation between stratigraphic units**

### **4.1 Introduction**

Geomagnetic chron 33r is usually associated with an interval of exclusively reversed magnetic polarity on most paleomagnetic charts, however, at least three studies have reported the presence of several short normal polarity intervals within the chron. Leahy and Lerbekmo (1995), studying outcrop samples from southern Alberta, Canada, identified several normal magnetozones within C33r. Normal polarity intervals were also observed by Montgomery et al. (1998) on chalk sequences in southern England. They argued that when compared with other European sequences (such as Gubbio in northern Italy (Lowrie et al. 1980)), the high sedimentation rates observed on their section allowed for higher magnetostratigraphic resolution, and therefore, the identification of shorter polarity intervals. In addition, continental sedimentary sequences from the Songliao Basin in northeast China, studied by He et al. (2012), have also shown the possible presence of polarity variations within C33r.

We report new magnetostratigraphic data from three cores from the Western Canada Sedimentary Basin (WCSB), which, based on previously published biostratigraphic constraints, are known to represent Santonian-Campanian time. The correlative section of the Geomagnetic Polarity Time Scale (GPTS) spans polarity chron 33r and its bounding reversals C34n-C33r and C33r-C33n. The primary objective of this study is to evaluate the paleomagnetic character of chron

\* A version of this chapter has been submitted for publishing to Geophysical Journal International reference GJI-S-13-0535

33r with respect to seafloor paleomagnetic profiles and the GPTS. Lerbekmo and Evans (2012) discovered the presence of so-called ‘tiny wiggles’ in chron 33n in a core from southern Alberta, Canada, and demonstrated that the durations of the geomagnetic polarity reversals represented by these ‘tiny wiggles’ have been underestimated. We investigate the presence and durations of additional reversals observed in the paleomagnetic profiles of three cores which correlate with ‘tiny wiggles’ identified in seafloor marine magnetic anomaly profiles, along with their utility as time-stratigraphic markers for correlation. In addition, magnetostratigraphy is used as a tool to facilitate robust age correlations between several stratigraphic units in southern Alberta.

## 4.2 Geologic Background

### 4.2.1 Regional Setting and Stratigraphic Units

Late Cretaceous rocks of the southern Alberta Plains are products of sedimentation in the Western Interior Seaway (Figure 4.1). During Santonian-Campanian time, 3rd-order marine cycles (Kauffman, 1977; Caldwell et al., 1993) distributed a succession of clastic material sourced from the Cordilleran orogen. From oldest to youngest, the stratigraphic units studied here are: First White Specks Member, Milk River Formation, Alderson Member (lower Lea Park Formation), Pakowki/upper Lea Park Formation, and Foremost Formation. The unconformity-bounded Alderson Member occupies a stratigraphic position laterally equivalent to the Milk River Formation, however, the two units are thought to be separated (at least in places) by an unconformity (Shurr and Ridgley, 2002; O'Connell, 2003; Pedersen, 2003).

The First White Specks Member (FWS), as defined by Nielsen et al. (2003), is the uppermost lithostratigraphic unit of the Niobrara Formation (Colorado Group). The unit is widespread in the southern WCSB, and is comprised primarily of

calcareous marine mudstone with coccolithic debris (white specks). The FWS is interpreted to represent a condensed section deposited during a sea level highstand

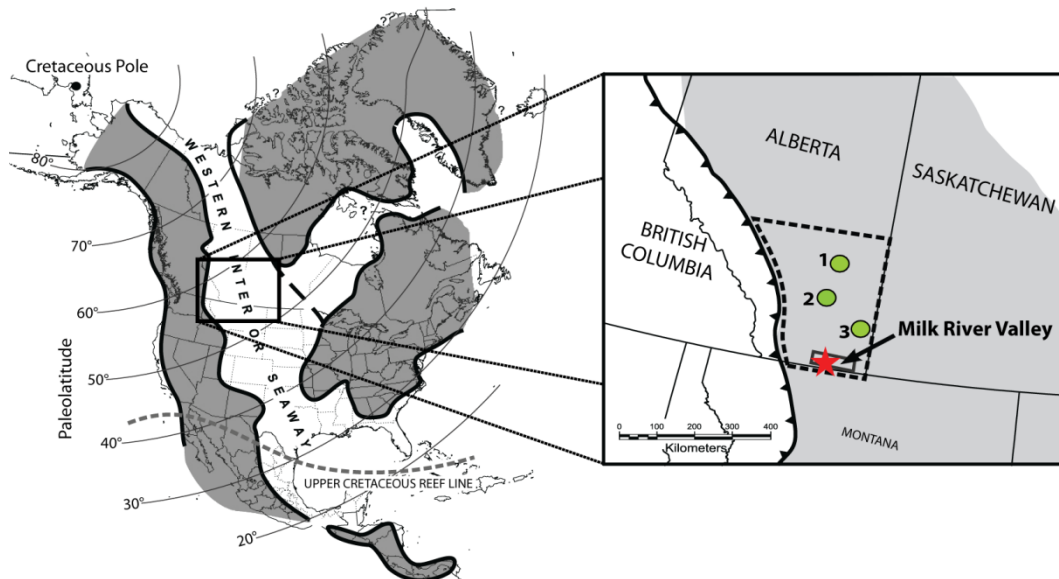


**Figure 4.1** Study area. Left: approximate distribution of Campanian marine deposits of the Western Interior Seaway (after Kauffman (1984) and Couillard and Irving (1975)). Right: locations of studied cores and localities referenced in the text. 1. Amoco B-1 Youngstown (ABY) well (51.61N, 111.05W). 2. ARC Brooks/Princess (ABP) well (50.66N, 111.55W). 3. Nexen Medhat (NM) well (50.21N, 110.13W). Star marks location of Writing-On-Stone Provincial Park.

(peak transgression), preceding the subsequent regression of the seaway and progradation of the Milk River Formation in southern Alberta (Kauffman, 1977; Leckie et al., 1994; Nielsen et al., 2003). The top of this unit is commonly used as a stratigraphic marker on well logs in the WCSB. The FWS is conformably overlain by the Telegraph Creek Member of the Milk River Formation in southern Alberta and Saskatchewan, and the Alderson Member and Lea Park Formation in progressively more distal regions to the north and east (Schröder-Adams et al., 1998; Nielsen et al., 2003; O'Connell, 2003).

The Milk River Formation of southernmost Alberta is a northward-tapering, sandy clastic wedge (Leckie et al., 1994; O'Connell, 2003) which contains transitional marine to continental sediments. Based on subsurface correlations, Tovell (1956) introduced a three-part lithostratigraphic subdivision of the Milk River Formation

comprised of the Telegraph Creek, Virgelle, and Deadhorse Coulee Members (in ascending stratigraphic order). The scheme of Tovell (1956) remains widely accepted, though several depositional interpretations and stratigraphic models have emerged over the years (e.g., Meijer Drees and Myhr, 1981; Meyer, 1998; Payenberg et al., 2003). The Telegraph Creek Member represents an open marine to shoreface transition, and contains interbedded marine shales and fine sands. The Virgelle Member is comprised of thick, massive packages of shoreface sandstone, and the Deadhorse Coulee Member contains nonmarine shales, siltstones, sandstones, and coal (Tovell, 1956; Payenberg et al., 2002). The entire succession is typically 80-100 m thick. The Milk River Formation (Telegraph Creek Member) rests conformably on top of the FWS. In southernmost Alberta, the Pakowki Formation overlies the Deadhorse Coulee Member of the Milk River Formation. Payenberg et al. (2002) demonstrated that a major hiatus (~2.5 Myr) is present at the Milk River-Pakowki contact in the outcrop area around Writing-On-Stone Provincial Park (WOSPP), based on isotope dates, palynology, and missing ammonite zones.

The Alderson Member of the Lea Park Formation was first introduced by Meijer Drees and Myhr (1981). The unit consists of bioturbated mudrocks, siltstone and very fine grained sandstone (O'Connell, 2010). Despite its original definition as a member of the Lea Park Formation, the Alderson Member is commonly referred as part of the Milk River Formation because of its distal lithology and stratigraphic position relative to the coarser-grained clastics of the Milk River Formation in southernmost Alberta. Meijer Drees and Myhr (1981) attempted to map the Milk River-Alderson shoreline in southern Alberta and used wireline logs to correlate the transition from near shore sediments in the south to the fine-grained marine sediments of the Lea Park Formation in the north. More recent work incorporating palynological and sedimentological evidence along with radiometric ages has shown the bulk of the Alderson Member to be significantly younger than the Milk River Formation exposed in southernmost Alberta in the vicinity of WOSPP (e.g., Ridgley, 2000; Payenberg et al., 2002; O'Connell, 2003;

Pedersen, 2003), bringing into the question the validity of such correlations. The upper boundary of the Alderson Member is marked by a widespread boundary chert pebble horizon easily recognizable in outcrop, core, and on wireline logs (Russell and Landes, 1940; Gill and Cobban, 1973; Meijer Drees and Myhr, 1981; Hamblin and Abrahamson, 1996; Payenberg, 2002; Pedersen, 2003). This boundary has long been interpreted as a transgressive ravinement surface associated with transgression of the Claggett/Pakowki/Lea Park Sea.

The Pakowki Formation is a marine shale which overlies the Milk River Formation in southern Alberta (Russell and Landes, 1940; Tovell, 1956); the two units are separated by the aforementioned unconformity, which is associated with the "Milk River Shoulder", a distinct anomaly on resistivity and porosity well logs. The lower Pakowki Formation contains numerous bentonite beds associated with the widespread Ardmore Bentonite zone, which has been dated at several locations in the Western Interior using radiometric methods and biostratigraphic constraints (Payenberg et al., 2002; Hicks et al., 1995), and thus provides an important time marker for the purposes of this study. The Pakowki Formation is equivalent to the upper Lea Park Formation in areas to the north and east. The top of the Pakowki Formation forms a complex, cyclical transition zone with the overlying Foremost Formation (McLean, 1971; Hamblin and Abrahamson, 1996).

The Foremost Formation (Belly River Group) is paralic in origin and represents a major pulse of clastic influx associated with the Laramide Orogeny and concurrent regression of the Pakowki Sea in southern Alberta. Lithologies range from offshore marine mudstones and siltstones to shoreface sands and coal beds (Slipper and Hunter, 1931; McLean, 1971; Hamblin and Abrahamson, 1996; Gordon, 2000). The Foremost Formation is overlain by nonmarine deposits of the Oldman and Dinosaur Park Formations.

#### **4.2.2 Studied Cores**

Despite being unoriented with respect to declination, cores are advantageous for the study of paleomagnetic reversals because they provide continuous, vertical (or nearly vertical) intervals of stratigraphic section well suited to regular sampling. Because the sampled cores were drilled vertically into the Earth, changes in the sign of magnetic inclination, which may also be supported by changes of 180° in magnetic declination, provide sufficient evidence for polarity change of the Earth's magnetic field (McElhinny and McFadden, 2000). Three cores from wells in southern Alberta, Canada, were selected to study the paleomagnetic character of Alderson-Milk River strata and adjacent units in southern Alberta (Figure 4.1). Cores were selected based on continuity with respect to the stratigraphic interval of interest as well as geographic distribution. The Amoco B-1 Youngstown (ABY; 34-30-08w4; 51.61N, 111.05W) was cored in 1969 and is a classic reference section for the WCSB. ABY is complete across approximately 2250 m of stratigraphic section representing Aptian through Campanian Stages. The palynology of ABY was discussed by Jarzen and Norris (1975) and Norris et al. (1975), providing a basic biostratigraphic backdrop for this key control point. In this study, approximately 664 specimens were derived from material collected from measured depths between 253-541 m in ABY. This depth range spans the lithostratigraphic interval from the upper FWS through lower Foremost Formation, and includes complete sections of the Alderson Member and Pakowki Formation. Lithologically, the interval exhibits an overall coarsening-upward trend from offshore marine deposits of the FWS to sandy, paralic deposits of the Foremost Formation, with the exception of the marine shales associated with the Pakowki/Claggett marine incursion, which are situated between the Alderson Member and the basal Foremost Formation. The Alberta Research Council Brooks/Princess core (ABP; 02-20-12w4; 50.66N, 111.55W) was cut in an exploratory coal hole drilled in 1983. Previously published work on ABP includes foraminiferal analysis by McNeil et al. (1995) and a detailed sedimentological interpretation given in Eberth and Hamblin (1993). 263 specimens were derived

from material collected from measured depths between 150-343 m in ABP. The depth range spans the lithostratigraphic interval from the upper Alderson Member through the lower Foremost Formation. Descriptions of ABY and ABP are given in Hamblin and Abrahamson (1996). Nexen Medhat 6-31-14-1 (NM; 31-14-01w4; 50.21N, 110.13W) was drilled in 2007 and contains a complete Alderson Member section at a more distal location where the Alderson Member is approximately 100m thick and gas-productive. 173 specimens were derived from material collected from measured depths between 371-488 m in NM. This depth range spans the lithostratigraphic interval from the FWS through the basal Pakowki Formation. A detailed description of the sedimentology of this core is provided in O'Connell (2010).

#### **4.2.3 Age Control**

A wealth of biostratigraphic information is available for calibration of the paleomagnetic data presented below. Regional zonal schemes for ammonite, foraminiferal, and palynological data have been previously established for the Upper Cretaceous of the Western Canada Sedimentary Basin (Gill and Cobban, 1973; Norris et al., 1975; North and Caldwell, 1975; Cobban, 1993; Nichols and Sweet, 1993; Kauffman, et al., 1993; Caldwell et al., 1993). In many places, radiometric ages corroborate these biostratigraphic schemes (e.g., Folinsbee et al., 1964; Thomas et al., 1990; Obradovich, 1993; Payenberg et al., 2002) and lend another degree of support to the regional age framework.

The First White Specks Member is associated with the Late Santonian *Desmoscaphites* ammonite zones and the inoceramid bivalve *S. Patootensis* in southern Alberta (Schröder-Adams et al., 1998), suggesting an Upper Santonian age. The age of the base of the Milk River Formation is based on ammonite specimens found in the Telegraph Creek Member near the international border belonging to the *Desmoscaphites bassleri* zone (Cobban, 1955; Gill and Cobban, 1973). The hiatus associated with the Milk River-Pakowki contact was proposed

by Payenberg (2002) and Payenberg et al. (2002), and was estimated to represent a time gap of approximately 2.5 Ma. The duration of the hiatus in this area is based on the absolute age of the Ardmore Bentonites above, and on the magnetic polarity reversal from chron 34 to 33r below, which was determined to lie within the Deadhorse Coulee Member (Leahy and Lerbekmo, 1995). In addition, palynological data support the presence of such a hiatus, as members of the *Aquillapollenites* complex were found to be largely missing in outcrop sections at WOSPP (Payenberg, 2002; See Payenberg et al., 2002 for detailed discussions regarding the palynological characteristics of the Milk River Formation). The regional extent of the hiatus remains largely uninvestigated. A few poor-quality specimens of *Scaphites hippocrepis* and *Baculites sp.* (smooth) have been found in distal Alderson Member cores from southwestern Saskatchewan (Ridgley, 2000), indicating that the large hiatus recognized at WOSPP may diminish toward distal sectors of the basin where Alderson Member sediments account for at least some of the missing time. In southernmost Alberta, in areas in and around WOSPP, the Ardmore Bentonites are dated at  $80.7 \pm 0.2$  Ma (Payenberg et al., 2002); they have also been dated at  $80.7 \pm 0.6$  Ma,  $80.8 \pm 1.4$  Ma, and  $81.0 \pm 0.7$  Ma in southern Montana and Wyoming (Hicks et al., 1995). The Ardmore Bentonites occur within close proximity to the base of the Pakowki Formation, and thus constrain the age of the onset of the Claggett transgression in southern Alberta (Payenberg et al., 2002). The Pakowki Formation has yielded ammonite specimens belonging to the *Baculites obtusus* and *Baculites mclearni* zones (Russell and Landes, 1940). Lerbekmo (1989) placed the chron 33r-33n boundary just above the base of the Foremost Formation in southernmost Alberta. This reversal corresponds to an approximate age of 79.5 on the GPTS and is therefore in agreement with the ages obtained for the underlying Ardmore Bentonites. Several radiometric bentonite ages ranging from approximately 72-76 Ma for the overlying Oldman and Dinosaur Park Formations (Belly River Group) in southern Alberta are given by Thomas et al. (1990) and Eberth and Hamblin (1993). As none of the samples measured in this study were taken from intervals stratigraphically higher than the Foremost Formation, the ages provided by

Thomas et al. (1990) and Eberth and Hamblin (1993) provide an upper age limit to the interval studied here. Consequently, the rocks analyzed in this study predate later Campanian magnetic polarity reversals associated with chron 32. Using the collective aforementioned age constraints, it is possible to bracket the 3 cored intervals studied here to within a combined age range of approximately 77-85 Ma. The respective section on the GPTS correlates to polarity C33r and its bounding reversals, as well as the uppermost and lowermost portions of C34n and C33n, respectively.

### 4.3 Methodology

Material collected from the ABY, ABP, and NM cores (continuous lengths of 254.2 m, 192.6 m and 117.4 m, respectively) was subjected to a rigorous multi-step process consisting of discrete core segment preparation, pilot testing, demagnetization treatment and paleomagnetic measurements, data analysis and filtering. Two primary criteria were used in selecting core segments for analysis: 1) orientation confidence; 2) relatively smaller grain size. If the orientation of a particular length of core was ambiguous or unclear to any degree, no segments were taken. Furthermore, segments were rarely collected from parts of the core immediately adjacent to box ends to avoid scenarios where sections may have been missing from above or below the core segments, and also to avoid sampling core tops which may have been damaged or contaminated by the drill bit. The sampling interval was approximately 1.5 m, which, based on a sedimentation rate for the Campanian of Alberta of ~60 m/Ma (Lerbekmo, 1989; J.F. Lerbekmo, personal communication), ensured the recognition of magnetic reversals with durations as short as 25,000 years. Between 2 and 5 cubic specimens ( $8 \text{ cm}^3$ ) were cut from each core segments. In total, 387 core segments were sampled yielding approximately 1100 discrete specimens from the ABY, ABP, and NM cores. In nearly all cases, more than one discrete specimen was derived from each core segment. The obtained inclination values were averaged for each core segment,

providing an additional measure of quality control and resulting in a robust dataset.

The magnetic mineralogy of the cores was investigated in representative specimens using thermal dependent magnetic susceptibility (MS) and isothermal remanent magnetization (IRM) experiments. All measurements were processed in the paleomagnetic laboratory at the Department of Physics, University of Alberta. Remanent magnetization measurements were made using a 2G Enterprises DC-squid cryogenic magnetometer, within a permalloy shielded room. Additionally the whole paleomagnetic laboratory room is shielded by an aluminum shield installed along the wall to suppress any industrial frequency electromagnetic noise to negligibly small level. The lab is built in the deep (second level) basement to avoid any microseismic noise. Magnetic susceptibility (MS) was measured with a Bartington susceptibility meter system. Demagnetization data was analysed using PMGSC software (Enkin, 1996).

Pilot specimens representative of a variety of lithologies and stratigraphic levels in each core were subjected to alternating field (AF) demagnetization with applied field steps of 5mT and 10mT up to 80mT. Based on their behaviour, an experimental protocol with demagnetization steps of 5mT up to 35mT was used for the ABY core, and demagnetization steps of 5mT up to 50mT were used for the ABP and NM cores. To ensure the reliability of the AF measurements, thermal demagnetization was applied to pilot specimens for each of the cores. The magnetic directions were determined by orthogonal diagrams (Zijderveld, 1967) and principal component analysis (Kirschvink, 1980).

## 4.4 Results

### 4.4.1 Rock Magnetism Results

Specimens from the ABY and NM cores were subjected to rock magnetic experiments. We assume rock magnetic characteristics are similar for the ABY and ABP cores, because of their relative proximity and the fact that they represent similar stratigraphic intervals. Figure 4.2 presents the results of MS and IRM experiments. MS measurements were consistent among all measured specimens and a marked high temperature peak at  $\sim 480^{\circ}\text{C}$ - $510^{\circ}\text{C}$  is observed, most likely related with the presence of magnetite or low titanium magnetite (Figure 4.2). Furthermore, MS increases above  $600^{\circ}\text{C}$ , indicating the creation of hematite in the specimens as a result of heating them in air. These characteristics are indicative of grains carrying a primary detrital remanent magnetization. All experiments were conducted in air, therefore, oxidation of the specimens is expected.

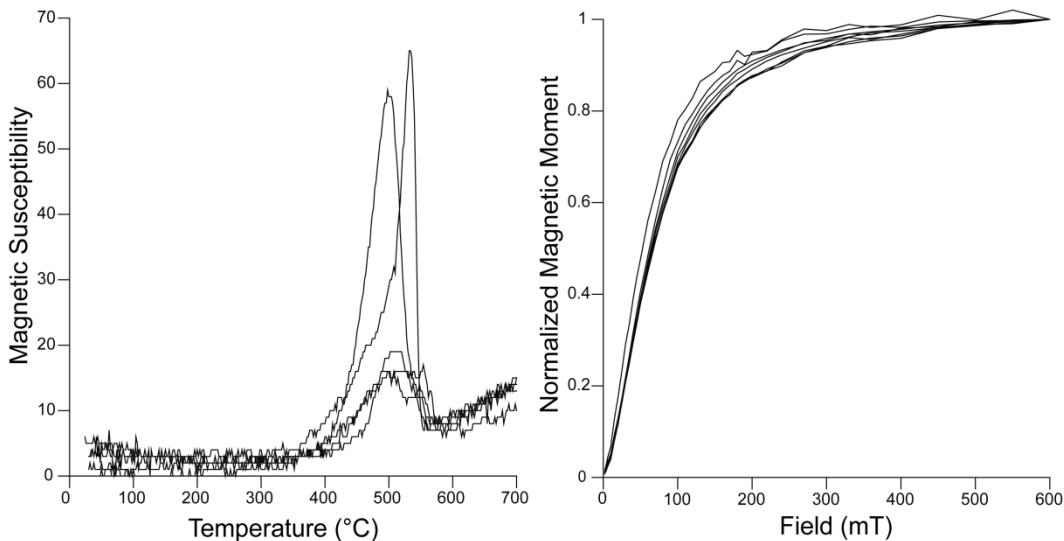


**Figure 4.2.** Results from thermal-dependent magnetic susceptibility (MS, left hand side) and isothermal remnant magnetization (IRM, right hand side) experiments for Amoco B-1 Youngstown (ABY) and Nexen Medhat (NM) cores.

IRM results typically acquired a saturation point at  $\sim 200$  mT, result consistent with the presence of magnetite or titanomagnetite in the specimens. At higher

demagnetization fields, increased IRM is observed. This characteristic is most likely related to the presence of high coercivity minerals such as hematite, which might be an indication of a later chemical remanent magnetization overprint (probably created in the laboratory).

Overall, thermal dependent MS and IRM experiments are consistent between the cores, confirming the presence of magnetite and/or titanomagnetite as primary carriers of magnetization and hematite as a chemical remanence created during the experimental procedure.

#### **4.4.2 Paleomagnetic Results**

Thermal demagnetization experiments showed to be consistent with AF experiments (Figure 4.3). However, due to the weak nature of the magnetization of sedimentary rocks, the majority of the specimens demagnetized using thermal experiments decayed very fast and only great circles could be used to determine the nature of the vector. For this reason, we used AF as the primary demagnetization technique.

For the ABY core, AF demagnetization was applied to 664 specimens (220 core segments) and revealed magnetizations with typical intensities on the order of  $1 \times 10^{-3}$  A/m. Some specimens presented a low coercivity component, probably of viscous origin, usually demagnetized at 10 mT (Figure 4.3). In the majority of the cases, a stable vector direction was observed between 15 mT and 35 mT and principal component analysis was used to determine the directions (Figure 4.3). However, some specimens did not behave as a stable direction during demagnetization, but instead demonstrated a trend along the great circle. In these cases, the polarity was determined by the course of the trend (Figure 4.3).

A total of 263 specimens from 108 core segments were subjected to AF demagnetization for the ABP core. Typical magnetization was on the order of

$1 \times 10^{-3}$ A/m to  $1 \times 10^{-4}$ A/m. The specimens showed a stable magnetic vector direction in the majority of the cases, which was usually acquired between 15 mT and 50 mT (Figure 4.3).

The NM core presented the lowest magnetization, typically on the order of  $1 \times 10^{-4}$ A/m. In total, 173 specimens from 72 core segments were measured. A stable vector direction was difficult to obtain, as the NRM was carried by a low coercivity phase, however, in the majority of cases, the underlying polarity was clear and followed a great circle trend (Figure 4.3).

Because the cores were only oriented with respect to the top and bottom of the core and not respect to declination, only inclination data could be used for analysis of polarity reversals. Low- and mid-inclination ( $\sim > \pm 30^\circ$ ) core segment values are, in the majority of the cases, not taken into account for the determination of magnetostratigraphic zonation because they could represent excursions of the magnetic field (Vandamme, 1994; Laj and Channell, 2007), insufficiency of the recording medium (Roberts and Winklhofer, 2004; Channell and Guyodo, 2004), or poor rates of sediment accumulation (Laj and Channell, 2007).

Histograms of inclinations for each core are shown in Figure 4.4. All inclination results obtained in the cores are included on the plots. Normal and reverse polarities for the characteristic remanent magnetization from the stable directions are distributed in nearly antipodal clusters for all cores, a result that corroborates the primary characteristic of the remanence. The ABY core average inclination for normal polarity is  $I=52.2^\circ$  ( $\sigma=11.6$ ) for 74 core segments and  $I=-49.5^\circ$  ( $\sigma=13.3$ ) for 84 reverse polarity core segments; the ABP core normal polarity average inclination is  $I=53.9^\circ$  ( $\sigma=10.7$ ) for 42 core segments and  $I=-51.8^\circ$  ( $\sigma=12.5$ ) for 41 reverse polarity core segments; the NM core average normal inclination polarity is

$I=60.1^\circ$  ( $\sigma=11.9$ ) for 18 core segments and its average reversal inclination is

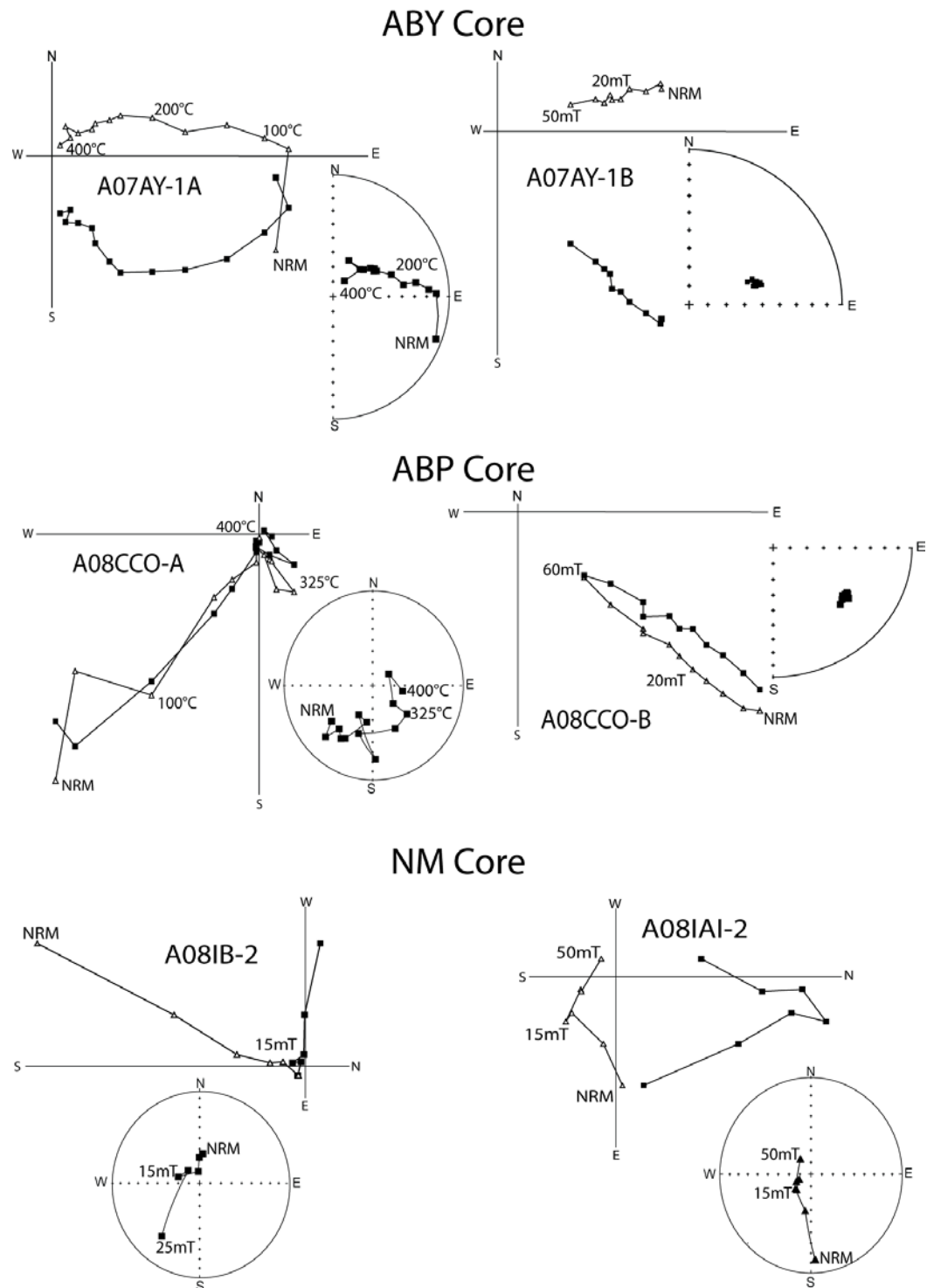


**Figure 4.3.** Equal-area projections, demagnetization orthogonal diagrams (Zijderveld, 1967) and intensity decay plots for the studied cores. Open (close) symbols in orthogonal plots represent projections onto the vertical (horizontal) plane. NRM: natural remanent magnetization.

$I = -49.5^\circ$  ( $\sigma = 13.1$ ) for 20 core segments. These inclinations are shallower than the expected inclination for the drilling sites ( $I = 65.4^\circ$ ,  $\alpha_{95} = 4.0^\circ$  for ABY;  $I = 64.8^\circ$ ,  $\alpha_{95} = 4.1^\circ$  for ABP;  $I = 64.3^\circ$ ,  $\alpha_{95} = 4.1^\circ$  for NM) calculated from the master APWP for North America at 80 Ma (Besse and Courtillot, 2002). Shallowing is usually observed in sedimentary rocks because of pre- and post-depositional compaction processes (King 1955; Butler 1992). If inclination shallowing was present in the studied cores, the observed inclination  $I_o$  could be related to the expected inclination  $I_a$  by Kent and Tauxe (2005):

$$\tan I_o = f \tan I_a, \quad (4.1)$$

where  $f$  is the flattening factor (King 1955), which has been found experimentally to lie between 0.4 and 0.6. Assuming  $f = 0.5$  (Figure 4.4), the bimodality of the inclination distribution is enhanced in the three cores, having a higher distribution

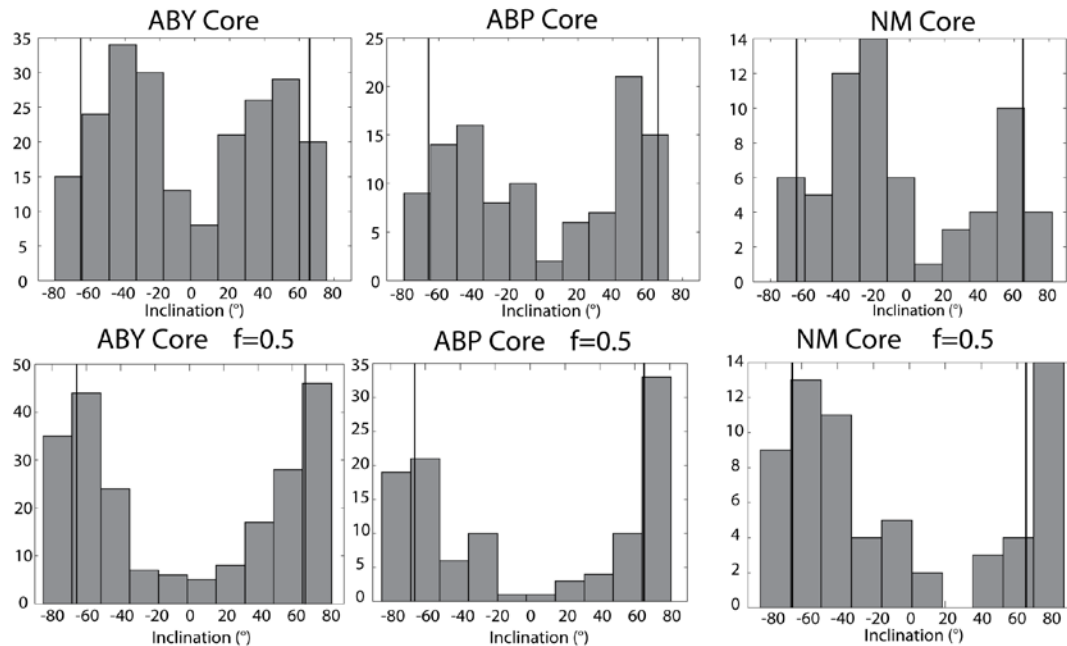


**Figure 4.4.** Inclination histograms for ABY, ABP and NM cores. The expected inclinations for each site are marked by the black straight lines ( $\pm 65.4^\circ$ ,  $\pm 64.8^\circ$ ,  $\pm 64.3^\circ$ , respectively).

of inclination close to the expected inclination. This effect is mainly observed in the ABY core (Figure 4.4). To further analyze the behavior of the inclination distribution, we also corrected the inclination with a flattening factor of  $f = 0.4$  and  $f = 0.6$ . For  $f = 0.4$ , the peak of the inclination distribution moved to higher inclination values in all cores, and for  $f = 0.6$ , the inclination distribution is very similar to the results obtained with  $f = 0.5$ . Although these results are consistent with sedimentary rocks that present inclination shallowing, they are not conclusive. The variations between our inclinations and the corrected ones are not significant enough, and the behavior of the inclinations in each core are different, therefore it is difficult to conclude whether or not inclination shallowing is a factor in southern Alberta.

#### 4.4.3 Magnetostratigraphy

Core segments were considered reliable if more than two specimens provided good directional information and if the mean inclination per segments is  $\sim < 30^\circ$ . To define a magnetostratigraphic zonation, more than one reliable core segment was preferred when defining a normal or reversed zone. However, in some cases normal/reverse zones were defined using only one high quality core segment. Inclination profiles and polarization zonations numbered from the top of the cores are presented in Figure 4.5.

The ABY core has a total of 9 reverse and 10 normal polarity zones, defined as YR and YN, respectively, in Figure 4.5a. Two major normal polarity intervals are observed between 511.43m and 482.16m (YN1) and 270.86m and 223.69m (YN10). Furthermore, eight well defined normal polarity features can be also observed (YN2, YN3, YN4, YN5, YN6, YN7, YN8 and YN9). The ABP core presents a total of 3 reverse and 3 normal zones (PR and PN, respectively, Figure 4.5b). A major normal polarity zone is observed at the top of the core, followed by two small normal polarity intervals at 442.80m (PN2) and 501.70m (PN3). NM core is dominated by long intervals of reverse polarity (Figure 4.5c). A total of 4

reverse and 5 normal polarity zones are observed (denoted by MR and MN, Figure 4.5c). Short reverse polarity intervals are observed at 419.60m (MN2), 405.00m (MN3) and 368.36m (MN4), while a well defined normal polarity zone is observed at 346.45m (MN5).

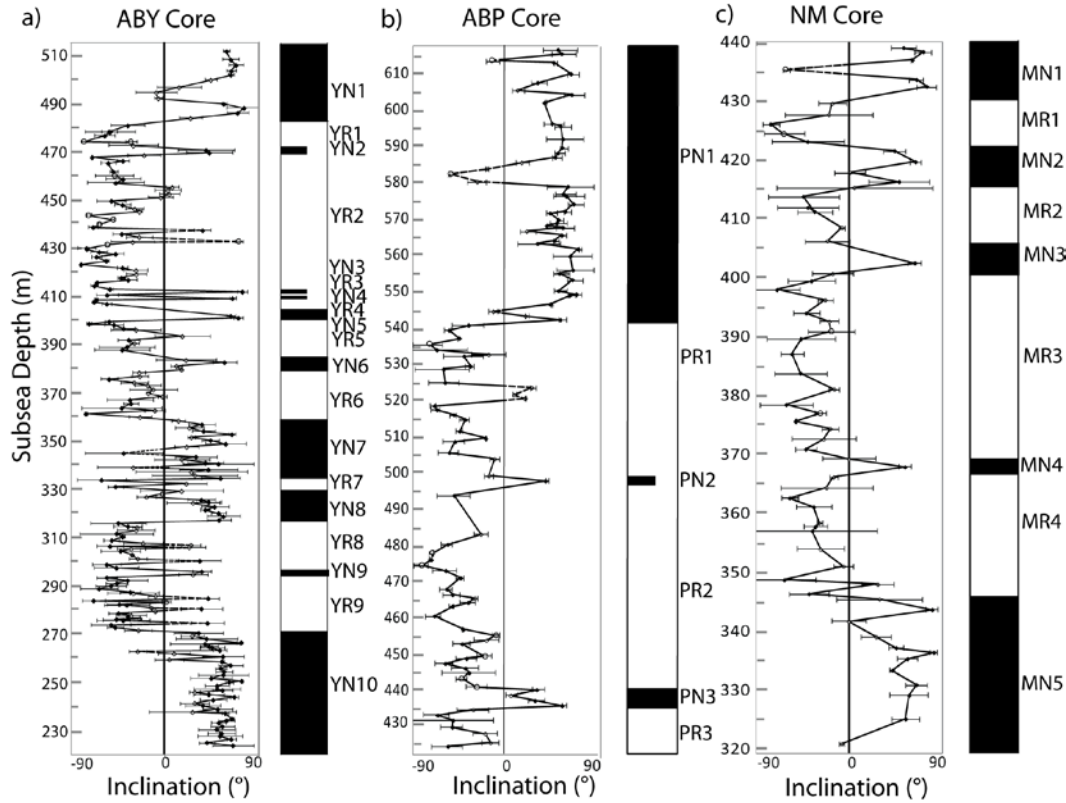


**Figure 4.5.** Inclination profiles and polarization zonations numbered from the top of each core. Close (open) diamonds represent core sections with inclination higher (lower) than  $\pm 30^\circ$ . Open circles represent low quality core sections. Dashed sections of the inclination profile represent core segments that were not considered as polarization zones. Subsea depth (m) with respect to ground elevation at well is shown. Error bars represent the standard deviation of the average inclination per core segment.

The magnetostratigraphic framework established between the studied cores, along with a superimposed lithostratigraphic breakdown for each core is presented in Figure 4.6. The correlation with the GPTS shown in Figure 4.6 is based upon the numerous age constraints discussed above, in conjunction with the reversal patterns established for the cores. The position of the C33r-C33n boundary is located at YN1-YR1 and PN1-PR1 (time line T5, Figure 4.6), thus the C33r-C33n polarity reversal is recorded in the lower Foremost Formation in the ABY and

ABP cores, albeit at slightly different lithostratigraphic positions. Lerbekmo (1989) and Leahy and Lerbekmo (1995) also place this reversal in the lowermost part of the Foremost Formation in the Milk River area within several meters of the top of the Pakowki Formation. In the NM core, the C33r–C33n boundary is difficult to determine because NM only extends ~2m above the top of the Alderson Member, thus the paleomagnetic character of the bulk of the Pakowki Formation is unknown at this location. The normal magnetozone observed at MN1 could represent a short polarity zone in C33r, however, correlation with paleomagnetic profiles of the other control points is suggestive of C33r–C33n being present in the uppermost Alderson Member at NM. Additionally, the C34n–C33r reversal, which nearly coincides with the Santonian–Campanian boundary (Obradovich, 1993) and the end of the long normal "Cretaceous normal polarity superchron" is clearly identifiable in the ABY core at YR9–YN10 and in the NM core at MR4–MN5 (time line T1, Figure 4.6). In both cores, the contact is located in the basal Alderson Member, providing the first empirical age (~83.5 Ma) for the lower Alderson Member in distal reaches of the Milk River–Alderson system. The C34n–C33r contact is not present in the ABP core because the core ends immediately below the Alderson–Pakowki contact.

Based on the age correlations with the GPTS and assuming a linear sedimentation rate for the sampled intervals, the average sedimentation rates were determined. For the ABY core, YN1–YR1 (C33r–C33n boundary) and YR9–YN10 (C34n–C33r boundary) were used as age markers for the calculation, which resulted in an average sedimentation rate of 50.9 m/Myr. For the ABP core, PN1–PR1 (C33r–C33n boundary) was used as an age marker. For a lower age boundary, we use the time line T4 (Figure 4.6), resulting in an average rate of 44.7 m/Myr. In the NM core, only the C34n–C33r limit is clearly defined, thus we again used time line T4 for an upper age boundary to obtain a value of 35.1 m/Myr. The higher sedimentation rate at ABY can explain the several short normal polarity magnetozones (YN2, YN3, YN4, YN5 and YN6) observed within C33r. These short geomagnetic events are not observed in the other two cores, possibly

because of varying sedimentation rates, and therefore, the ability to record the geomagnetic polarity transitions. In addition, a somewhat denser sampling scheme for the ABY core may also be a contributing factor. Furthermore, normal magnetozones YN7-YN8 in the ABY core correlate very well with normal zone PN3 in the ABP core and normal zones MN2 and MN3 in the NM core (time lines T4 and T3 in Figure 4.6).

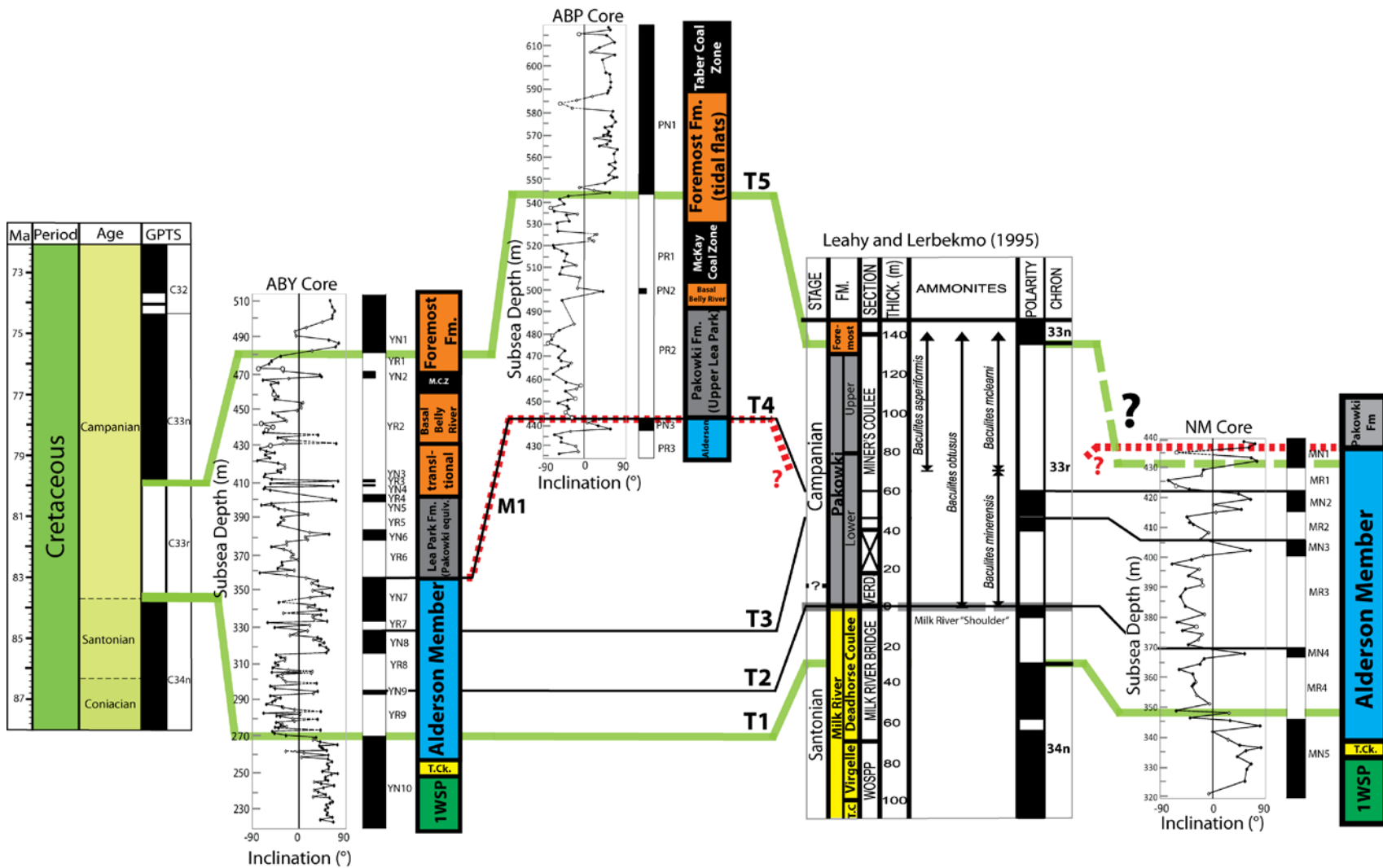


**Figure 4.6.** Time correlation between the studied magnetostratigraphic sections. Lithostratigraphic units are also illustrated for each location. Green lines represent the C33n-C33r and C33r-C34 boundaries in each of the studied cores as well as those established by Leahy and Lerbekmo (1995) in the Milk River Valley. Chron boundaries are correlated to the Geomagnetic Polarity Timescale (GPTS) (Ogg and Smith, 2004). Black lines present our correlation of microchrons. T1-T5 denote established timelines referenced in the text. Red short-dashed line represent the base of the Pakowki Formation, M1. Small question marks represent the Pakowki transgression (refer to manuscript for discussion). Large question mark represents the ambiguity to determine the C33n-C33r. Inclination profile plotting convention as in Figure 4.5, error bars are not illustrated.

## 4.5 Discussion

Figure 4.7 presents the comparison of the composite magnetostratigraphic profile of the studied sites and several magnetostratigraphic studies for the Upper Cretaceous. To create the composite profile, the ABY core was selected as the reference core and correlation lines in Figure 4.6 were used as a guide to adjust for the ABP and the NM cores. We included all the available magnetostratigraphic profiles that are reliably described in the literature and show short polarity intervals within C33r. The presence of the normal polarity intervals within C33r between the different cores is quite consistent and correlates well with the tiny wiggles C33r.*a* and C33r.*b* of Bouligand et al. (2006) (black arrows in Figure 4.7). Lerbekmo and Evans (2012) argued that the duration of tiny wiggles on oceanic crustal blocks is seriously underestimated and showed that the polarity intervals determined from their core is at least an order of magnitude larger than those implied by marine magnetic anomaly patterns. Our results are consistent with those of Lerbekmo and Evans (2012). Our most prominent short normal polarity intervals (shown with grey correlation lines in Figure 4.7) have estimated durations of 500.0 kyr (first correlation interval, Figure 4.7) and 278.2 kyr (second correlation interval, Figure 4.7) compared to a duration of 10 kyr for C33r.*a* and 16 kyr for C33r.*b* (Bouligand et al. 2006). Assuming an average sedimentation rate of 50.8 m/Myr for the ABY core, we estimate the double event to be centered at approximately 81.6 Ma and 82.1 Ma. These ages do not fit exactly with the estimations of Bouligand et al. (2006) for “tiny wiggles” *a* and *b*. This may be attributed to varying rates of sedimentation. We incorporate the age

estimations of the “tiny wiggles” *a* and *b* of Bouligand et al. (2006) to our study and readjust the age of the double normal polarity magnetozone to be centered at 80.4 and 81.6 Ma.

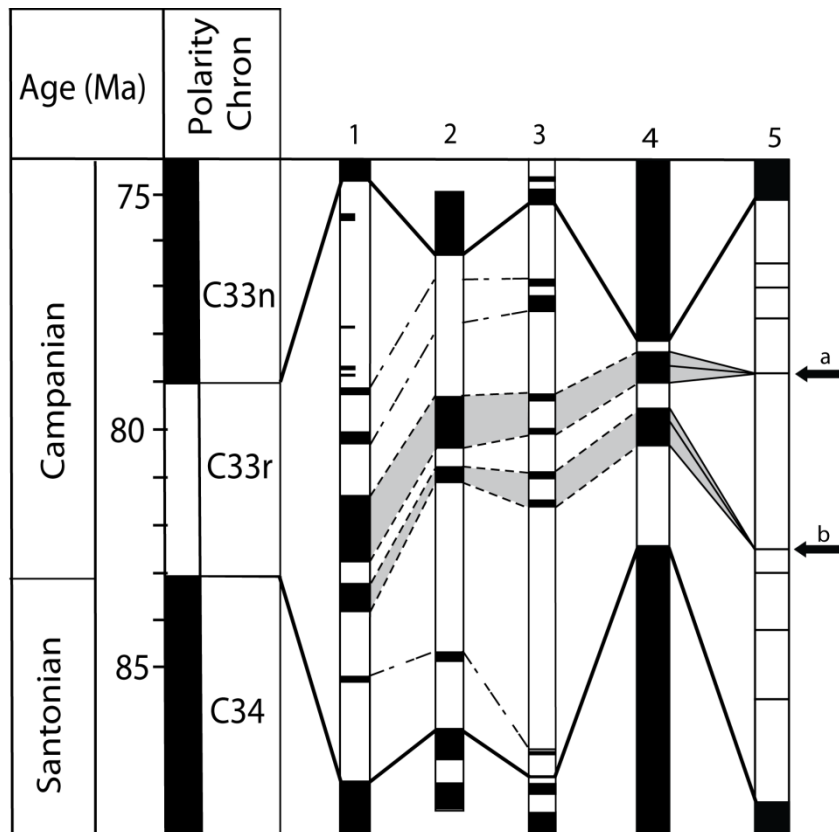


**Figure 4.7.** Correlation between composed magnetostratigraphic profile of the studied cores and Upper Cretaceous cores. Shade area represents the interpreted correlation between the cores. Black arrows represent tiny wiggles *a* and *b* of Boulingand et al. (2006). 1. This study. 2. Leahy and Lerbeckmo (1995). 3. Montgomery et al. (1998). 4. He et al. (2012), second interpretation of their core. 5. Bouligand et al. (2006).

The stratigraphic implications of the time framework presented in Figure 4.6 underscore the complexity and interrelated nature of the contiguous depositional units which comprise the Late Santonian-Early Campanian of southern Alberta. The position of the C34n-C33r boundary within the lowermost Alderson Member provides the first convincing evidence of the age of these gas-bearing strata in distal reaches of the Alderson depositional system (~83.5 Ma). When correlated

with the C34n-C33r boundary of Leahy and Lerbekmo (1995), time equivalency is demonstrated between the lowermost Alderson Member and at least the upper ~20 m of the Deadhorse Coulee Member in southernmost Alberta (Figure 4.6). This correlation suggests that nonmarine deposits of the Deadhorse Coulee Member were a proximal component of the Alderson depositional system in southeastern Alberta. This correlation is in general agreement with the interpretation discussed in Shurr and Ridgley (2002; their figure 9; unconformity "B-2").

The occurrence of the C34n-33r boundary in the NM core in this study is in partial conflict with the chronostratigraphic framework put forth by Payenberg et al. (2002), who reasoned that the entire Alderson Member is younger than the entire Milk River Formation (including the Deadhorse Coulee Member), based largely upon contrasting palynological assemblages observed in correlative units. They did not, however, include palynological analysis of the Alderson Member itself in their study. Additionally, the temporal resolution of palynostratigraphy may not be high enough to resolve such details in this case. It is proposed here that the age framework given by Payenberg et al. (2002) be modified slightly to show partial time equivalency between the Deadhorse Coulee Member and the lowermost Alderson Member. O'Connell et al. (1992, 1999) and O'Connell (2003) also interpreted the entire Alderson Member to be younger than the entire Milk River Formation based on the presence of a regional unconformity separating the two units ("basal Alderson unconformity") and supporting palynological data, however, these data remain unpublished thus the sampling locations/depths are unknown.

The basal Alderson unconformity proposed by O'Connell et al. (1992) and later discussed by O'Connell et al. (1999) and O'Connell (2003,2008) has been described as a major sequence boundary characterized by the presence of a chert pebble horizon. We do not disagree with the interpretation of an event-significant surface at this horizon in Alderson cores, however, we suggest that in its more

proximal reaches in southernmost Alberta, the contact is more likely to be present in the lower Deadhorse Coulee Member in the WOSPP area, even though it has not yet been recognized in outcrop. In a clastic stratigraphic sequence, subaerial unconformities are overlain by nonmarine deposits when preserved (Catuneanu, 2006), such as those which dominate the Deadhorse Coulee Member, though they can be difficult to recognize (Fanti and Catuneanu, 2010 and references therein). The notion that the entire Alderson Member is younger than the Milk River Formation in southern Alberta and completely separated from it by a major regional unconformity is contradictory to the data presented here.

The magnetostratigraphic correlation shown in Figure 4.6 has interesting implications with regard to the onset of the Pakowki transgression in southern Alberta. When the transgressive ravinement surface at the base of the Pakowki Formation (M1 in Figure 4.6) is correlated within the context of the magnetostratigraphic framework, its diachronous nature becomes apparent. Timeline T4 (Figure 4.6) coincides with M1 at ABY and ABP indicating similar depositional conditions in areas to the north. The occurrence of the same reversal at the same lithostratigraphic boundary provides some measure of evidence for erosion and missing time at this contact. In contrast to the correlation between ABY and ABP, T4 occurs approximately 12 m below M1 in the NM core, indicating that the Pakowki transgression occurred at least somewhat later at this location. When correlated to the magnetostratigraphic interpretation of Leahy and Lerbekmo (1995), T4 shows a striking difference between the age of the Pakowki transgression in the Milk River Valley versus areas to the north, as 60m of Pakowki shales are present between M1 and T4 in Leahy and Lerbekmo's section. Timeline T4 suggests that the Pakowki transgression probably progressed from west to east, but may have simultaneously progressed from south to north, at least on a subregional scale.

The relative position of T5 between ABY, ABP, and Leahy and Lerbekmo's (1995) section may also yield insight into the diachronous nature of the Foremost

Formation, which appears to become younger in a southerly direction. The relative thicknesses of the Foremost sections at ABY and ABP are indicative of higher sedimentation rates to the north, which may signify closer proximity to sediment source areas and/or more accommodation, and therefore support this idea. Furthermore, timeline T5 (Figure 4.6) highlights the possibility of time equivalency between the lower Foremost Formation and the uppermost Alderson Member at the NM core. Genetic linkages between the Alderson Member and the Pakowki and lower Foremost Formations cannot be ruled out, and in fact, seem likely. The work by O'Connell et al. (1992) and Payenberg et al. (2002) demonstrated palynological similarity between the Alderson Member and the Pakowki Formation, though they did not suggest any depositional link between the two units.

## 4.6 Conclusions

Based on the correlation presented in Figure 4.6 and Figure 4.7, we conclude the following:

- 1) The presence of short polarity intervals within chron 33r is evident in the three studied cores. The durations of these intervals are consistent with previous studies of “tinny wiggles” in sedimentary sections, and are more than an order of magnitude longer than those observed in the marine magnetic anomaly pattern interpretations.
- 2) The presence of C34n-C33r in the lower Alderson Member in the NM core provides the first empirically-derived age (~83.5 Ma) for this unit in southern Alberta.
- 3) Time-equivalency is demonstrated between the Deadhorse Coulee Member in the Milk River Area and the lower Alderson Member in southeastern Alberta, suggesting a probable genetic link between these units. In the same way, this

correlation contradicts the presence of a persistent regional unconformity which completely isolates the Alderson Member from the Milk River Formation.

4) The Pakowki transgression appears to have both west-to-east and south-to-north directional components. It occurred first in the Milk River Valley, followed by areas near the ABY and ABP cores, and later in areas further to the east near the NM core.

5) Average sedimentation rates in the studied cores of southern Alberta generally decrease from west to east; rates of 50.8 m/Myr, 44.7 m/Myr and 35.1 m/Myr were observed in the ABY, ABP and NM cores, respectively. This is consistent with the sedimentation rate of 57.0 m/Myr reported for the CPOG Strathmore core (~100km west of ABY) by Lerbekmo and Evans (2012).

In the case of the Santonian-Campanian of the southern Alberta Plains, high-resolution magnetostratigraphy using core proved to be a revealing tool with respect to stratigraphic relationships and the timing of important geologic events. No other tool is capable illuminating these items with such clarity and precision. Regardless of absolute ages, the ability to correlate relative moments in time across a basin is demonstrated.

## Bibliography

Besse, J., Courtillot, V., 2002. Apparent and true polar wander and the geometry of the geomagnetic field for the last 200 Myr. *Journal of Geophysical Research*, 107(0), 1–33. doi:10.1029/2000JB000050.

Bouligand, C., Dymond, J., Gallet, Y., Hulot, G., 2006. Geomagnetic field variations between chronos 33r and 19r (83–41 Ma) from sea-surface magnetic anomaly profiles. *Earth and Planetary Science Letters*, 250, 541–560.

Butler, R.F. 1992. Paleomagnetism: magnetic domains to geologic terranes. Blackwell Scientific Publications, Boston, MA. pp. 238.

Caldwell, W.G.E., Diner, R., Eicher, D.L., Fowler, S.P., North, B.R., Stelck, C.R., von Holdt Wilhelm, L., 1993. Foraminiferal biostratigraphy of Cretaceous marine cyclothem, in Caldwell, W.G.E. and Kauffman, E.G. (eds.), Evolution of the Western Interior Basin. Special Paper - Geological Association of Canada, no. 39, p. 477-520.

Catuneanu, O., 2006. Principles of Sequence Stratigraphy. First Edition, Elsevier, Amsterdam, 375 p.

Channell J.E.T, Guyodo, Y. 2004. The Matuyama Chronozone at ODP Site 982 (Rockall Bank): Evidence for decimeterscale magnetization lock-in depths. In: Channell et al. (eds.) AGU Geophysical Monograph Seminar, 145: Timescales of the Geomagnetic Field, pp. 205–219. Washington, DC: AGU.

Cobban, W.A., 1955. Cretaceous rocks of northwestern Montana. In Lewis, P.J. (ed.), Billings Geological Society, Sixth Annual Field Conference, Guidebook: 107–119.

Cobban, W.A. 1993. Diversity and distribution of Late Cretaceous ammonites, Western Interior, United States. In Evolution of the Western Interior Basin. Edited by W.G.E. Caldwell and E.G. Kauffman. Geological Association of Canada Special Paper 39, pp. 435–451.

Couillard, R., Irving, E., 1975. Palaeolatitude and reversals: evidence from the Cretaceous Period, in Caldwell, W.G.E. (ed.), *The Cretaceous System in the Western Interior of North America*, *Special Paper Geological Association of Canada*, no. 13, p. 21-29.

Eberth, D.A., Hamblin, A.P., 1993. Tectonic, stratigraphic, and sedimentologic significance of a regional discontinuity in the Upper Judith River Group (Belly River wedge) of southern Alberta, Saskatchewan, and northern Montana, *Canadian Journal of Earth Sciences*, v. 30, no. 1, p. 174-200.

Enkin, R.J., 1996. A computer program package for analysis and presentation of paleomagnetic data, Pacific Geoscience Center, Geological Survey of Canada.

Fanti, F., Catuneanu, O., 2010. Fluvial sequence stratigraphy: the Wapiti Formation, west-central Alberta, Canada. *Journal of Sedimentary Research*, 80, 320-338.

Folinsbee, R.E., Baadsgaard, H., Cumming, G.L., Nascimbene, J., 1964. Radiometric dating of the Bearpaw Sea, *Bulletin of the American Association of Petroleum Geologists*, v. 48, p. 525.

Gill, J.R., Cobban, W.A., 1973. Stratigraphy and geologic history of the Montana Group and equivalent rocks, Montana, Wyoming, and North and South Dakota. U.S. Geological Survey Professional Paper, no. 776, 37p.

Gordon, J., 2000. Stratigraphy and Sedimentology of the Foremost Formation in Southeastern Alberta and Southwestern Saskatchewan. Unpublished Master's thesis, University of Regina, Regina, Saskatchewan, 110 p.

Hamblin, A. P., Abrahamson, B.W., 1996. Stratigraphic architecture of "Basal Belly River" cycles, Foremost Formation, Belly River Group, subsurface of southern Alberta and southwestern Saskatchewan. *Bulletin of Canadian Petroleum Geology*, v. 44, no. 4, p. 654-673.

He, H., Deng, C., Wang, P., Pan, Y., Zhu, R., 2012. Toward age determination of the termination of the Cretaceous Normal Superchron. *Geochemistry Geophysics Geosystems*. 13, no. 1, doi:10.1029/2011GC003901

Hicks, J.F., Obradovich, J.D., Tauxe, L., 1995. A new calibration point for the Late Cretaceous time scale; the  $^{40}\text{Ar}/^{39}\text{Ar}$  isotopic age of the C33r/C33n geomagnetic reversal from the Judith River Formation (Upper Cretaceous), Elk Basin, Wyoming, USA, *Journal of Geology*, v. 103, no. 3, p. 243-256.

Jarzen, D.M., Norris, G., 1975. Evolutionary significance and botanical relationships of Cretaceous angiosperm pollen in the western Canada interior. *Geoscience and Man*, 11: 47-60.

Kauffman, E. G., 1977. Geological and biological overview; Western Interior Cretaceous basin. *The Mountain Geologist*, v. 14, no. 3-4, p. 75-99.

Kauffman, E. G., 1984. Paleobiogeography and evolutionary response dynamic in the Cretaceous Western Interior Seaway of North America, in Westermann, G.E.G. (ed.), Jurassic-Cretaceous Biochronology and Paleogeography of North America. *Special Paper - Geological Association of Canada*, 27, 273-306.

Kauffman, E. G., Sageman, B. B., Kirkland, J. I., Elder, W. P., Harries, P. J., Villamil, T., 1993. Molluscan biostratigraphy of the Cretaceous Western Interior Basin, North America, in Caldwell, W.G.E. and Kauffman, E.G. (eds.), Evolution of the Western Interior Basin. *Special Paper - Geological Association of Canada*, 39, 397-434.

Kent, D.V., Tauxe, L., 2005. Corrected Late Triassic latitudes for continents adjacent to the North Atlantic. *Science*. 307, 240-244.

King, R.F., 1955. The remanent magnetism of artificially deposited sediments. *Mon. Not. R. Astr. Soc. Geophys. Suppl.*, 7, 115–134.

Kirschvink, J.L., 1980. The least-squares line and plane and the analysis of paleomagnetic data. *Geophysical Journal of the Royal Astronomical Society*, 62, 699-718.

Laj, C., Channel, J.E.T., 2007. Geomagnetic Excursions. In: Treatise on Geophysics, Schubert, G., eds., Elsevier, Los Angeles, U.S.A, Volume 5, 373–416.

Leahy, G. D., Lerbekmo, J. F., 1995. Macrofossil magnetobiostratigraphy for the upper Santonian- lower Campanian interval in the Western Interior of North America: comparisons with European stage boundaries and planktonic foraminiferal zonal boundaries. *Canadian Journal of Earth Sciences*, 32, 247–260.

Leckie, D.A., Bhattacharya, J.P., Bloch, J., Gilboy, C.F., Norris, B., 1994. Chapter 20, Cretaceous Colorado/Alberta Group of the Western Canada Sedimentary Basin: *in* Mossop, G., and Shetson, I., compilers, Geological Atlas of the Western Canada Sedimentary Basin, Calgary: Canadian Society of Petroleum Geologists and Alberta Research Council, p. 335–352.

Lerbekmo, J. F., 1989. The Stratigraphic position of the 33-33r (Campanian) polarity chron boundary in southeastern Alberta. *Bulletin of Canadian Petroleum Geology*, 37 (1), 43–47.

Lerbekmo, J. F., Evans, M. E., 2012. Cryptochrons and tiny wiggles: New magnetostratigraphic evidence from chronos 32 and 33 in Western Canada. *Physics of the Earth and Planetary Interiors*, 202-203, 8–13. doi:10.1016/j.pepi.2012.05.004

Lowrie, W., Channell, J.E.T., Alvarez, W., 1980. A review of magnetic investigations in Cretaceous pelagic carbonate rocks. *Journal of Geophysical Research*, 85, 3597-3605.

McElhinny, M.W., McFadden, P.L., 2000. Paleomagnetism, Continents and Oceans. Academic Press, 386 p.

McLean, J.R., 1971. Stratigraphy of the Upper Cretaceous Judith River Formation in the Canadian Great Plains. Report - Saskatchewan Research Council, Geology Division, no. 1, 96 p.

McNeil, D.H., Wall, J.H., Eberth, D.A., 1995. Parasequences and foraminiferal distributions in the Campanian Foremost Formation of southern Alberta. Proceedings of the Oil and Gas Forum '95, Geological Survey of Canada, Open File 3058, p. 93-97.

Meijer Drees, N.C., Myhr, D.W., 1981,. The Upper Cretaceous Milk River and Lea Park Formations in southeastern Alberta. *Bulletin of Canadian Petroleum Geology*, 29(1), p. 42-71.

Meyer, R., 1998. Sedimentology, petrology and permeability characterization of the Upper Cretaceous, Virgelle Member, Milk River Formation, Writing-On-Stone Provincial Park, Alberta, Canada. Doctoral dissertation, University of Calgary, Calgary, AB, Canada, pp. 456.

Montgomery, P., Hailwood, E.A., Gale, A.S., Burnett, J.A., 1998. The magnetostratigraphy of Coniacian–late Campanian chalk sequences in southern England. *Earth and Planetary Science Letters*, v. 156, no. 3–4, p. 209–224, doi:10.1016/S0012-821X(98)00008-9.

Nichols, D.J., Sweet, A.R., 1993. Biostratigraphy of Upper Cretaceous non-marine palynofloras in a north-south transect of the Western Interior Basin. In Caldwell, W.G.E., and Kauffman, E.G. (eds.), Evolution of the Western Interior Basin, *Geological Association of Canada, Special Paper* 39: 539–584.

Nielsen, K.S., Schröeder-Adams, C.J., Leckie, D.A., 2003. A new stratigraphic framework for the upper Colorado Group (Cretaceous) in southern Alberta and southwestern Saskatchewan, Canada, *Bulletin of Canadian Petroleum Geology*, v. 51, no. 3, p. 304-346.

Norris, G., Jarzen, D. M., Awai-Thorne, B. V., 1975. Evolution of the Cretaceous terrestrial palynoflora in Western Canada in Caldwell, W.G.E. (ed.), Cretaceous System in the Western Interior of North America, Special Paper - Geological Association of Canada, no.13, p. 333-364.

North, B.R., Caldwell, W.G.E., 1975. Foraminiferal faunas in the Cretaceous System of Saskatchewan. in Caldwell, W.G.E. (ed.), Cretaceous System in the

Western Interior of North America, *Special Paper - Geological Association of Canada*, no.13, p. 303-331.

Obradovich, J.D., 1993. A Cretaceous time scale, in Evolution of the Western Interior Basin, in Caldwell, W.G.E. and Kauffman, E.G. (eds.), Evolution of the Western Interior Basin. *Special Paper - Geological Association of Canada*, 39, p. 379-398.

O'Connell, S.C., 2003. The unknown giants – low-permeability shallow gas reservoirs of southern Alberta and Saskatchewan, Canada. Canadian Society of Petroleum Geologists annual meeting, 2003, extended abstract.

O'Connell, S., 2008. Low Permeability gas reservoirs of the Alderson Member; Milk River Formation, Southern Alberta - a shallow gas core workshop; Belfield Resources Inc., Calgary.

O'Connell, S.C., 2010. Unconventional, low-permeability offshore marine reservoir facies, with hatal conglomerates developed at internal stratigraphic unconformity surfaces - the Alderson member of the Milk River formation, Upper Cretaceous, southern Alberta and Saskatchewan. Conference Abstracts, GeoCanada 2010 –Working with the Earth, Calgary, May 10-14, 2010.

O'Connell, S.C., Bhattacharya, J.P., Braman, D.R., 1992. Sequence stratigraphy of the Upper Cretaceous Milk River and Lea Park Formations, Alberta, Annual Meeting Abstracts - American Association of Petroleum Geologists and Society of Economic Paleontologists and Mineralogists Annual Convention, Program and Abstracts, p. 98.

O'Connell, S.O., Campbell, R., Bhattacharya, J., 1999. The stratigraphy, sedimentology, and reservoir geology of the giant Milk River gas field in southeastern Alberta and Saskatchewan. Canadian Society of Petroleum Geologists Annual Meeting, Abstract 99-83-O.

Ogg, J. G., Smith, A.G., 2004. The geomagnetic polarity time scale, in Geologic Time Scale 2004, edited by F. M. Gradstein, J. G. Ogg, and A. G. Smith, pp. 63–86, Cambridge Univ. Press, Cambridge, U. K.

Payenberg, T. H. D., 2002. Integration of the Alderson Member in Southwestern Saskatchewan into a litho- and chronostratigraphic Framework for the Milk

River/Eagle Shoreline in Southern Alberta and north-central Montana; *in* Summary of Investigations 2002, Volume 1, Saskatchewan Geological Survey, Sask. Industry and Resources, Misc. Rep.,4.1, 134–142.

Payenberg, T. H. D., Braman, D. R., Davis, D. W., Miall, A. D., 2002. Litho- and chronostratigraphic relationships of the Santonian – Campanian Milk River Formation in southern Alberta and Eagle Formation in Montana utilising stratigraphy , U – Pb geochronology , and palynology. *Canadian Journal of Earth Sciences*, v. 39, p. 1553-1577.

Payenberg, T.H.D., Braman, D.R., Miall, A.D., 2003. Depositional environments and stratigraphic architecture of the Late Cretaceous Milk River and Eagle Formations, southern Alberta and north-central Montana; relationships to shallow biogenic gas. *Bulletin of Canadian Petroleum Geology*, v. 51, no. 2, p. 155-176.

Pedersen, P.K., 2003. Stratigraphic relationship of Alderson (Milk River) strata between the Hatton and Abbey-Lacadena pools, southwestern Saskatchewan, preliminary observations, in Summary of Investigations 2003, v. 1, Saskatchewan Geological Survey, Sask. *Industry and Resources, Misc. Rep.*,4.1, Paper A-11, 11 p.

Ridgley, J. L., 2000. Lithofacies architecture of the Milk River Formation (Alderson Member of the Lea Park Formation), southwestern Saskatchewan and southeastern Alberta; its relation to gas accumulation; Summary of Investigations 2000; Volume 1, Saskatchewan Geological Survey, No. 2000-4.1.

Roberts, A. P., Winklhofer, M., 2004. Why are geomagnetic excursions not always recorded in sediments? Constraints from post-depositional remanent magnetization lock-in modelling, *Earth and Planetary Science Letters*, 227(3-4), 345-359, doi:doi:10.1016/j.epsl.2004.07.040.

Russell, L. S., Landes, R. W., 1940. Geology of the southern Alberta plains. Geological Survey of Canada, Memoir 221, pp. 223.

Schröder-Adams, C. J., Adams, P. J., Haggart, J., Leckie, D. A., Bloch, J., Craig, J., McIntyre, D.J., 1998. An integrated paleontological approach to reservoir

problems; Upper Cretaceous Medicine Hat Formation and First White Speckled Shale in southern Alberta. *Canadian Palaios*, 13, 361-375.

Shurr, G. W., and Ridgley, J. L., 2002. Unconventional shallow biogenic gas systems. *American Association of Petroleum Geologist Bulletin*, 86(11), 1939-1969.

Slipper, S. E., and Hunter, H. M., 1931. Stratigraphy of Foremost, Pakawki, and Milk River Formations of Southern Plains of Alberta. *Bulletin of the American Association of Petroleum Geologists* 15(10), 1181-1196.

Thomas, R.G., Eberth, D.A., Deino, A.L., Robinson, D., 1990. Composition, radioisotopic ages, and potential significance of an altered volcanic ash (bentonite) from the Upper Cretaceous Judith River Formation, Dinosaur Provincial Park, southern Alberta, Canada. *Cretaceous Research*, 11(2), 125-162.

Tovell, W. M., 1956. Some aspects of the geology of the (Upper Cretaceous) Milk River and Pakawki Formations (southern Alberta). Doctoral dissertation, University of Toronto, Toronto, ON, Canada, 113+ p.

Vandamme D (1994) A new method to determine paleosecular variation. *Physics of the Earth and Planetary Interiors*, 85, 131–142.

Zijderveld, J.D.A., 1967. A.C. demagnetization of rocks, analysis of results. In: Methods in paleomagnetism, D.W. Collinson, K.M. Creer, and S.K. Runcorn, eds., Elsevier, Amsterdam, 254–286.

# **Chapter 5**

## **Revised apparent polar wander path for Siberia during the Phanerozoic: Application of a new fitting technique**

### **5.1 Introduction**

The existence of Siberia as an independent stable platform can be traced back with accuracy from the breakup of Rodinia (~800 Ma) until the end of the Paleozoic Era, when it became part of Eurasia (Cocks and Torsvik 2007; Kuzmin et al. 2010). Different continental blocks have accreted to Siberia since the Precambrian time forming one of the largest tectonic structures on Earth – the Siberian continent. Its size and longevity make Siberia a crucial part of any global tectonic reconstruction. This is the reason why an accurate description of its apparent polar wander path (APWP) is fundamental. However, the paleomagnetic dataset of Siberian poles is still quite sparse and incomplete compared to many other continents.

This contribution is a continuation of the work developed in Kravchinsky and Kabin (2005). The available paleomagnetic pole list is updated with recently published poles from the Paleozoic and Mesozoic Eras. In order to ensure the reliability of the data, only poles available in international journals and that follow the Van der Voo's (1993) selection criteria, are considered. In terms of the APWP construction, two main techniques are explored. In the first approach, the APWP was approximated using a least squares fit computed through singular value decomposition. This method has never been used before for APWP constructions but it is widely used in geophysical problems that deal with sparse data sets (Zhdanov, 2002). The second technique used was a smoothing cubic spline technique, similar to the one used by Cocks and Torsvik (2007), to construct the most recent Siberian APWP. The effectiveness of both approaches has been

demonstrated by comparison with the very well resolved APWP for Europe (Torsvik et al., 2001).

The next step on the analysis was to apply and compare both techniques to construct the Siberian APWP for the Phanerozoic Eon. For construction of the Siberian APWP in the Mesozoic Era, two possible scenarios discussed in the literature are considered: Siberia regarded as a consolidated component of Eurasia since the Triassic as proposed by Cocks and Torsvik (2007), Torsvik et al. (2012) and Pavlov 2012; and Siberia as an independent block at least until the late Cretaceous (Metelkin et al. 2010).

## 5.2 Methodology

### 5.2.1 Paleomagnetic Data Selection

Using the International Association of Geomagnetism and Aeronomy (IAGA) Global Paleomagnetic Database, paleomagnetic poles were selected to compose an up-to-date APWP of the Siberian platform for Paleozoic and Mesozoic eras ranging from 538 Ma (Lower Cambrian) up to 75 Ma. There is a large discrepancy regarding the poles older than 538 Ma related to the possibility that the Siberian platform might not have been fully amalgamated by this time (see a review of the problem in Kravchinsky et al. (2001) and Pavlov et al. (2004)). Hence these older poles are not included in the analysis. Instead, the analysis is limited to Lower Cambrian poles (those younger than 538 Ma).

The locations of the sampling sites for these poles are shown in Figure 5.1. Selected paleomagnetic poles and the estimations of their reliability are presented in Figure 5.2 and Table 5.1. Figure 5.2 presents only poles between 200 Ma and 538 Ma because of the two possible scenarios of Siberia location, which are discussed in this chapter introduction. Only paleomagnetic poles that have been recently published for which geological settings and laboratory techniques are

adequately described in accessible peer reviewed journals, are included. The data were graded according to Van der Voo's (1993) classification system that consists of seven reliability criteria shown below:

- Well determined age and the assumption that the magnetization age is the actual rock age
- Adequate statistics and sufficient number of samples
- Proper documentation and demagnetization techniques
- Field tests to constrain the age of magnetization
- Structural control and tectonic coherence with the involved craton or block
- Presence of reversals
- No resemblance to paleopoles of younger age

In order for a pole to be considered for analysis, a minimum of three Van der Voo's criteria above, should be met. This minimum requirement is based on typical analysis done in literature.

Based on the work of Gurevitch (1984) and Pavlov and Petrov (1996), the Siberian southern poles between 407 Ma to 550 Ma have been rotated, to take into account the opening of the Viluy Basin (see Figure 5.2, right hand side). The poles were corrected respect an Euler pole of latitude 60°N, longitude 120°E and angle of 13° (Cocks and Torsvik, 2007).

Poles between 75 Ma and 190 Ma, in table 5.1, were obtained from the work of Metelkin et al. (2010) and Pavlov (2012). Pavlov (2012) also studied the differences between Siberian and European APWP during the Mesozoic. He concluded that the present day paleomagnetic data indicates that the consolidation of the Northern Eurasian continent was completed by the end of the Permian, from the very beginning of the Mesozoic Era. Therefore, the Siberian and East European platforms were parts of a single rigid megablock and the Meso-Cenozoic segment of the European APW path can be used as the reference for the

Siberian Platform. However, Pavlov (2012) uses paleomagnetic poles from folded areas that are usually not used to construct APWPs. In addition, he used a “palliative approach that implies finding the pro and contra arguments for the coincidence of the corresponding segments of the European and Siberian paths” to reach the aforementioned conclusions (Pavlov, 2012). These are the reasons why not all the poles presented in Pavlov’s contribution (2012) are summarized in Table 5.1.

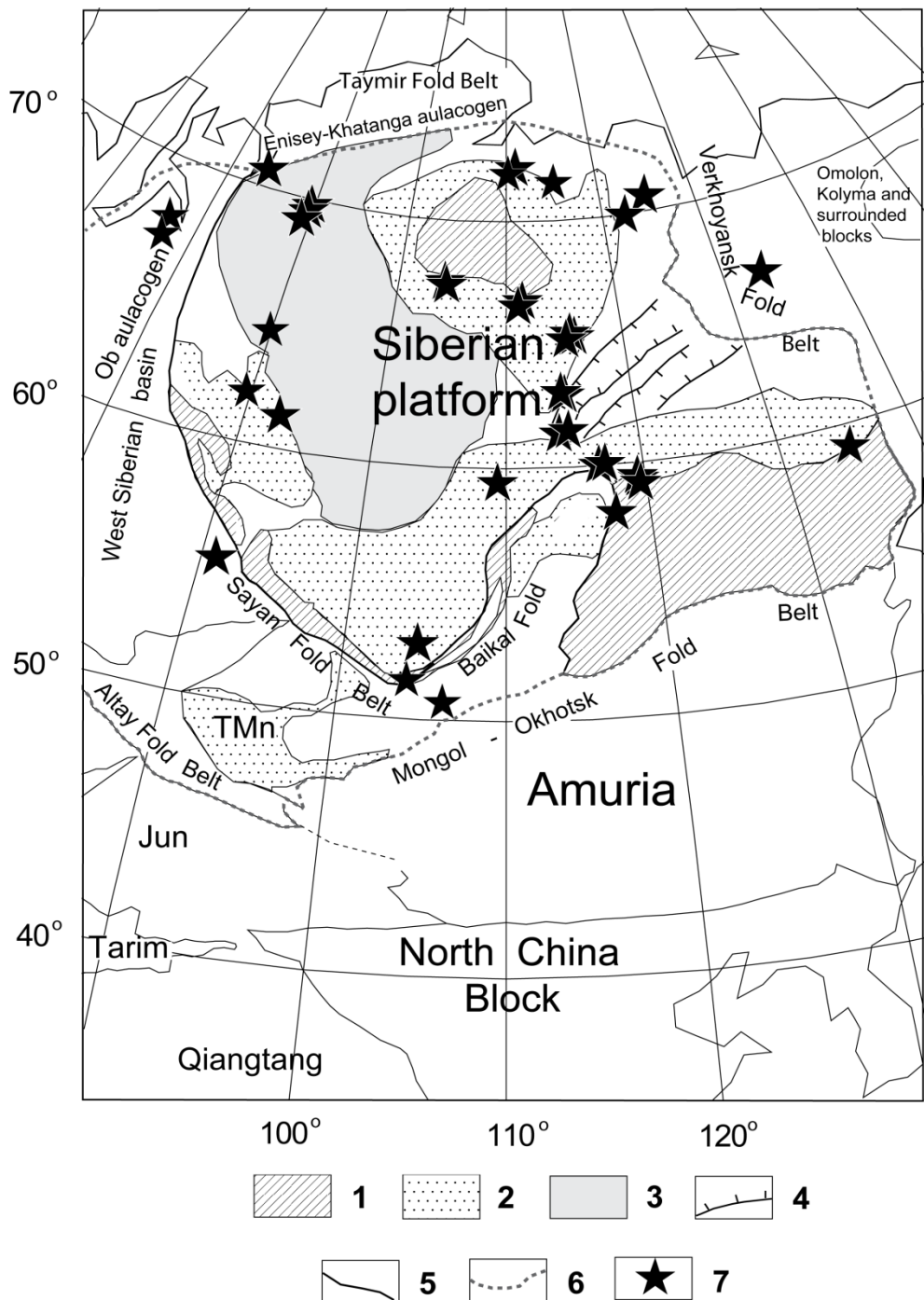


**Figure 5.1.** Simplified geological structure of Siberia and surrounding regions modified from Kravchinsky et al. (2002). 1: Precambrian shields; 2: Riphean and Palaeozoic sediment cover; 3: Permo-Triassic traps; 4: Viluy palaeorift; 5: edge of Precambrian platform; 6: Middle–Late Palaeozoic border of Siberian block. Names of blocks: TMn: Tuva-Mongolian, Jun: Jungar ; 7: paleomagnetic study sampling localities.

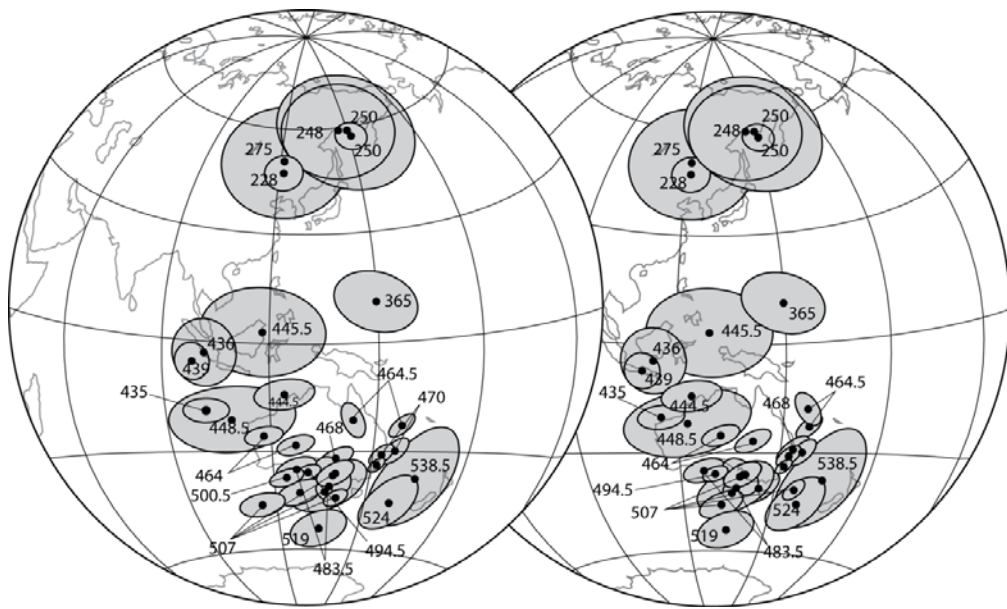


**Figure 5.2.** Selected paleomagnetic poles with 95% confidence ovals for the Siberian APWP construction. Left hand side plot represents the selected poles without rotation for Wenlock (~426.2 Ma) to Emsian (~402.3 Ma) times. Right hand side corrected poles with respect to an Euler pole of latitude 60°N, longitude 120°E and angle of 13°. Poles from 75 Ma to 200 Ma are not presented.

**Table 5.1.** Selected paleomagnetic poles for Siberian platform and their reliability. Selected paleomagnetic poles for Siberian platform. Formation – Geological formation name were sample was acquired, B (N) – number of sites (poles) included in the statistics, Mean Age – age in Ma. Q – classification factor due to Van der Voo (1993) (7 is the best score) Pole Lat (Long) – Paleomagnetic pole latitude (longitude),  $dp/dm$  – semi-axes of the confidence cone of the paleomagnetic pole, Site Lat (Long) – sampling site coordinates. Ref – Reference.

Formation	B(N)	Mean Age (Myr)	Q	Pole Lat	Pole Long	$dp$ (°)	$dm$ (°)	Site Lat (°N)	Site Long (°E)	Ref.
Minusa trough	16 (243)	75	6	82.8	188.5	6.7	5.7	54.9	90.3	Metelkin et al. 2007b
Khilok Fm., Transbaikalia	3 (25)	120	4	72.3	186.4	6.0	6.0	52.0	108.0	Metelkin et al. 2004
Verkhoyansk Trough	11 (93)	130	4	67.2	183.8	7.9	7.5	67.3	133.3	Metelkin et al. 2008
Anabar Bay	(209)	145	6	76.9	179.3	4.7	4.8	73.90	113.1	Housa et al., 2007
Ichetuy Formation	18 (156)	155	5	63.6	166.8	8.9	8	53.5	107.0	Metelkin et al. 2007a.
Badim Formation	12 (86)	155	5	64.4	161	7.3	6.7	51.8	112.0	Kravchinsky et al. 2002b
Verkhoyansk Trough	4 (40)	165	4	59.3	139.2	5.8	5.7	67.3	133.3	Metelkin et al. 2008
Monostoy River	5	190	6	43.3	131.4	22.7	23.6	51.1	106.8	Cogné et al. 2005
South Taimyr*	13 sites	228	6	47.1	121.6	5	5	74.8	100.6	Walderhaug et al., 2005

**Table 5.1. Continuation**

Formation	B(N)	Mean Age (Myr)	Q	Pole Lat	Pole Long	dp (°)	dm (°)	Site Lat (°N)	Site Long (°E)	Ref.
South Taimyr*	10 sites	248	6	59.3	145.8	14	15	74.9	100.5	Walderhaug et al., 2005
Western Taimyr*	(31)	250	7	59	150	18.4	16.9	72.9	84.0	Gurevitch et al., 1995
Siberian Traps Mean Pole*	8 sites	250	7	57.2	151.1	4	4	62.5	90.0	Pavlov et al., 2007
South Siberia*	5 dykes (31)	275	4	50.5	121.4	16.8	16.5	51.8	104.0	Pisarevsky et al., 2006
Basalts and kimberlites*	11 localities	365	4	11.1	149.7	12	8	64.6	114.7	Kravchinsky et al., 2002a
Lena River, Nyuva river	(56)	435	5	-18.6	101.9	6.4	3.3	60.7	116.3	Shatsillo et al., 2007
Lena river	(15)	436	3	-3	102	9	9	60.0	116.0	Rodionov et al., 1982
Nyuaya River	5 (39)	439	5	-5.5	98.6	4.9	4.9	60.7	116.3	Shatsillo et al., 2007
Moyer river*	(20)	444.5	4	-13.9	124.1	8.3	4.2	67.5	104.0	Gallet and Pavlov, 1996
Ust'kut Formation	(6)	445.5	5	3.1	118.1	17.9	12.3	60.5	116.4	Torsvik et al., 1995
Lena River Sediments	(17)	448.5	5	-21.1	109	17.8	9.2	60.5	116.4	Torsvik et al., 1995
Krivaya Luka	(40)	464	5	-25.6	117.9	5.2	2.6	59.7	118.1	Iosifidi et al., 1999
Krivaya Luka	(123)	464	5	-28.2	127.1	5.1	2.6	59.7	118.1	Iosifidi et al., 1999
Moyer River Sediments*	(32)	464.5	4	-22.7	157.6	4.1	2.1	67.5	104.0	Gallet and Pavlov, 1996
Kudrino Section	(125)	464.5	6	-21.1	143.4	2.7	5.3	57.7	108.0	Pavlov et al., 2008
Krivaya Luka Formation	(26)	468	4	-32	139	5	2.5	59.8	118.1	Torsvik et al., 1995
Moyer River Sediments*	(45)	470	4	-29.8	156.6	4.4	2.4	67.5	104.0	Gallet and Pavlov, 1996
Guragirskya*	(87)	470	5	-30.9	152.7	3.7	2.1	68.0	88.8	Gallet and Pavlov, 1998
Moyer River Sediments*	(144)	478	4	-33.9	151.7	2.5	1.4	67.5	104.0	Gallet and Pavlov, 1996
Surinsk Formation	6 (259)	480	5	-42.2	128.1	6.1	3.3	58.3	109.6	Surkis et al., 1999
Moyer River Sediments*	(15)	483.5	4	-40.3	137.5	10.6	6.2	67.5	104.0	Gallet and Pavlov, 1996
Kulumbe River Sediments*	(45)	483.5	5	-35.2	127.2	5.5	3.1	68.0	88.8	Pavlov and Gallet, 1998

**Table 5.1 Continuation**

<b>Formation</b>	<b>B(N)</b>	<b>Mean Age (Myr)</b>	<b>Q</b>	<b>Pole Lat</b>	<b>Pole Long</b>	<b>dp (°)</b>	<b>dm (°)</b>	<b>Site Lat (°N)</b>	<b>Site Long (°E)</b>	<b>Ref.</b>
Moyer River Sediments*	(22)	494.5	4	-37.0	138.4	4	6	67.5	104	Gallet and Pavlov, 1996
Kulumbe River Sediments*	(155)	494.5	5	-36.1	130.7	3.4	2	68.0	88.8	Pavlov and Gallet, 1998
Verkholensk Formation	2 (53)	500.5	4	-37.7	124.0	4.6	2.3	58.5	109.7	Rodionov et al., 1998
Kulumbe Formations*	(128)	507	7	-41.9	136.2	1.8	2.9	68.0	88.8	Pavlov and Gallet, 1998
Khorbusuonka River Sediments	2 (158)	507	5	-43.7	140.0	3.3	2.0	71.5	124.0	Gallet et al., 2003
Yunkualyabit-Yuryakh *	3 (38)	507	5	-36.4	139.2	5.2	3	70.9	122.6	Pisarevsky et al., 1997
Maya River	(113)	507	6	-45.8	115.0	5.9	3.3	59.5	134.5	Pavlov et al., 2008.
Khorbusuonka River Sediments*	(35)	519	5	-53.3	135.0	7.2	5.1	71.5	124.0	Gallet et al., 2003
Erkeket Formation*	8 (23)	524	5	-44.8	158.7	8.8	5.7	70.9	122.6	Pisarevsky et al., 1997
Kessysa Formation*	(12)	538.5	5	-37.6	165.0	15.4	9.2	70.9	122.6	Pissarevsky et al., 1997
<b>Corrected South Poles</b>										
Lena River, Nyuva river	(56)	435	5	-19.9	115.4	6.4	3.3	60.7	116.3	Shatsillo et al., 2007
Lena river	(15)	436	3	-4.4	113.7	9	9	60.0	116.0	Rodionov et al., 1982
Nyuaya River	5 (39)	439	5	-7.2	110.6	4.9	4.9	60.7	116.3	Shatsillo et al., 2007
Ust'kut Formation	(6)	445.5	5	3.5	129	17.9	12.3	60.5	116.4	Torsvik et al., 1995
Lena River Sediments	(17)	448.5	5	-21.6	122.8	17.8	9.2	60.5	116.4	Torsvik et al., 1995
Krivaya Luka Formation	(40)	464	5	-25	132.2	5.2	2.6	59.7	118.1	Iosifidi et al., 1999
Krivaya Luka Formation	(123)	464	5	-26.6	141.6	5.1	2.6	59.7	118.1	Iosifidi et al., 1999
Kudrino Section	(125)	464.5	6	-17.8	156.7	2.7	5.3	57.7	108.0	Pavlov et al., 2008
Krivaya Luka Formation	(26)	468	4	-29.1	153.7	5	2.5	59.8	118.1	Torsvik et al., 1995
Surinsk Formation	6 (259)	480	5	-40.4	144.8	6.1	3.3	58.3	109.6	Surkis et al., 1999
Verkholensk Formation	2 (53)	500.5	4	-36.3	140.1	4.6	2.3	58.5	109.7	Rodionov et al., 1998
Khorbusuonka River Sediments	2 (158)	507	5	-40.6	156.5	3.3	2.0	71.5	124.0	Gallet et al., 2003
Maya River	(113)	507	6	-45.4	132.9	5.9	3.3	59.5	134.5	Pavlov et al., 2008

\*Poles from Northern Siberia

### **5.2.2 Mathematical Approach**

A number of methods have been used to determine the APWPs for different continents. Gould (1969) suggested the regression model on the sphere, in which colatitudes and longitudes were regressed independently as parametric functions of the time variable. Irving (1977) proposed a method of averaging using a moving time window of fixed width. Thompson and Clark (1981, 1982) constructed the best-fitting smooth polar path by a method of least squares. They used cubic splines and iterative bi-square weighting, based on the residuals of the smoothly varying spline functions. Clark and Thompson (1984) used the least squares spline functions on the data projected onto a tangent plane about the North Pole. Jupp and Kent (1987) suggested the alternative approach of transferring (“unwrapping”) the spherical data onto a plane and then applying standard fitting techniques of smoothing and interpolation. Le Goff et al. (1992) proposed a statistical method based on the inertia matrix and the parameters of the Fisher distribution (Fisher, 1953). McFadden and McElhinny (1995) suggested a method of averaging the paleomagnetic poles assuming the Fisher distribution.

Schettino and Scotese (2005) applied non-parametric spline regression analysis to construct APW paths for major continents from 200 Ma to the present.

In practice, all of those smoothing methods agree well when an extensive APWP dataset is available. For example, the large data set of Europe for the last 180 Ma, Besse and Courtillot (2002) demonstrated that APWPs constructed using different smoothing techniques, (moving windows and cubic splines), allowed the reconstruction of a very well defined cusp (short segment with sharp curvature).

Determining the APWP for older geological times where the data points are quite isolated still remains a serious problem. Furthermore, for particular geological epochs, rocks are often missing. For example, Early–Middle Devonian rocks are very poorly represented in the Siberian platform and consequently, it would never be possible to obtain accurate and reliable paleomagnetic data for this time

interval. As with any incomplete geophysical dataset, an interpolation method can be used. In this contribution, two methods that enable the APWPs calculations for both large and small datasets are explored.

In the first approach, singular value decomposition (SVD) is used to perform the least squares method (LSM) fit. It is generally more stable numerically than other techniques, such as those based on a solution of the normal equations (De Boor 2001; Press et al. 2007). Mathematically, the problem reduces to finding coefficients  $a_j$  and  $b_j$  in the expansion

$$\lambda(t) = a_1 f_1 + a_2 f_2 + \cdots + a_j f_j, \quad (5.1)$$

and

$$\varphi(t) = b_1 g_1 + b_2 g_2 + \cdots + b_j g_j,$$

where  $t$  is time,  $\lambda$  is latitude,  $\varphi$  is longitude and  $j=1,2,\dots,m$ . The choice of functions  $f$  and  $g$  is, to a large degree arbitrary, as long as they are linearly independent. Possibly, the most straightforward choice is polynomials:  $f_j = g_j = t^j$ , where  $j=1,2,\dots,m$ . However, many other possibilities, such as trigonometric functions, may be considered. In this paper the usage of polynomial basis functions is discussed, as well as rational functions of the form

$$f_j = \frac{1}{1+q(t_j-T)^2}, \quad (5.2)$$

where  $t$  is time,  $q$  is a polynomial function of the difference between the time and a small variations  $T$ . In all cases  $f_j=g_j$  is chosen, although nothing in the method imposes this limitation.

Another important choice that needs to be made in applying this formalism is related to the number  $m$  of functions on the basis. In this specific case,  $m$ , cannot be larger than the number of the available data points,  $n$ . If  $m$  is chosen to be equal to  $n$ , then finding the coefficients of the expansion becomes a matter of

simple interpolation (Lagrange interpolation, if polynomial functions are used), and the resulting interpolating curve will pass exactly through all available points. While sometimes useful, this approach tends to produce spurious oscillations between the interpolated points that grow in amplitude as the number of reference points (and therefore, the degree of the interpolating polynomial), increases. A common method to reduce these undesired oscillations is to use cubic spline interpolation.

This method restricts the order of the interpolating polynomial to 3, but describes the resulting curve with a different polynomial between different reference points. Cubic spline interpolation once again generates a curve passing exactly through the reference points. Cubic splines are by far the most common approach to modeling data that are known with good accuracy and good time resolution. However, in constructing an APWP for Siberia, our data is sparse, with only a few available data points that are non-uniformly distributed in time. Therefore, it is natural to choose  $\mathbf{m}$  to be less than  $\mathbf{n}$ . In this case, the determination of the coefficients  $\mathbf{a}$  and  $\mathbf{b}$ , becomes the problem of solving an over-determined system of linear equations, which can be written in matrix notation as:

$$\lambda(t) = \sum_{j=1}^{\mathbf{m}} a_j f_j \quad \Rightarrow \quad \lambda = \mathbf{a}f, \quad (5.3)$$

and

$$\varphi(t) = \sum_{j=1}^{\mathbf{m}} b_j g_j \quad \Rightarrow \quad \varphi = \mathbf{b}g, \quad (5.4)$$

where  $\lambda$  and  $\varphi$  are a  $\mathbf{n} \times 1$  matrix,  $\mathbf{a}$  and  $\mathbf{b}$  are a  $\mathbf{n} \times \mathbf{m}$  matrix and  $f$  and  $g$  are a  $\mathbf{m} \times 1$ . This system can be solved in least square sense, minimizing  $\|\mathbf{a}f - \varphi\|_2$  and  $\|\mathbf{b}g - \lambda\|_2$ . There are several algorithms that can be used to solve the system of equations, of which singular value decomposition (SVD) is the most robust and numerically stable method (for further discussion of the method please refer to De Boor, 2001; Press et al., 2007; Zhdanov, 2002). In terms of the SVD, a  $\mathbf{n} \times \mathbf{m}$  matrix  $\mathbf{A}$  can be factorized as:

$$\mathbf{A} = \mathbf{U}\mathbf{Q}\mathbf{V}^T, \quad (5.4)$$

where  $\mathbf{U}$  is  $n \times m$  column orthogonal matrix,  $\mathbf{Q}$  is a  $m \times m$  diagonal matrix with positive or zero elements, and  $\mathbf{V}^T$  is the transpose of a  $m \times m$  orthogonal matrix. The minimal solution then will be given by (only solution for the latitude is shown, result is similar for the longitude):

$$f = \mathbf{V}\mathbf{Q}^{-1}\mathbf{U}^T\lambda , \quad (5.5)$$

Although SVD is computationally more intensive than the other alternatives, this consideration is absolutely insignificant for the problems we are dealing with.

The APWP computed by a least square method (LSM) in general does not pass exactly through any of the available reference points, but show the general tendency of the paleomagnetic pole distribution. This seems to be the most reasonable approach to modeling relatively few inexact data points. The closer  $m$  is chosen to  $n$ , the closer the resulting curve will be to the data points, but also the larger the oscillations between the data points will be. On the other hand, the smaller  $m$  is chosen, the smoother the curve will be, but at the same time the further it will be from the available points. The optimal value of  $m$  has to be found by experimenting in every particular case.

In the second approach, the Siberian APWP is best fitted using a smoothing technique: smoothing cubic spline. The data were not weighted with any particular criteria, although the poles themselves have been chosen following the Van der Voo criteria. De Boor (2001) gives a detailed description of the smoothing spline method and FORTRAN subroutines that have been modified for APWP application. De Boor (2001) discusses that the spline is more effective than just a standard interpolation and that it is efficient only when sufficient accurate function values are available.

The smoothing parameter  $S$  in the cubic spline method is a parameter that can be

changed enough without firm restraint to reach a desired approximation for data. Generally speaking, smaller  $S$  causes smoothed curve to pass closer to the data points, and larger  $S$  smoothens the curve more, but may not pass very close to the original data points especially in small and scattered datasets.

De Boor (2001) provides a general discussion of both methods. He argues that the smoothing cubic spline is chosen with slightly more degrees of freedom than a number of available data points that causes a conceptual difficulty. In practice it may cause excessively effective approximation and thus transcribe the noise. De Boor (2001) concluded that the LSM approach should be considered first among approximating kin methods because it is derived from an inner product and leads to solving a linear system of equations with no exceeded number of chosen parameters.

The procedure used for the APWP construction is as follows:

- (1) A running average with a window of 10 Myr is applied to the poles. The average confidence circle  $A_{95}$  is calculated following the procedure described by McFadden and McElhinny (1995). If there is only one pole for the time period then the confidence circle  $A_{95}$  is calculated from the semi-radiiuses of the oval of 95% confidence  $dp$  and  $dm$  using the approximate formula given in Khramov (1987).
- (2) For the LSM using SVD a polynomial of degree  $m$  is fitted to the averaged data using the least squares method. The normalized time  $t = \frac{t-t_{min}}{t_{max}-t_{min}}$  is used as the argument of the polynomial.
- (3) For the cubic smoothing technique, different smoothing parameters  $S$  are chosen until satisfactory smoothing is achieved.
- (4) The  $A_{95}$  is linearly interpolated between the poles.

## 5.3 Results

### 5.3.1 European APWP

Different types of functions and different number of applied polynomials were used in the LSM (Figure 5.3 and Figure 5.4) to create the APWP of Europe. The European paleomagnetic dataset for the interval between 150 Ma and 300 Ma from Torsvik et al. (2001) (their Table 1b) was used for the APWP construction. Comparative analysis demonstrates that the choice of polynomials does not play an important role in the proposed procedure (Figure 5.3). Both APWPs demonstrate almost identical results in terms of confidence circles  $A_{95}$  that run from 4 to 11 degrees (not shown in Figure 5.3 for clarity), the reason why in further analysis only polynomial are used as based functions. It is important to note that the choice of basic functions, in this case polynomials, is to a large extent arbitrary. Any set of linearly independent functions, for example trigonometric functions, can be used instead.

To further test the reliability of the approach, the APWP for Europe was compared with the SVD least squares method. Torsvik et al. (2001) constrained the APWP using the spherical spline weighted by the  $Q$  factor (Van der Voo's reliability criteria). The resulting curves for the LSM were constrained using  $m=6$  and  $m=10$  polynomials (Figure 5.4). The difference is statistically insignificant in terms of confidence circles  $A_{95}$  (they all overlap at more than 80%, not shown in Figure 5.4). The principal difference between the APWP constructed with the spherical spline and the APWP's constructed using the SVD least squares method is in the time interval of 175–195 Ma. The spherical spline APWP has a cusp and the SVD least squares APWP does not.

The cusp observed in Figure 5.4 could be an artifact caused by the nature of the spline smoothing discussed in De Boor (2001), as well as with the irregular distribution of the European paleomagnetic poles during the Mesozoic. The curve

is shifted toward the pole with the age 192 Ma. In the LSM, the cusp does not appear even when a higher number of polynomials are applied (values from 5 to 15 were tried). A small difference can be also seen near the 300 Ma although both methods indicate the turn of the curve. Generally speaking, a smaller number of applied polynomials correspond to a higher degree of smoothing.

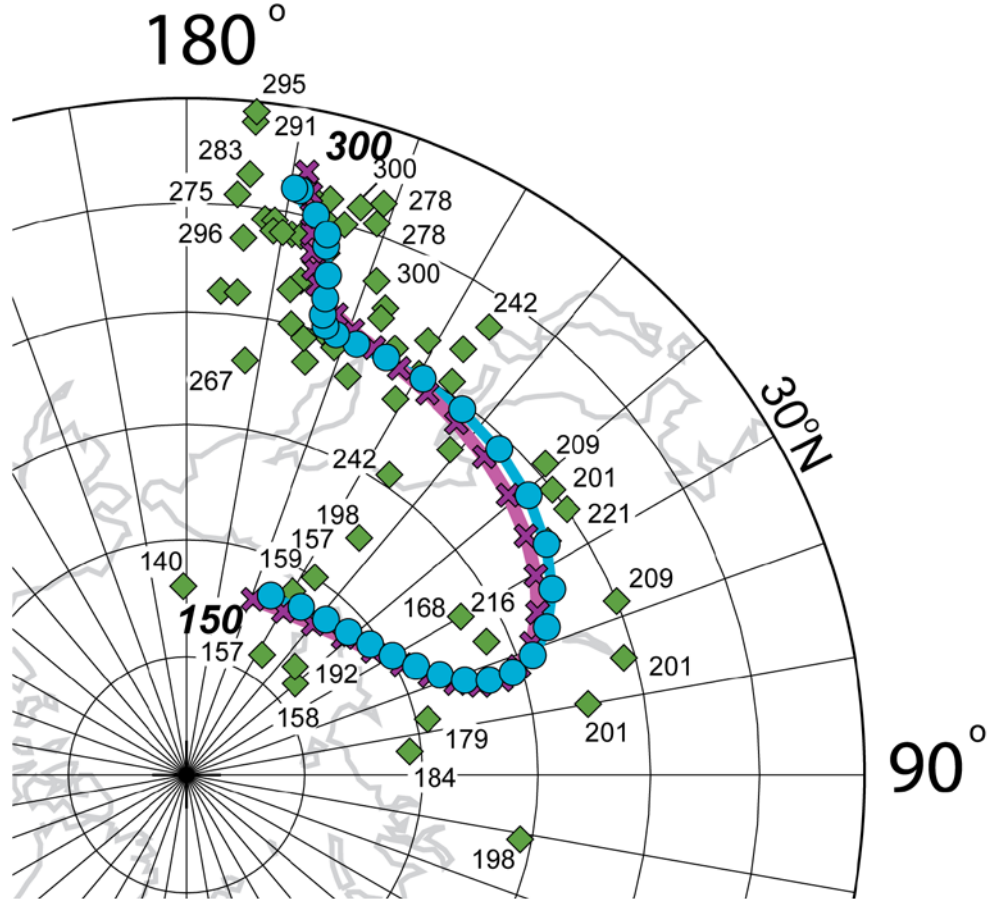


**Figure 5.3.** Comparison between European APWPs, constrained with SVD least squares method using different set of polynomials. Circles: polynomial function with  $t^k$  set of polynomials. Crosses: rational functions as a set of polynomials. The 95% confidence circles are not shown for clarity. Number of polynomials is the same ( $m=10$ ) for both curves. The individual poles are taken from the Table 1b of Torsvik et al. (2001). Ages are in Ma.

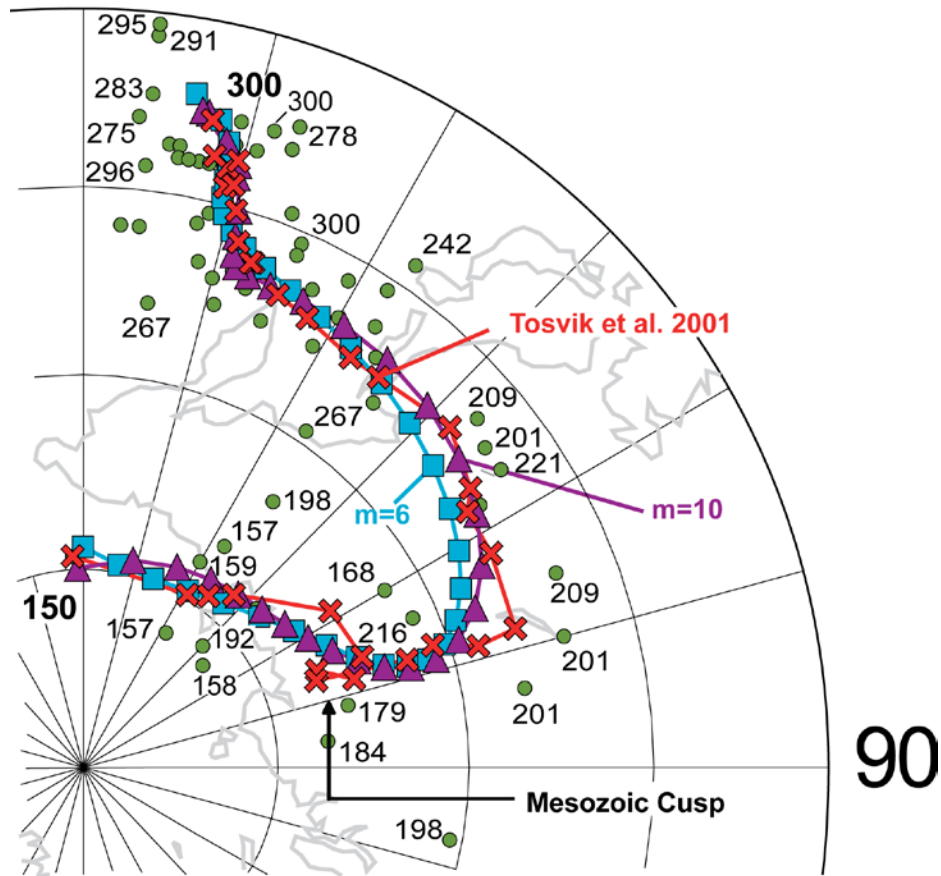


**Figure 5.4.** Comparison between European APWPs, constructed with the SVD least squares method using different number of polynomials. The 95% confidence circles are not shown for clarity. Number of polynomials is 6 for the blue curve (squares), and 10 for the purple path (triangles). Red crosses and path is the APWP of Europe from Torsvik et al. (2001) (their Table 2). Individual paleomagnetic poles from Table 1b of Torsvik et al. (2001) are shown as green circles, nearby numbers indicate the ages (in Ma) of the individual poles. Black arrow marks the European APWP Mesozoic cusp reported by Torsvik et al. (2001).

Figure 5.5 illustrates the smoothing cubic spline approach with different smoothing parameters (15 and 30). Higher smoothing parameter  $S$  translates into a higher degree of the curve smoothing. The obtained results are similar to Torsvik et al. (2001) and a cusp near 175–195 Ma and another one around 250–260 Ma are observed. The two curves are almost identical to the APWP published by Torsvik et al. (2001) with statistically negligent variations. The highest difference occurs at the end of the dataset because the obtained curves are more age

dependent (Torsvik et al. curve is weighted by the  $Q$  factor), and therefore, come closer to the group of the poles between 270–300 Ma.

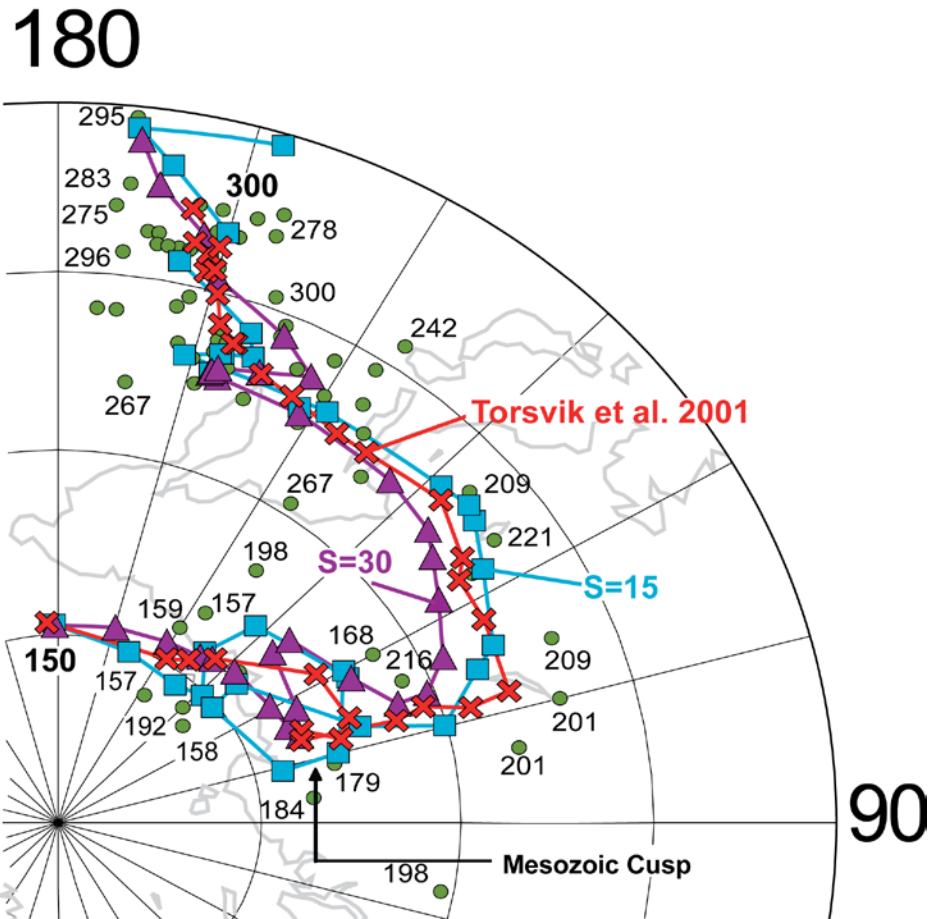


**Figure 5.5.** Comparison between European APWPs constructed with the smoothing spline method using different smoothing parameter  $S$  (squares  $S=15$  and triangles  $S=30$ ). The 95% confidence circles are not shown for clarity. The APW paths are plotted in 10 Myr step poles. Red crosses and path is the APWP of Europe from Torsvik et al. (2001) (their Table 2). Individual paleomagnetic poles from Table 1b of Torsvik et al. (2001) are shown as green circles, nearby numbers indicate the ages (in Ma) of the individual poles. Black arrow marks the European APWP Mesozoic cusp reported by Torsvik et al. (2001).

These results show that the LSM and smoothing cubic spline are suitable techniques determining APWP's when applied to extensive data sets.

### 5.3.2 APWP for the Siberian Platform

Figure 5.6 presents the behavior of the techniques when applied to the scattered and sparse dataset of Siberia from Table 5.1. For LSM (left hand side, Figure 5.6) polynomials of order 5, 6 and 10 were used. There are noticeable differences between all three APWPs. There are only 4 poles for Siberia in the age interval between 250 and 460 Ma, interval in which the number of polynomials determines the oscillation of the curves. The curve constructed using 10 polynomials provides a more undulating path in this age interval and the curve with only 5 polynomials is the smoothest one. Also, for poles older than ~520Ma, the curve with  $m=10$  follows closer the distribution of points and is markedly different from the other 2 curves. To reconstruct Siberian data between 200 Ma and 540 Ma,  $m=6$  appears to strike the right balance: it shows the general tendency of the poles and does not over fit them. Furthermore, the paths reconstructed with the spline method (smoothing parameter equal to 10, 20, 30 and 40, right hand side Figure 5.6) demonstrates less rippling within individual paths and is closer to the individual poles. In this case  $S=30$  seems to show the best fit to Siberian data.

Figure 5.7 compares the best fitting lines obtained using the discussed methods ( $m=6$  and  $S=30$ ) with Cocks and Torsvik (2007) APWP for Siberia. Cocks and Torsvik (2007) constructed their APWP using a spherical spline method. The path followed by the different methods is very similar. The main difference between the paths (Figure 5.7a) probably lies in that Cocks and Torsvik (2007) weigh their data with respect to Van der Voo's quality factor. They ensure that the path is firmly anchored to the most reliable data and only loosely guided by the rest (Torsvik et al. 1996). Figure 5.7b compares the latitudinal drift of each path with respect to a reference point at 65°N, 105°E. Differences are observed in the interval between 250 Ma 460 Ma. This can be explained by the lower number of data points (only 4 points) in this interval of time, reason why the fitting of the line will depend largely on the fitting technique. However, the general tendency of the lines is consistent.

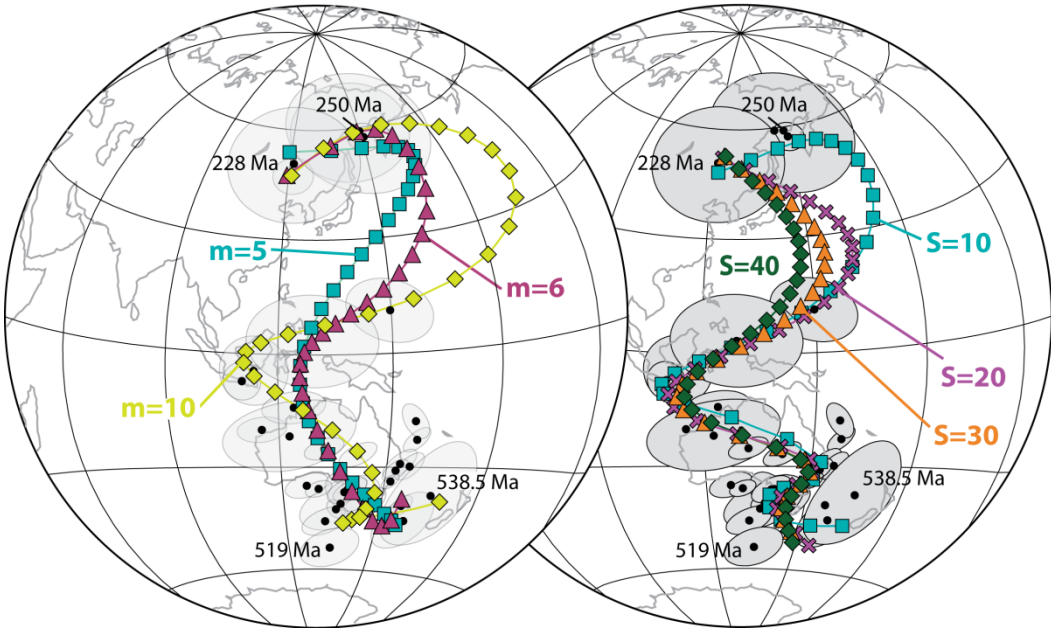
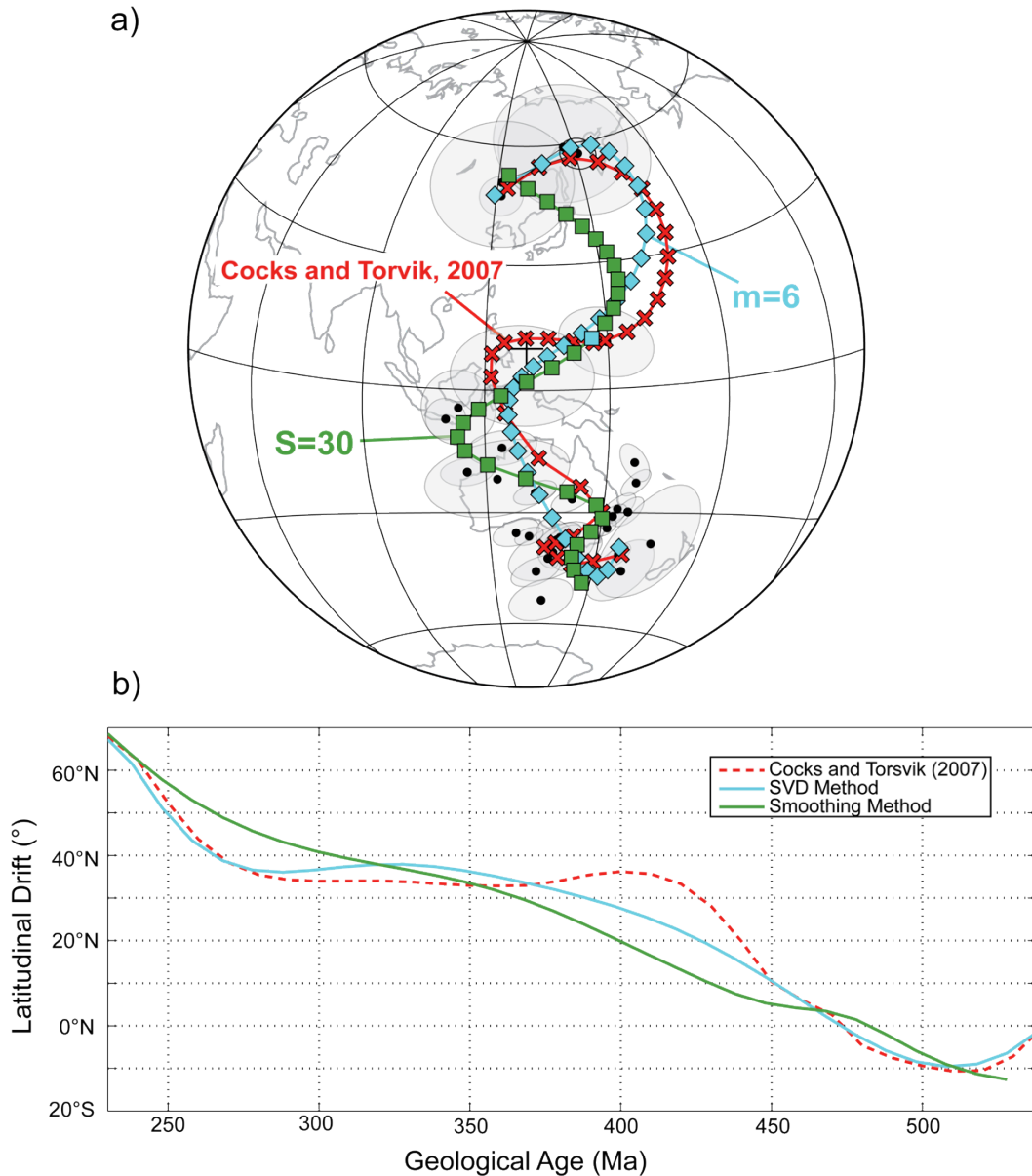


**Figure 5.6.** Comparison between Siberian APWP's for 200 Ma to 538.5 Ma (Table 5.1). Left hand side: APWP's created using least square method solve through SVD. Squares:  $m=5$ . Triangles:  $m=6$ . Downward triangles:  $m=7$ . Diamonds:  $m=10$ . Right hand side: APWP's constructed with cubic smoothing method. Squares:  $S=10$ . Crosses:  $S=20$ . Triangles:  $S=30$ . Diamonds:  $S=40$ . Right hand side: APWP's created using cubic smoothing. Squares:  $S=10$ . Crosses:  $S=20$ . Triangles:  $S=30$ . Diamonds:  $S=40$ . Siberian poles are shown as black circles and their corresponding A95 circle of confidence is shown as a grey shaded area. The 95% confidence circles for the APWP's are not shown for clarity. A10 Ma averaging window was used for the APWP's construction.

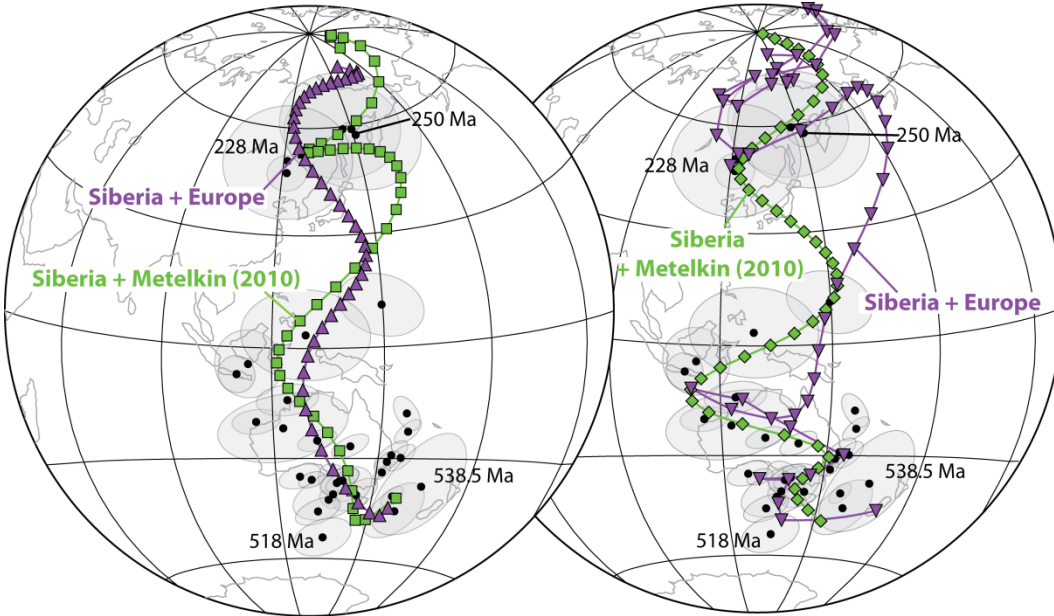
So far, the APWP constructions have only been based on the existent poles for Siberia between 200 Ma and 540 Ma. The next step is to include Mesozoic Era poles for Siberia. Two possible scenarios are considered: In the first, Siberia is a consolidated component of Eurasia since the Triassic as proposed by Cocks and Torsvik (2007), Torsvik et al. (2012) and Pavlov (2012), where European poles from 75 Ma to ~200 Ma from Torsvik et al. (2001, their Table 1b) are included to Siberian data set; and in the second, Siberia is an independent block at least until the late Cretaceous as proposed by Metelkin et al. (2010), where poles from Metelkin et al. (2010) are included in the data set (Table 5.1).

Figure 5.8 presents the results for the curve fitting using the two discussed methods. For the LSM the curves fit nicely the data set. In this case  $m=10$  is the best fitting polynomial. Although during the Mesozoic interval the reconstructed

paths do not coincide, both paths turn to the right and tend to the present location of the paleomagnetic pole for Eurasia. Between  $\sim$ 250 Ma and  $\sim$ 370 Ma there is a marked difference in the longitude of the paths, probably because of the sparse data set in this period of time.



**Figure 5.7.** a) Best fitting lines obtained using LSM using SVD ( $m=6$ ) and cubic smoothing ( $S=30$ ) techniques and Cocks and Torsvik (2007) Siberian APWP's. b) Latitudinal drift for the three paths presented in a).



**Figure 5.8.** Left hand side: APWP constructed with SVD least squares method. Right hand side, APWP constructed with cubic spline smoothing method. Comparison paths including Metelkin et al. (2010) Siberian poles vs. European poles from Torsvik et al. (2001) during the Mesozoic are shown. Individual paleomagnetic poles for this interval are not shown. Green squares/diamonds: Metelkin's poles and Siberian poles; purple triangles (up/down): European and Siberian poles.

The smooth cubic spline method (right hand side, Figure 5.8) with  $S=30$  is consistent with the least square method but presents large differences between both data sets. In this case, the path is less smooth for the Mesozoic interval. Both curves turn to the right and tend to the present location of the paleomagnetic pole for Eurasia. However, for the Siberian plus European data set, the path during the Mesozoic is complex and probably marked by artifacts created by the fitting method. A misfit, as the one observed with the LSM, can also be seen between  $\sim 250$  Ma and  $\sim 370$  Ma, period of time when the data set is sparse.

For this reconstruction, the least squares method solved through SVD presents a better fit to the data set because it does not present large variations related to the scarcity of the data. It is clearly more stable. For the smoothing cubic spline the curve passes closer to the individual poles, which is not the best fitting when dealing with sparse data sets.

The presented analysis is primary based on a qualitavite study of the fitting curves, which might not be the most realiable method to determine the goodness of the fitting. In order to improve the method, the development of an objective criterion to choose the best fitting line for Siberian APWP is required. For this we propose to use the least squares method error analysis (e.g. calculating the misfit and penalty functions) to systematically determine the best fitting line. Such work is a subject of future study.

Analyzing the latitudinal drift and the APWP velocity of a reference point with respect to the least squares method APWP (Figure 5.9) it is evident that there is a difference between the nature of the path during Mesozoic times. Nevertheless, both paths show the same tendency and the difference could be related to the uncertainty of the paleomagnetic poles for Siberia during this period of time. It is important to note that in Table 5.1, there is only one pole per date for the Mesozoic time, i.e. for 75 Ma there is only one pole, and no average can be obtained. Therefore, when the average paleomagnetic pole is calculated, there will be only one pole, and the nature of the APWP path is going to be biased by the low number of data. Furthermore, although small variations are observed in the APWP velocity, both curves are quite consistent and show the same general tendency.

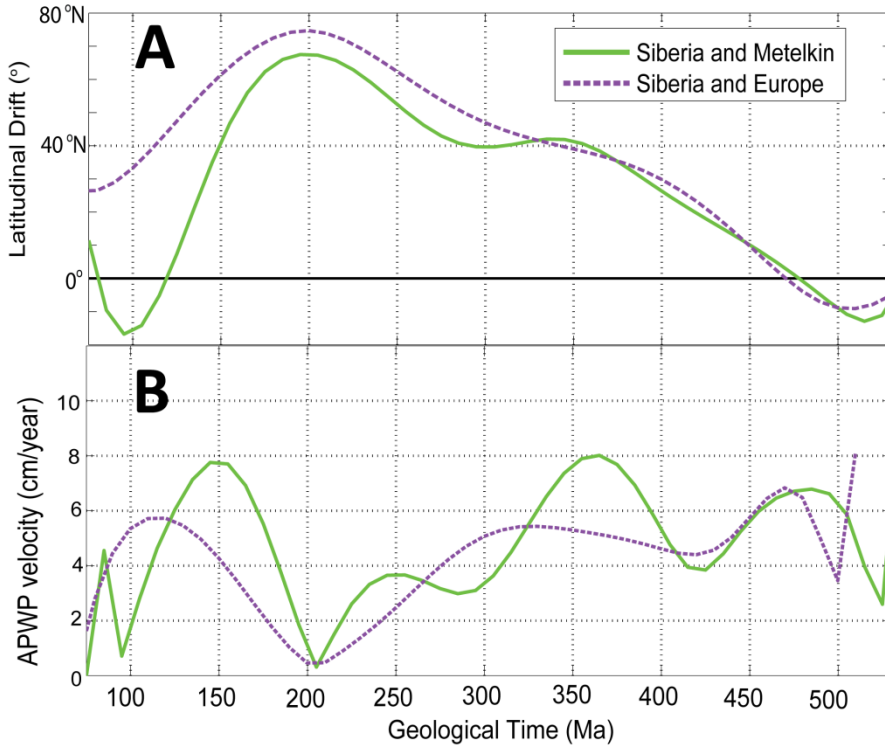


**Figure 5.9.** A: Latitudinal drift for a reference point at 65 N and 105 E. B: APWP migration velocity. Both plots were based on SVD least squares APWP path from Figure 5.8.

## 5.4 Conclusions and Future Work

This study updated the apparent polar wander path of Siberia along the Phanerozoic Eon using an innovative and new statistical approach. Two techniques to fit curves to the paleomagnetic poles have been tested on the extensive data set of Europe and on the sparse data set of Siberia. The first method used, the least squares fit computed through singular value decomposition (SVD), presented smooth paths and provided a good fit to the general tendency of the paleomagnetic poles for both data sets (extensive and sparse). The second one, the smoothing cubic spline method, is more sensitive to small features (like cusps) and presents a less smooth fitting to the data.

The APWP for Siberia data sets including Metelkin et al. (2010) poles and European poles (Torsvik et al. 2010) during the Mesozoic were also studied. For this data set, the least square method presented the best fit. Although both paths

followed the same general tendency during the Mesozoic, there is a wide difference between both paths around 100 Ma (Figure 5.0A). This feature could be probably associated with the uncertainties on the paleomagnetic poles for Siberia during this period of time. To be certain of Metlkin's assumption, a large density of data is required.

Supported by the results of this study, it can be concluded that the least square method solved through singular value decomposition is reliable and works well for large and sparse data sets. It also provides advantages with respect to smoothing cubic spline techniques when working with sparse data sets. Furthermore, a distinction between the position of Siberia during the Mesozoic cannot be established from this contribution, because of the low density of data for this period of time, which creates an APWP with low time and space resolution.

Several steps can be done in future research to improve Siberian APWP and the fitting techniques:

- The fitting techniques should be weighted with respect to the  $Q$  parameters of Van der Voo to ensure that the reconstructed path is firmly anchored to the most reliable data and only loosely guided by the rest.
- To further compare the nature of the APWPs it is important to create a quantitative way to calculate the error of the fitting that should include the error of the average of the paleomagnetic poles. For this least squares misfit and error analysis is recommended to be explored in future work.
- The APWP created for this contribution does not provide information with respect to the longitudinal location of Siberia through time. Following the work developed by Kuzmin et al. (2010) and Smirnov and Tarduno (2010), the absolute paleoposition of Siberia platform could be

reconstructed with respect to the present day location of the Icelandic hot spot and above the African LLSVP during the Paleozoic Eon.

- Further paleomagnetic data are required to solve for the location of Siberia through time. The fitting technique can only help to a certain limit, and more poles are required.

## Bibliography

- Besse, J., Courtillot, V., 2002. Apparent and true polar wander and the geometry of the geomagnetic field over the last 200 Myrs, *Journal of Geophysical Research*, 107, 1–31.
- Clark, R.M., Thompson, R., 1984. Statistical comparison of palaeomagnetic directional record from lake sediments. *Geophysical Journal of the Royal Astronomical Society B*, 47, 482–488.
- Cocks, L. R.M., Torsvik, T.H., 2007. Siberia, The wandering northern terrane, and its changing geography through the Paleozoic. *Earth-Science Reviews*, 82, 29–74.
- Cogné, J-P., Kravchinsky, V.A., Halim, N., Hankard, F., 2005. Late Jurassic-Early Cretaceous closure of the Mongol-Okhotsk Ocean demonstrated by new Mesozoic palaeomagnetic results from the Trans-Baikal area (SE Siberia). *Geophysical Journal International*, 163(2), 813-832.
- De Boor, C., 2001. A practical guide to splines. Springer-Verlag, New York.
- Fisher, R., 1953. Dispersion on a sphere, *Proceedings Royal Society London*, Ser. A, 217, 295–305.
- Gallet, Y., Pavlov, V., 1996. Magnetostratigraphy of the Moyero river section (north-western Siberia): constraints on geomagnetic reversal frequency during the early Palaeozoic, *Geophysical Journal International*, 125, 95–105.
- Gallet, Y., Pavlov, V.E., 1998. Magnetostratigraphy from the Kulumbe river reference section (NW Siberian platform). *Fizika Zemli*, 12, 60-69. In Russian.
- Gallet, Y., Pavlov, V., Courtillot, V., 2003. Magnetic reversal frequency and apparent polar wander of the Siberian platform in the earliest Palaeozoic, inferred from the Khorbusinka river section (northeastern Siberia). *Geophysical Journal International*, 154, 829-840.

Gurevitch, E.L., 1984. Palaeomagnetism of the Ordovician deposits of the Moyero River sequence. *Palaeomagnetic Methods in Stratigraphy*. VNIGR, St Petersburg, pp. 35–41 (In Russian).

Gould, A.L., 1969. A regression technique for angular variates. *Biometrics*, 25, 683–700.

Gurevitch, E., Westphal, M., Daragan-Suchov, J., Feinberg, H., Pozzi, J.P., Khramov, A.N., 1995. Paleomagnetism and magnetostratigraphy of the traps from Western Taimyr (northern Siberia) and the Permo-Triassic crisis. *Earth and Planetary Science Letters*, 136, 461-473.

Housa, V., Pruner, P., Zakharov, Kostak, M., Chadima, M., Rogov, A., Slechta, S., Mazuch, M., 2007. Boreal-Tethyan correlation of the Jurassic-Cretaceous boundary interval by magneto- and biostratigraphy. *Stratigraphy and Geological Correlation*, 15(3), 297-309.

Iosifidi, A.G., Khramov, A.N., Rodionov, V.P., Pisarevskii, S.A., Popov, V.V., 1999. Geomagnetic reversals in the Early Paleozoic: 2. A nonsynchronous record of Middle Ordovician reversals in the Berezovskaya section, Southern Siberian platform. *Fizika Zemli (Physics of the Earth)*, 1, 28–37. In Russian.

Irving, E., 1977. Drift of the major continental blocks since the Devonian, *Nature* 270, 304–309.

Jupp, P.E., Kent, J.T., 1987. Fitting smooth paths to spherical data. *Applied Statistic*, 36, 34–36.

Khramov, A.N., 1987. Paleomagnetology. Springer-Verlag, Berlin.

Kravchinsky, V.A., Konstantinov, K.M., Cogné, J.-P., 2001. Palaeomagnetic study of Vendian and Early Cambrian rocks of South Siberia and Central Mongolia: was the Siberian platform assembled at this time? *Precambrian Research*, 110, 61–92.

Kravchinsky, V.A., Konstantinov, K.M., Courtillot, V., Savrasov, J.I., Valet, J.-P., Cherniy, S.D., Mishenin, S.G., Parasotka, B.S., 2002a. Palaeomagnetism of East Siberian traps and kimberlites: two new poles and palaeogeographic

reconstructions at about 360 and 250 Ma, *Geophysical Journal International*, 148, 1–33.

Kravchinsky, V.A., Cogné, J.-P., Harbert, W.P., Kuzmin, M.I., 2002b. Evolution of the Mongol- Okhotsk Ocean as constrained by new palaeomagnetic data from the Mongol-Okhotsk suture zone, Siberia. *Geophysical Journal International*, 148, 34–57.

Kravchinsky, V.A., Kabin, K., 2005. Apparent Polar Wander Path for Siberian Platform. American Geophysical Union, Fall Meeting 2005, abstract #GP11A-0007.

Kuzmin, M.I., Yarmolyuk, V.V., Kravchinsky, V.A., 2010. Phanerozoic hot spot traces and paleogeographic reconstructions of the Siberian continent based on interaction with the African large low shear velocity province. *Earth-Science Reviews*, 102, 29–59.

Le Goff, M., Henry, B., Daly L., 1992. Practical method for drawing a VPG path, *Physics of the Earth and Planetary Interiors*, 70, 201-204.

McFadden, P.L., McElhinny, M.W., 1995. Combining groups of paleomagnetic directions or poles. *Geophysical Journal International*, 22, 2191-2194

Metelkin, D.V., Gordienko, I.V., Zhao, X., 2004. Paleomagnetism of Early Cretaceous volcanic rocks from transbaikalia: argument for Mesozoic strike-slip motions in central Asian structure. *Russian Geology and Geophysics*, 45(12), 1404-1417.

Metelkin, D.V., Gordienko, I.V., Klimuk, V.S., 2007a. Paleomagnetism of Upper Jurassic basalts from Transbaikalia: new data on the time of closure of the Mongol-Okhotsk Ocean and Mesozoic intraplate tectonics of Central Asia. *Russian Geology and Geophysics*, 48, 825-834.

Metelkin, D.V., Kazansky, A. Yu., Bragin, V.Yu., Tsel'movich, V.A., Lavrenchuk, A.V., Kungurtsev, L.V., 2007b. Paleomagnetism of the Late Cretaceous intrusions from the Minusa trough (southern Siberia). *Russian Geology and Geophysics*, 48, 185-198.

Metelkin, D.V., Vernikovsky, V.A., Kazansky, A. Yu., Kashirtsev, V.A., Bragin, V. Yu., Kungurtsev, L.V., 2008. The Mesozoic Apparent Polar Wander Path for the Siberian domain of the Eurasian plate. *Doklady Earth Sciences*, 418, 62-67.

Metelkin, D.V., Vernikovsky, V.A., Kazansky, A.Y., Wingate, M.T.D., 2010. Late Mesozoic tectonics of Central Asia based on paleomagnetic evidence. *Gondwana Research*, 18, 400–419.

Pavlov, V.E., Petrov, P.Y., 1996. Paleomagnetic investigation of the Riphean sediments of the Turukan region. *Fizika Zemli*, 3, 71–81 (In Russian).

Pavlov, V.E., Gallet, Y., 1998. Upper Cambrian to Middle Ordovician magnetostratigraphy from the Kulumbe River section (northwestern Siberia). *Physics of the Earth and Planetary Interiors*, 108, 49–59.

Pavlov, V.E., Gallet, Y., Shatsillo, A.V., Vodovozov, V.Yu., 2004. Paleomagnetism of the Lower Cambrian from the Lower Lena River Valley: Constraints on the Apparent Polar Wander Path from the Siberian Platform and the Anomalous Behavior of the Geomagnetic Field at the Beginning of the Phanerozoic. *Izvestiya, Physics of the Solid Earth*, 40, #2, 114–133. Translated from *Fizika Zemli* 2, 28–49.

Pavlov, V.E., Courtillot, V., Bazhenov, M.L., Veselovsky, R.V., 2007. Paleomagnetism of the Siberian traps: New data and a new overall 250 Ma pole for Siberia. *Tectonophysics*, 443, 72-92.

Pavlov, V., Bachtadse, V., Mikhailov, V., 2008. New middle Cambrian and middle Ordovician palaeomagnetic data from Siberia: Llandelian magnetostratigraphy and relative rotation between the Aldan and Anabar-angara blocks. *Earth and Planetary Science Letters*, 276, 229-242.

Pavlov, V., 2012. Siberian paleomagnetic data and the problem of rigidity of the Northern Eurasian Continent in the Post-Paleozoic. *Izvestiya, Physics of the Solid Earth*, 48, 721-737.

Pisarevsky, S.A., Gurevich, E.L., Khramov, A.N., 1997. Palaeomagnetism of Lower Cambrian sediments from the Olenek River section (northern Siberia):

palaeopoles and the problem of magnetic polarity in the Early Cambrian. *Geophysical Journal International*, 130, 746-756.

Pisarevsky, S.A., Gladkochub, D.P., Donskaya, T.A., De Waele, B., Mazukabzov, A.M., 2006. Palaeomagnetism and geochronology of mafic dykes in south Siberia, Russia: the first precisely dated Early Permian palaeomagnetic pole from the Siberian craton. *Geophysical Journal International*, 167, 649-658.

Press, W.H., Teukolsky, S.A., Vetterling, W.T., Flannery, B.P., 2007. Numerical recipes: The art of scientific computing. Cambridge University Press, pp. 1262.

Rodionov, V.p., Osipova, E.P., Pogarskaya, I. A., 1982. Pole number 10023. In: Kramov, A.N. (Ed.), Paleomagnetic Directions and Paleomagnetic Pole: Data for USSR, Issue 5, Materials of the WDC-B, Moscow, pp. 12 and 38 (in Russian).

Rodionov, V.P., Khramov, A.N., Pisarevsky, S.A., Popov, V.V., Iosifidi, A.G., 1998. Geomagnetic reversals in Early Palaeozoic. 1- Late Cambrian reversal recorded in Ichera section, south of the Siberian platform. *Fizika Zemli*, 12, 50-59.

Schettino, A., Scotese, C. R., 2005. Apparent polar wander paths for the major continents (200 Ma to the present day): a palaeomagnetic reference frame for global plate tectonic reconstructions, *Geophysical Journal International*, 163, 727-759.

Shatsillo, A.V., Paverman, V.I., Pavlov, V.E., 2007. Middle Paleozoic segment of the apparent polar wander path from the Siberian plateau: New paleomagnetic evidence for the Silurian of the Nyuya-Berezovskii facial province. *Izvestiya, Physics of the Solid Earth*, 43, 880-889.

Smirnov, A. V., Tarduno, J. A., 2010. Co-location of eruption sites of the Siberian Traps and North Atlantic Igneous Province: Implications for the nature of hotspots and mantle plumes. *Earth and Planetary Science Letters*, 297 (3-4), 687-690.

Surkis, Y. F., Westphal, M., Rodionov, V.P., Khramov, A.N., Gurevich, E.L., 1999. Geomagnetic reversals in early Paleozoic. 3- Reversals recorded in Lowe Ordovician redbeds, Mandra section. *Fizika Zemli*, 5, 3-13. In Russian.

Thompson, R., Clark, R.M., 1981. Fitting polar wander paths, *Physics of the Earth and Planetary Interiors*, 27, 1–7.

Thompson, R., Clark, R.M., 1982. A robust least-squares Gondwanan apparent polar wander path and the question of palaeomagnetic assessment of Gondwanan reconstructions. *Earth and Planetary Science Letters*, 57, 152–158.

Torsvik, T.H., Tait, J., Moralev, V.M., McKerrow, W.S., Sturt, B.A., Roberts, D., 1995. Ordovician palaeogeography of Siberia and adjacent continents, *Journal of Geology of the royal Society of London*, 152, 279–287.

Torsvik, T.H., Smethurst, M.A., Meert, J.G., Van der Voo, R., McKerrow, W.S., Brasier, M.D., Sturt, B.A., Walderhaug, H.J., 1996. Continental break-up and collision in the Neoproterozoic and Palaeozoic: a tale of Baltica and Laurentia. *Earth-Science Reviews*, 40, 229–258.

Torsvik, T.H., Van der Voo, R., Meert, J.G., Mosar, J., Walderhaug, H.J., 2001. Reconstructions of the continents around the North Atlantic at about the 60th parallel. *Earth and Planetary Science Letters*, 187, 55–69.

Torvik, T.H., Van der Voo, R., Preeden, U., Mac Niocaill, C., Steinberger, B., Doubrovine, P.V., van Hinsbergen, D.J.J., Domeier, P., Gaina, C., Tohver, E., Meert, J.G., McCausland, P.J.A., Cocks, L.R.M., 2012. Phanerozoic polar wander, palaeogeography and dynamics. *Earth Science Reviews*, 144 (3-4), 325–368.

Van der Voo, R., 1993. Paleomagnetism of the Atlantic, Tethys and Iaperus Oceans. Cambridge University Press, Cambridge, U.K., pp. 411.

Walderhaug, H.J., Eide, E.A., Scott, R.A., Inger, S., Golionko, E.G., 2005. Palaeomagnetsim and  $^{40}\text{Ar}/^{39}\text{Ar}$  geochronology from the South Taimyr igneous complex, Arctic Russia: a Middle–Late Triassic magmatic pulse after Siberian flood-basalt volcanism. *Geophysical Journal International*, 163, 501–517.

Zhdanov, M.S., 2002. Geophysical inverse theory and regularization problems. Elsevier Science B.V. Amsterdam, The Netherlands. pp. 619.

# **Chapter 6**

## **Conclusions**

This dissertation presents different applications of paleomagnetism to investigate the intensity of the dipolar field during the Permo-Triassic; the age of kimberlite magmatism in the Siberian platform; the geochronostratigraphic framework of the southern part of the Western Canada Sedimentary Basin and the detailed nature of Chron 33r; and the apparent polar wander path of Siberia. The obtained results show the versatility of paleomagnetism as a tool to unravel the evolution of the planet. All the objectives of the thesis were fulfilled and the main conclusions for each of the chapters are summarized below.

The first study explored the existence of a low dipolar field intensity of the geomagnetic field during the Permo-Triassic boundary. For this purpose, specimens from eastern (areas of the kimberlite pipes Sytikanskaya, Yubileinaya and Aikhal) and northwestern (extrusions near Noril'sk city) locations of the Siberian trap province were subject to paleointensity measurements. The paleomagnetic directions derived from the experiments (eastern localities:  $D=107.5^\circ$ ,  $I=75.5^\circ$ ,  $k=82.8$ ,  $\alpha_{95}=5.3^\circ$ ,  $N=10$  sills; northwestern localities:  $D=95.1^\circ$ ,  $I=71.8^\circ$ ,  $k=35.2$ ,  $\alpha_{95}=15.7^\circ$ ,  $N=4$  outcrops) agree with the expected directions calculated from the reference paleomagnetic poles of Pavlov et al. (2007) ( $D=100.6^\circ$ ,  $I=80.1^\circ$ ,  $\alpha_{95}=2.8^\circ$  for the eastern localities and  $D=84.7^\circ$ ,  $I=74.9^\circ$ ,  $\alpha_{95}=3.0^\circ$  for the northwestern locality). The northwestern specimens did not meet the reliability criteria for paleointensity and were not used for the mean virtual dipolar moment (VDM) calculations. The eastern locality results have VDM values of  $6.01 \pm 1.45 \times 10^{22}$  Am<sup>2</sup>, which are distinctly higher compared to previous studies by Heunemann et al. (2004) and Shcherbakova et al. (2005) suggesting: (1) a low intensity of the magnetic field is not a characteristic during the Permo-Triassic boundary; and (2) the Mesozoic dipole low cannot be

extended until this period of time. Discrepancies between the present results and previous studies could possibly be explained by the existence of multidomain grains in the northwestern specimens of the previous studies. The new results suggest that the geomagnetic field intensity at the Permo-Triassic boundary was very close to the observed present-day values.

The second contribution in this dissertation explores the application of paleomagnetism to geological dating. Paleomagnetic poles were determined for four Siberian diamond bearing kimberlite pipes (Eastern Udachnaya, Western Udachnaya, International, and Obnazhennaya). The poles were compared with the Siberian apparent polar wander path (APWP) of Cock and Torsvik (2007) for the Paleozoic interval and to Besse and Courtillot (2002) and Torsvik et al. (2008) APWP for the Mesozoic interval. The ages of the kimberlites fall into three groups spanning from the Early Silurian to the Late Jurassic. Early Silurian to Late Devonian ages are most likely related to magmatism during the early and main formation stages of the Viluy rift. Middle–Late Jurassic magmatism could be associated with subduction processes that took place in the present day northeast margin of the Siberian platform during this time period.

The third research topic consisted of applying magnetostratigraphic analysis as a dating tool on three deep drilling cores that penetrate Santonian-Campanian strata in southern Alberta, Canada. Chrons 34n and 33r were clearly identified from the studied sections. Normal polarity zones were observed within C33r, previously described as reverse polarity over its entire length. The most prominent short normal polarity intervals have durations of 500 kyr and 278.2 kyr. This result correlates well with previously published data and provide evidence with respect to the duration of the so-called “tinny wiggles” in the continental sedimentary sections. Furthermore, the presence of C34n-C33r in the lower Anderson Member geological formation provides the first empirical age (~83.5 Ma) for this key stratigraphic unit in southern Alberta. In addition, the definition of the age boundaries helps to create new genetic links between the Deadhorse Coulee

Member in the Milk River Area and the lower Alderson Member in southern Alberta.

In the fourth and last chapter of this dissertation I constructed a new APWP for Siberia. The paleomagnetic data set used for the analysis was up-dated to the most recent and reliable poles available in the literature. Two techniques to fit curves to the paleomagnetic poles were used and compared with the extensive data set of Europe and with the sparse data set of Siberia. The least squares fit computed through singular value decomposition (SVD) presented smooth paths and provided a good fit to the general tendency of the paleomagnetic poles for both data sets (extensive and sparse). The smoothing cubic spline method is more sensitive to small features (like cusps) and presents a less smooth fitting to the data. In addition, Siberian APWP including Metelkin et al. (2010) poles and European poles (Torsvik et al. 2001) during the Mesozoic were also studied. For this data set, the least squares method presented the best fit. It can be concluded that the least squares method solved with singular value decomposition is a reliable method that works well for large and sparse data sets and provides advantages respect to the smoothing cubic spline techniques when working with sparse data sets. Furthermore, a distinction between the two possibilities for Siberian location during the Mesozoic era, i.e., Siberia as consolidated part of Eurasia since the Triassic and Siberia as an independent block at least until late Cretaceous, cannot be established from this contribution, because the time and space resolution of the APWP is not sufficient.

## Future work

Although the contributions presented in this dissertation shed more light on the understanding of the evolution of Siberia and the Western Canada Sedimentary Basin, several comments are in order:

- The nature of the intensity of the Earth's magnetic field during the Permo-Triassic boundary and especially the characteristic of the field during the Siberian trap basalt eruption, cannot be determined without more paleointensity data. This is necessary in order to have a statistically representative result. Furthermore, to ensure the quality of the paleointensity method it is important to have a well-defined set of statistical parameters. I found complicated to define and “choose” the best parameters; this point is already addressed and various research groups continue working on developing and adapting the paleointensity statistical apparatus.
- The work in this thesis demonstrates the effectiveness of paleomagnetic dating. It could be applied more often for dating geological processes. However, paleomagnetic dating requires well-developed APWPs for all regions. It is fundamental to create and improve such reference tools.
- To gain a better understanding of the evolution of the Western Canada Sedimentary Basin, especially of the Alderson Member in southern Alberta, is fundamental to extend the magnetostratigraphic analysis done in the area. It would be advantageous to analyze cores from southern Saskatchewan and north of the USA. In addition, the cores I analyzed presented differences with the expected inclination for North America, a variation that can be attributed to inclination shallowing. In my contribution I did not explore this problem in depth. It would be interesting to analyze the nature of the shallowing and to further compare

with the well-studied inclination shallowing problem for the same time interval in central Asia.

- For the Siberian APWP construction, the fitting technique should be weighted with respect to the  $Q$  parameters of Van der Voo to ensure that the reconstructed path is firmly anchored to the most reliable data and only loosely guided by the rest. Also, a least squares misfit analysis should be explored to systematically determine the goodness of the fitting line. Furthermore, the APWP created for this contribution does not provide information with respect to the longitudinal location of Siberia through time. Following the work developed by Kuzmin et al. (2010) and Smirnov and Tarduno (2010), the paleoposition of the Siberian platform could be absolutely reconstructed with respect to the present day location the Icelandic hot spot and above the African large low shear velocity province during the Paleozoic.

## Bibliography

Cocks, L.R.M., Torsvik, T.H., 2007. Siberia, the wandering northern terrane, and its changing geography through the Paleozoic. *Earth-Science Reviews*, 82, 29–74.

Besse, J., Courtillot, V., 2002. Apparent and true polar wander and the geometry of the geomagnetic field over the last 200 Myrs. *Journal of Geophysical Research*, 107, 1–31.

Heunemann, C., Krasa, D., Soffel, H.C., Gurevitch, E., Bachtadse, V., 2004. Directions and intensities of the Earth's magnetic field during a reversal: results from the Permo-Triassic Siberian trap basalts, Russia. *Earth and Planetary Scientific Letters*, 218, 197– 213.

Kuzmin, M.I., Yarmolyuk, V.V., Kravchinsky, V.A., 2010. Phanerozoic hot spot traces and paleographic reconstructions of the Siberian continent based on interaction with the African large low shear velocity province. *Earth-Science Reviews*, 102, 29–59.

Metelkin, D.V., Vernikovsky, V.A., Kazansky, A.Y., Wingate, M.T.D., 2010. Late Mesozoic tectonics of Central Asia based on paleomagnetic evidence. *Gondwana Research*, 18, 400–419.

Shcherbakova, V.V., Shcherbakov, V.P., Vodovozov, V.V., Sycheva, N.K., 2005. Paleointensity at the Permian-Triassic boundary and in the late Permian. *Izvestiya, Physics of the Solid Earth*, 41, 931–944.

Smirnov, A. V., Tarduno, J. A., 2010. Co-location of eruption sites of the Siberian Traps and North Atlantic Igneous Province: Implications for the nature of hotspots and mantle plumes. *Earth and Planetary Science Letters*, 297 (3-4), 687–690.

Torsvik, T.H., Van der Voo, R., Meert, J.G., Mosar, J., Walderhaug, H.J., 2001. Reconstructions of the continents around the North Atlantic at about the 60th parallel. *Earth and Planetary Science Letters*, 187, 55–69.

Torsvik, T.H., Muller, D.R., Van Der Voo, R., Steinberger, B., Gaina, C., 2008. Global plate motion frames: toward a unified model. *Reviews of Geophysics*, 46, 1–44.